EROSION AND SEDIMENTATION ON THE CARNEGIE RIDGE, EASTERN EQUATORIAL PACIFIC

A Thesis

by

CAROLINE KELLY BROOKS

Submitted to the Office of Graduate and Professional Studies of
Texas A&M University
in partial fulfillment of the requirements for the degree of

MASTER OF SCIENCE

Chair of Committee,	Mitch Lyle
Committee Members,	Franco Marcantonio
	Niall Slowey
Head of Department,	Deborah Thomas

December 2014

Major Subject: Oceanography

ABSTRACT

The Carnegie Ridge is an aseismic ridge that bounds the south flank of the Panama Basin. Dynamic sedimentation around Carnegie Ridge is shown by evidence of erosion, dissolution and re-deposition of pelagic sediments where erosive episodes have carved out relict landscapes. I examine three aspects of these features: 1) What are the mechanisms involved in the erosive episodes; 2) Can the ages of the erosive events be constrained; and finally 3) Can the transport mechanism be identified?

The extent of erosion and re-deposition was studied during the R/V Melville cruise MV1014 from October to November 2010 to compare with geochemical estimates of sediment focusing. The MV1014 cruise acquired geochemical, geological and geophysical data to compare with earlier surveys and scientific drilling.

Large-scale erosion, presumably driven by massive, density-driven deepwater spillover events from the Peru Basin, created a prominent valley named Sand Dune Valley in the study area. A second, smaller valley, known as Western Valley, was likely formed by medium-scale erosion catalyzed by a ridge jump with subsequent normal faulting forming a fault scarp which has intensified near-bottom currents. Smaller-scale erosional events created small-scale surface sediment truncation. Utilizing a seismic stratigraphy developed by comparing seismic horizons to the sediment columns at DSDP Site 157 and ODP Site 846, and exposure of diagenetic chalk along the valley floors allowed a reconstruction of the timing of these highly erosive episodes.

Two major erosive episodes are proposed to have occurred at ~5 Ma and ~3Ma which removed as much as 75 km^3 of sediment. The erosive episodes may be linked to a

ridge jump of the Galapagos hotspot at ~5-4 Ma and the final closing of the Isthmus of Panama ~3Ma.

Sediment transport regimes for the Quaternary were determined using horizons dated at 2 Ma (PL-2), 1.7 Ma (PL-1) and 84 ka (Q-84). Isopachs created using the three horizons concluded that the dominant transport regime occurs to the NW of the study area with strong lateral transport to the sides of the valleys.

DEDICATION

For my son, Blake Michael Tatro.

ACKNOWLEDGEMENTS

I would like to thank my committee chair, Dr. Lyle, and my committee members, Dr. Sager, Dr. Marcantonio, and Dr. Slowey for all of their guidance through this process. Thanks to Dan'l Lewis for all his camaraderie and help with data acquisition, processing and interpretation. I would like to thank Chris Paul for his help with bathymetry, and everyone in the Oceanography Department that has assisted this research process. A special acknowledgment goes out to STEM for my research grant.

I would like to thank my friends and family for all their support through the years.

NOMENCLATURE

CR	Carnegie Ridge
SDV	Sand Dune Valley
WV	Western Valley
ODP	Ocean Drilling Project
DSDP	Deep Sea Drilling Project
Ma	Unit of time equal to 1 million years, 10^6 years
ka	Unit of time equal to 1thousand years, 10^3 years
CTD	Conductivity-Temperature-Depth, Measures water characteristics
JC	Jumbo Core
PC	Piston Core
GC	Gravity Core
MC	Multi-Core
WC	Water Cast
CDP	Common Depth Point
BSR	Bottom-Simulating Reflector

TABLE OF CONTENTS

Page

LIST OF FIGURES

Page

LIST OF TABLES

Page

1. INTRODUCTION

Deep sea sediments are an important archive of climatic signals and it is vital to know how these sediments are deposited and over what area the paleoceanographic signals are averaged in order to understand what signals are recorded. The Carnegie Ridge, the southern boundary of the Panama Basin, is a prime location to study how sediments record and preserve climate signals under varying transport conditions. Equatorial upwelling in this location, driven by the southeast trade winds, is strong and causes high productivity all across the Panama Basin. The surface-ocean properties of the eastern equatorial Pacific are also sensitive to inter-annual to decadal variability in addition to long-term climate changes associated with the Pleistocene ice ages (van Andel, 1973).

The Panama Basin is partly isolated from the rest of the Pacific, because of the basin's two ridge systems (Figure 1), Galapagos hotspot traces on the Cocos plate (Cocos Ridge) and on the Nazca plate (Carnegie Ridge). Jumping of the Cocos-Nazca spreading center to either side of the Galapagos hotspot over the Neogene (Werner, et al., 2003) caused variation of topography along the Cocos and Carnegie Ridges. The latest jump occurred about 5 million years ago and connected the Carnegie Ridge to the Galapagos Islands. The jump also allowed the Cocos-Nazca spreading center to propagate into the Panama Basin in its present configuration (Werner, et al., 2003)

The bathymetric relief of the ridges interacts with deepwater flow to create variability in sedimentation and erosion near the ridges (van Andel & Malfait, 1980). Within the Panama Basin, deposition of calcareous nannofossil ooze occurs in sedimentary packages as much as 600m thick, with a mean thickness of 400m (van Andel,

et al., 1971). In areas prone to erosion, as much as 400m of sediment are missing, presumably removed by erosion.

Malfait and van Andel (1980) showed that the Carnegie Saddle region of Carnegie Ridge (the low-lying part of Carnegie Ridge between 87° and 85°W, Figure 1) has high variability of erosion and sediment transport and is a natural lab for understanding the dynamics of sediment movement in a pelagic environment. Also, this same region is the center of a dispute about estimating horizontal sediment transport and sediment focusing via geochemical versus geophysical/geological evidence (Francois, et al. 2004; Lyle, et al. 2005). For this reason, the extent of erosion and re-deposition was studied by seismic reflection profiling during the R/V Melville cruise MV1014 from October to November 2010 to compare with geochemical estimates of sediment focusing from sediment cores collected on the same cruise (Figure 2). This thesis reports on the results from the seismic reflection survey.

2. BACKGROUND

2.1 Geologic Setting

The Panama Basin is isolated from the Pacific Ocean basin by the Cocos Ridge to the northwest and by the Carnegie Ridge to the south (Figure 1). Despite its close proximity to Central and South America and separation from the main Pacific Ocean, the Panama Basin has most features of typical oceanic basins including an active mid-ocean ridge, abyssal hill topography and depths reaching ~5000m in the trench near the Colombia continental margin (van Andel, et al., 1971). Oceanic crustal ages in the MV1014 study area (Figure 3) increase from ~3Ma in the NW upper portion to ~13 Ma near the saddle (Meschede & Barckhausen, 2000). The crustal age of Carnegie Ridge increases from west to east because of its hotspot origin (Figure 3).

Located at the southern edge of the Panama Basin, the Carnegie Ridge was formed during tectonic initiation of the Galapagos hot spot and interaction with the Cocos-Nazca spreading center (CNS) around 22.7 Ma (Hey, 1977; Lonsdale & Klitgord, 1978; Meschede & Barckhausen, 2000; Werner, et al., 2003; Harpp, et al., 2004). Magnetic anomalies indicate that seafloor spreading separated the once conjoined Malpelo and Carnegie Ridges between 14.5 and 9.5 Ma (Figure 1, Figure 4), (Werner, et al., 2003; Harpp, et al., 2004).

The Carnegie Ridge trends east-west, is ~600 km long, and is up to ~300 km wide (Werner, et al., 2003). The ridge itself has a topographic relief of ~ 2000m and is a natural extension of the Galapagos Platform (Sallares & Charvis, 2003; Werner, et al., 2003). The Carnegie Ridge is divided by a saddle depression ~84°W to 87°W, referred to as the

Carnegie Saddle. The deep topography at the Carnegie saddle creates a sill ~2300 m deep which restricts exchange of deep water with the Peru Basin to the south (Lonsdale, 1977). The formation of this sill is associated with a southward ridge jump between 14.5 to 11 Ma (Figure 4) that resulted in a shift of the hotspot to the Cocos Ridge and decrease of magma production along the Carnegie Ridge (Werner, et al., 2003). To the west of the saddle, Carnegie Ridge transitions into the Galapagos Islands Platform and to the east of the saddle the ridge rises to ~ 1500 m before terminating at the Peru-Chile Trench along the Ecuadorian continental margin (Malfait, 1974; van Andel & Malfait, 1980).

Due to the Carnegie Ridge's unique position and unique evolution of the Cocos-Nazca Spreading Center through geologic time, sediments within the Panama Basin record changes in ocean circulation, biological productivity, tectonism and climate. Panama Basin's equatorial location and trapping of continentally-derived sediment in the trenches near South America causes sedimentation to primarily be of biogenic origin and be composed of siliceous calcareous ooze. However, aeolian dust is deposited at a low rate, and there are a significant number of volcanic ash layers originating from South and Central America (Mienert, 1984). There is also hemipelagic deposition of clays within 300 km of the coast (Singh, et al., 2011).

Most deep-sea deposition regimes are characteristically represented by pelagic drape but there can be strong interaction between deepwater flow and the sedimentation, and pelagic drape is not the only depositional regime located within the basin. The crest of the Carnegie Saddle is bare of sediments and deep channels have been cut into older

pelagic sediment deposits on the north side of Carnegie Ridge (Malfait, 1974; van Andel & Malfait, 1980).

Using textural analysis Van Andel (1973) estimated that winnowed, fine-grained material from the surrounding volcanic ridges contributes 40-50% of total sediment accumulation in Panama Basin. From a geochemical perspective; however, Singh et al., (2011) suggests that sediment eroded from high standing topography is not a dominant factor in sediment accumulation based on Th systematics. I propose that density driven deepwater circulation is an important sediment transport mechanism within the basin. Near-bottom currents ~30 cm/s (1 km/hr) have been recorded, with mean speeds ~7cm/s, as well as the presence of barchans dunes in an erosional valley in the Carnegie Ridge, with a mean transport direction into the NW Panama Basin (Malfait, 1974; Lonsdale & Malfait, 1974; van Andel & Malfait, 1980).

2.2 Previous Work

Much of the study of the Panama Basin results from work at Oregon State University over 40 years ago, including Panama Basin structure, morphology and tectonic history (van Andel, et al., 1971); the distribution and composition of the sediments (Plank, et al., 1973); the texture and dispersal of sediments (Moore, et al., 1973; van Andel & Heath, 1973) and erosive regimes and mechanisms (Malfait, 1974; van Andel & Malfait, 1980; Figure 5). The sediments of the Panama Basin and the Carnegie Ridge have been studied by two scientific drilling legs: DSDP Leg 16, and ODP Leg 202. Five drill sites have been drilled on or near the Carnegie Ridge: DSDP 156 and 157, ODP 1238, 1239, and 1240 (Figure 6). These sites provide geologic framework with

which to base the MV1014 Panama Basin seismic survey and shed further light on the sedimentation and erosional patterns since the beginning of the late Miocene. The ridges surrounding the Panama Basin create topographical relief that enables sedimentation and erosion atypical of most deep-sea environments. Erosion is an important factor in many areas close to the Carnegie Ridge and has carved out two valleys; the larger crossed by seismic tracklines 7, 9, and 11, and the smaller crossed by trackline 8 (Figure 2). The larger valley was named Sand Dune Valley for the presence of barchan sand dunes found on its seafloor and the smaller was named Western Valley (Lonsdale, 1980).

The Carnegie Saddle region of the Carnegie Ridge has been previously surveyed in 1971 using analog seismic reflection, coring, and subbottom profiling (van Andel & Malfait, 1980; Figure 5) and in 1972 and 1974 using a deep-towed geophysical package (Lonsdale & Malfait, 1974). Five different environments were discovered in the area encompassing the Carnegie Ridge ranging from terraces to basalt scarps to manganese-encrusted valley floors (van Andel & Malfait, 1980). Seismic reflection profiles and free-fall cores acquired on the YALOC-71 survey and piston cores acquired on the COCOTOW deep-tow survey in 1974 revealed unconformities prevalent across the Panama Basin (Figures 7 and 8.) The first deep tow survey conducted in 1972, SOUTHTOW revealed a semi-consolidated chalk floor of the Sand Dune Valley. A dredge sample taken along the fault scarp at the northern terminus of the Sand Dune Valley also revealed basaltic basement with chert as the base of the sedimentary package (Lonsdale, 1980). In 1973, drilling on DSDP Leg 16 allowed the dating of the volcanic basement and provided the first description of the complete sediment package at Site 157.

High-resolution seismic profiles were collected before drilling, allowing a basic seismic stratigraphy to be developed. In 2003, ODP conducted Leg 202 with the main objective of investigating timing and processes of late Cenozoic climatic and oceanographic changes in the southeast Pacific (Tiedmann, et al., 2007), which drilled Site 1240 in the Panama Basin just north of the Carnegie Saddle.

2.3 Unconformities, Seismic Horizons, and Diagenesis

Several cores from previous surveys found unconformities (Figure 7; Free-fall cores Y71-3-32FF3/FF4 taken aboard YALOC-71 and COCOTOW 13P, (Lonsdale & Malfait, 1974; Lonsdale, 1980). The free-fall cores recovered by YALOC-71 are near MV1014 Line 5 and determined through nannofossil biostratigraphy that the unconformity in the region is mid Pliocene in age. A thin veneer of late Pleistocene sediment overlies late Miocene or early Pliocene sediments (Figure 8) demonstrating a major sediment loss since the beginning of the Pliocene (Lonsdale & Malfait, 1974). Slightly to the northwest on MV1014 Line 12, a second unconformity Pleistocene in age was also found, demonstrating a second change in sedimentation patterns (Figure 8; Malfait, 1974). Here Quaternary sand dunes were sampled and found to lie unconformably over a Pliocene-aged sequence (Lonsdale, 1980).

Hiatuses are common in the basal sediment section of Carnegie Ridge. ODP Leg 202 Sites 1238 and 1239, on the easternmost Carnegie Ridge, have a hiatus just above basalt occurring during the middle Miocene (Mix, et al., 2003; Mix, et al., 2003). In the Carnegie Saddle region, DSDP Site 157's oldest sediments date to around 10 Ma, about 1.5 million years younger than the basaltic crust (van Andel, et al., 1971). There is another

hiatus or extreme slowing of sedimentation occurring at the Miocene-Pliocene boundary between 300 and 330 mbsf (van Andel, et al., 1971). Below 345 mbsf, the Site 157 section has been diagenetically altered, with ooze altered to chalks and limestone. Basalt basement was recovered at 434 mbsf.

Site 157 offers the closest fully recovered core with penetration to basement with which to base an approximate age model that allows dating of seismic reflectors occurring around the Sand Dune Valley and Western Valley. Site 157 is offset from the MV1014 Panama Basin survey Transit Line 5 by 37 kilometers (Figure 6 and Figure 9). Site 157 has reflectors which document dates of nannofossil ooze deposition and reflect induration down hole with the ooze compacting into chalk and then reprecipitating into cherty limestone. These reflectors can then be correlated to major occurrences of erosional episodes that carved out these dynamic valleys.

Scientists, age dating Site 157 using biostratigraphy, found the sediment directly above basaltic basement to be late Miocene (Discoaster neohamatus Zone, ~10Ma, Table 1; van Andel, et al., 1971). However, due to poor recovery, spotty occurrences and a general overall lack of preserved faunal abundances deep within the cored sections due to diagenesis, the basal date is poorly controlled. The oldest sediment above the chert-chalk sequence is about 6 Ma, just below the top occurrence of calcareous nannofossil *Discoaster quinqueramus* (5.58 Ma, van Andel & Heath, 1973).

The oldest cherts present are mid-Miocene to mid-Pliocene, but the age is poorly constrained because of poor nannofossil preservation (Gartner, 1973). With greater constraints on biostratigraphical zones (Table 1) and the addition of ODP Leg 138 Site 846

which is located south of the Galapagos hotspot (Figure 6), it is most likely that the oldest sediments at Site 157 are ~10Ma and the irregularity of dating the lower unit of the core resulted from indurated chert, poor preservation of both silica and carbonate microfossils, and perhaps periods of erosion eradicating whole units of sediment.

3. DATA ACQUISITION AND PROCESSING

Data used in this thesis were acquired aboard the R.V. Melville MV1014 expedition from October to November 2010. The MV1014 Panama Basin Survey was designed to compare geochemical and geophysical estimates of sediment focusing following the overall trackline shown in Figure 1. Two sites, one on the Cocos Ridge and one on the Carnegie Ridge, had extensive seismic reflection surveys. A third site, in the Peru Basin, located south of the Panama Basin studied sedimentation within the south Pacific gyre. This thesis is based on the MV1014 Carnegie Ridge survey (Figure 2).

Data were collected using multi-channel 2-D seismic reflection, high-resolution digital 3.5 kHz sub-bottom profiler, swathmap bathymetry, various coring techniques (piston, gravity, jumbo and multi-core) and CTD water casts onboard the R/V Melville. The Carnegie Ridge Survey consists of 13 tracklines that range from roughly 0° N to 2° S and between 84°W to 86° W (Figure 2). Seismic data were collected with a 40-channel Geometrics Geo-eel hydrophone streamer towed at 7 knots. Transit seismic reflection lines were also collected between sites at 10 knots using a 16 channel streamer. The seismic source was dual GI (Generator-Injector) seismic sources, using 45c.i generator, and 105 c.i. injector. During both survey and transit mode, seismic acquisition shots were fired every 10 seconds. Digital data were collected for 7 seconds on each shot, digitized at 1 ms.

Digital data collected on previous cruises (ODP Leg 92 and NEMO-03) were included where they passed through the Carnegie Ridge survey area to expand the data set. Due to the vertical resolution of these survey's seismic sections, the extra data were

solely used for calculating a total sediment isopach map within the Panama Basin (Figure 9). Analysis that involved finer resolution, such as comparing sedimentation rates on epoch scales were made with seismic and 3.5 kHz data obtained during the MV1014 Panama Basin cruise.

Seismic reflection data from MV1014 were uploaded into ProMAX. A bandpass filter of 25-30-120-135 and Automatic Gain Control was applied. Prior to stacking, a Normal Moveout (NMO) correction was applied and then the data were stacked using a CDP/Ensemble Stack. The CDP stacked data were then migrated using the F-K Stolt method and a constant velocity of 1480 m/s. Before uploading the seismic data into interpretation software, the ship position data were used to locate each shotpoint. The position of each shotpoint was set equal to the ships position four shotpoints previously to accommodate the offset between the ship and the first CDP.

The seismic data are presented in European Polarity whereby a positive reflection coefficient and a high acoustic impedance contrast produces a negative amplitude or trough reflection.

4. SEISMIC STRATIGRAPHY

Typical deep-sea sedimentation is a drape of many nearly horizontal strata over basement topography resulting from millions of years of accumulation of biogenic ooze free of extreme currents. The Carnegie Ridge, with its uplifted topography, volcanic origin, and exposure to significant bottom currents has a much more dynamic sedimentation environment, with erosion, sediment slumping, and sediment focusing into basins as evident in these combined vertical seismic profiles showing a transect from NW- SE in the survey area (Figure 10).

4.1 Equatorial Pacific Seismic Sequences

The goal of seismic stratigraphy is to categorize common bedding that occurs in packages to identify paleodepositional regimes. It is well known that the equatorial Pacific has distinctive depositional events through the Neogene that cause variations in carbonate content and acoustic impedance (Mayer, et al., 1986; Bloomer, et al., 1995; Liao & Lyle, 2014). Traditional approaches to identifying seismic sequences were used and combined with distinctive methods developed uniquely for this area. Special approaches are necessary because of erosion and induration and lithification of sequences. This process leads to diagenesis of foraminiferal ooze creating heightened reflections in sequences and a cherty seismic sequence above basaltic crust with an erosive surface (Figure 10, Figure 11). The change in lithification or induration from biogenic ooze to chalk to chert or limestone can be diagnosed seismically as a change in reflection strength caused by an increase in both velocity and density as the softer substrate compacts and gets harder, which in turn delivers a stronger seismic return (Figure 13). Below the

transformation from chalk to chert or limestone there is often an attenuation of seismic amplitude, as differences between layers get smaller and differences in acoustic impedance between rock and basalt get smaller.

4.2 Identifying and Dating Seismic Horizons

Seven stratigraphic seismic horizons (Figure 11) were identified throughout the survey area within the seismic reflection sequences; Seafloor (SF), PL-1, PL-2, P-1, LM-1, LM-1a, and Acoustic Basement (AB). Lettering for the seismic horizons define geologic ages of proposed sequence boundaries. PL-1 and PL-2 reflect seismic sequences that are Pleistocene in age, P-1 represents a Pleistocene to Pliocene sequence and LM-1 and LM-1a represent Late Miocene seismic sequence boundaries. Surface sediment ages for the seafloor were calculated from MV1014's multi-cores 9 and 16 (Figure 2). Sediment cores taken on the MV1014 survey penetrated less than 20 m and do not provide adequate control for sedimentation older than the late Pleistocene. Ages for the older seismic horizons are based on drillcore data from ODP Leg 202 Sites 1238, 1239 and 1240 (Mix, et al., 2003); Leg 138 Site 846 (Bloomer, et al., 1995); DSDP Legs 68 and 69 Site 504, 505 (Beiersdorf & Natland, 2007); and DSDP Leg 16 Site 157 (van Andel & Heath, 1973). These cores were incorporated into the working data set due to their recovery of sediment all the way down to basement. Locations for these cores are shown on Figure 6.

4.3 Mapping of Sedimentary Units

Seismic horizons are discussed and ages assigned in the next few sections. They were in part used to produce isopach maps of sediment deposition on the northern flank of Carnegie Ridge. Seismic data were uploaded into Kingdom Suite for interpretation.

Pinch-outs of sedimentary packages were observed to enable postulation of sediment package extent and distribution within the study area. Seismic packages constrained by major horizons of interest (Figure 11) described in the rest of section 4, were mapped out to study sedimentation and erosion from the Miocene to the present.

4.4 Subbottom Profiler Seismic Horizon Q-84

The youngest seismic horizon, Q-84 (Figure 14) is associated with an 84 ka ash layer and was identified in the subbottom profiler data. 3.5 kHz acoustic energy was generated with a hull-mounted transducer and was digitally recorded during MV1014. The sub-bottom profiling data gives detailed acoustic reflection images of the top 50 m of the sediment column. Prominent reflections occur from ash layers in the sediment due to the strong acoustic impedance contrast with biogenic sediments. One ash layer has been identified as ash layer "D" (Los Chocoyos Ash) dated at 84 kbp (Drexler, et al., 1980) based upon correlation of the subbottom reflection profile and the ash depth in a piston core taken next to Site 1240 (ME0005-24JC; Lyle, et al., 2005). In ME0005-24JC, the ash layer "D" occurred at 980 cm and is 10 cm thick.

4.5 Pleistocene Horizons PL-1 and Pl-2; Pelagic Sequences

Using ODP Site 1240 (Figure 1, Figure 2, Figure 6; 0°1.311 N, 86°27.758 W), a Pleistocene age model for the study area was developed (Figure 15). Site 1240 subdivides its total sediment package into three subunits 1A, 1B and 1C based on visual core description, smear slide analysis, and sediment physical properties (van Andel & Heath, 1973). Subunit 1A is a nannofossil ooze with diatoms, while Subunit 1B has higher diatom content relative to the other subunits. Subunit 1B also has a lower

GRA bulk density and higher P-wave velocity (Mix, et al., 2003; Figure 15). The boundary between subunit 1A and 1B should be marked by a positive reflection or peak (European Polarity acoustic impedance decrease) marked as Horizon PL-1, caused by the shift into a seismic sequence with a characteristically faster P-wave velocity but lower density. As the sediments are unconsolidated, density changes have a higher impact on acoustic impedance than the smaller accompanying velocity change (Janik, et al., 2004). Additionally, there should be a negative reflection or trough (European Polarity acoustic impedance increase) associated with the boundary between subunits 1B and 1C, Horizon PL-2, demonstrating the transition back into a slower but denser material (Figure 15). These horizons, PL-1 and PL-2, represent the division of subunits and were dated using biostratigraphy of three microfossil groups (Mix, et al., 2003) and reflect ages of 1.7 Ma for PL-1 and 2 Ma for PL-2. Although, the horizons bound sequences indicative of pelagic deposition (Figure 11), the horizons are not continuously present throughout the study area due to the vast change in depositional environments and periods of erosion as evident in core samples identifying a Pleistocene unconformity (Figure 8).

4.6 Pliocene and Miocene Seismic Horizons

Two seismic stratigraphies have been developed for the eastern equatorial Pacific (Bloomer, et al., 1995) and for Cocos Ridge (Liao & Lyle, 2014) based upon reflections from lithologic boundaries where $CaCO_3$ changes content and where the associated density change produces a reflection. Not only does acoustic energy reflect from lithologic change marking a change in sedimentation, it also can be reflected from lithification caused by diagenesis in the sediment column, like the formation of chalk and

chert in these carbonate sequences when the buried sediment compacts and then warms and the biogenic silica dissolves and reprecipitates. Lyle and his colleagues (2000) suggested, based upon appearance of chert in young sediments along the California continental margin, that chert would quickly form when sediments warmed to about 25°C. Within the equatorial Pacific, this is shown by the appearance of chert at Site 847 in 7 Ma sediments at a depth of 250 mbsf. Here Carnegie Ridge seismic horizons are integrated within this framework (Figure 12, Figure 16).

4.6.1 Horizon P-1; Onlap Sequence

P-1 is a sinuous, prominent peak correlating to Horizon R1-t at Site 846. Seismic reflections within this unit become indurated from overburden and illustrate a heightened reflection strength. This could be indicative of ooze lithifying into a stiffer substrate. In areas with proximity to the Carnegie Ridge in the Panama Basin study area, the horizon marks the top of an onlap sequence differing from the normal pelagic sequences bound by horizons PL-1 and PL-2 above.

4.6.2 Horizon LM-1; Onlap Sequence

LM-1 is denoted by a sinuous, prominent trough correlating to a change in $CaCO_3$ concentration right above Horizon R4 at Site 846, which marks the base of a higher sedimentation rate interval. This seismic horizon also marks an increase in carbonate content (50%-70%) that causes a heightened reflection strength of reflectors deeper in section from induration of sediments (Mienert, 1984). This horizon marks the top of a second onlap sequence which differs from the sequence above by the heightened reflectors throughout the package suggesting a lithified substrate like chalk.

4.6.3 Unconformable Horizon LM-1a

LM-1a is a highly erosive surface present in the southern portion of the study area and is interpreted to represent the transition into cherty chalk or limestone, because it is at the right depth for this transition based on typical geothermal gradients, and the seismic characteristics are similar to the basaltic crust beneath. The horizon is an unconformable surface, where the erosion of hard, lithified sediment creates a very chaotic, pronounced reflector within the carbonate substrate indicative of a hardground paloeseafloor, marking a large change in environment of deposition in the geologic past. The beds below the reflector are parallel whereas the bedding patterns above the reflector reflect a change in deposition with exemplary angled bedding (Figure 11, Figure 12). For this reason a lithological correlation with Site 846 cannot be made. However, the horizon is marked on Site 846's $CaCO_3$ plot where an extreme decrease in carbonate concentration is observed and marks the top of a cherty ooze transformation to demonstrate time and overburden required for the diagenetic transition to occur and to postulate on approximate ages this occurs within the equatorial Pacific.

4.6.4 Acoustic Basement

Acoustic Basement (AC) was picked as a prominent, high-amplitude trough marking hard substrate. The basement is noted as acoustic because it may be either massive chert/limestone or basalt. Similarities in velocity between highly indurated chert/limestone and basalt makes it difficult to delineate between the two.

4.7 Age Dating Pliocene and Miocene Seismic Horizons

To approximately age date P-1 and LM-1, DSDP Leg 16 Site 157 and ODP Leg 138 Site 846 were used to create age models based on $CaCO_3$ content (Figure 16). Site 846 has a seismic stratigraphy from Bloomer et al., (1995) and a $CaCO_3$ profile which can be correlated to the CaCO3 profile in Site 157, which in turn is near to Transit Line 5 and Line 7 (Figure 6, Figure 9). ODP Leg 16 Site 157 is the closest drill site to Sand Dune Valley that has a full sediment package (~400m) and basalt basement. While Site 846 is closer to the Galapagos (Figure 6), its use as a proxy is advantageous due to the seismic stratigraphy from Bloomer et al., (1995) and the incorporation of well-logs used to make a synthetic seismogram for seismic reflection profile correlation. Synthetic seismograms enable precise dating of horizons of interest. Using percent carbonate ($CaCO_3$) vs. depth (m) plots, Site 157 was correlated to Site 846 (Figure 16; Table 2) and used to approximately age two horizons in the Carnegie Ridge survey; P-1 (~2.2 Ma), LM-1 (~5.3 Ma). The age of LM-1a, because it is erosional, will not be the same across the site and therefore cannot be correlatable with Site 846. It marks only the beginning of a hard, eroded sequence.

5. RESULTS

Calcareous ooze is a major biogenic sediment type noted for a high velocity and density gradient with depth (Hamilton, 1976). Significant changes in both density and velocity may occur when the carbonate content changes with depth (Mayer, et al., 1986). When analyzing seismic reflection profiles, bulk density has a direct influence on acoustic impedance, defined by the relation ρV_p, bulk density times P-wave velocity. Reflection coefficients can then be determined to calculate actual horizons representative of changes in carbonate content and diagenesis (Figure 12). The carbonate content variations throughout seismic sections are a good guide to reflection coefficients and therefore to seismic events (Mienert, 1984). Due to the dynamic geologic evolution of the Panama Basin and Carnegie Ridge, many seismic horizons are present on reflection profile, which illustrate a large variability in depositional environment.

First, the seismic horizons indicative of the seafloor and acoustic basement were identified to create a sediment isopach map (Figure 9), and to locate anomalous thicknesses of sediment to indicate focusing or erosion. Minibasins created from uplift of the volcanic ridge emplacement create sediment traps (Figure 17). The volcanic ridge's pinnacles that are numerous and essential to minibasin genesis also provide relief for many gravity deposits such as slumps (Figure 17). Secondly, seismic horizons PL-1 and PL-2 from Site 1240 were used to map Pleistocene isopachs. Finally, seismic horizons representing the Pliocene to Miocene package were correlated with DSDP Leg 16 Site 157 and Leg 138 Site 846 to unravel the Panama Basin's depositional history and propose a

time line for erosional processes that carved Sand Dune Valley out of the pelagic landscape.

5.1 Sediment Packages

Sediment package thicknesses will be discussed in the following paragraphs with emphasis on anomalously high and anomalously low packages. The absence of core data within the study area for the seismic packages occurring from the Pliocene and late Miocene result in the use of empirical data for average velocities of carbonate oozes, chalks and cherts in the equatorial Pacific.

5.1.1 Total Sediment Accumulation, North and South Flank of Carnegie Saddle

The total sediment thickness isopach map was created in Kingdom Suite using the seafloor (SF) and basement seismic horizons (AC, Figure 9). An equation for thickness was used as denoted:

(1) Total Sediment Thickness=((SF(s)-AC(s))/2)*V_c,

where **Vc=1600 m/s** and **s=TWTT**

This resultant total sediment isopach map is juxtaposed with the bathymetric map of the north flank of Carnegie Saddle. There is significant variability to sediment isopachs and they do not appear to be typical pelagic sediment drape. Typical sediment thickness is ~400m in the survey area but some areas have thicknesses up to 600m and other areas are essentially bare of sediment. Thick sediments are found both in the deeper minibasins to the north of Carnegie Ridge (Figure 17) but also on the Carnegie Ridge itself. Surprisingly, one of the thickest sediment accumulations occurs just to the east of the erosional Sand Dune Valley. Also, it should be noted that the thickest sediment

accumulation lies on the southern flank of the Carnegie Ridge on Transit Line 5 transecting into Peru Basin. Accumulations up to 700 m are present here.

Erosion has also dissected some areas down to exposed basement near the ridge crest or down to the manganese-encrusted, semi-indurated chalky floor of Sand Dune Valley and Western Valley. They are marked by rectangles (Figure 9). Lines 7, 8 and 9 form a cross sectional view of the erosional Western Valley and Sand Dune Valley (Figure 10). It is unclear where the sediment removed from Sand Dune Valley went. There is no anomalous accumulation of sediments below the mouth of the valley. Instead, there is an anomalous accumulation to the east. Such a deposition pattern suggests that the loss of sediment was not from slumping but from grain-by-grain, mechanical erosion.

5.1.2 Anomalous Sediment Package Thickness

Figure 9 shows the thickest accumulations of sediment and are placed into categories according to proximity to the Carnegie Ridge and depth. 'Octagons' denote areas of deposition occurring around a depth of 2200m and deposition on the northern flank of the ridge around the highly erosive valley areas showing lateral transport of sediment sourced from the Peru Basin to the south. The 'triangle' packages denote deposition at depths of 2500m-3000m and are located at the base of the northern flank of the ridge suggesting downslope transport. Finally, 'ellipse' packages occur in basins that are deeper than 3000m and are characteristic of basin infill. The erosive valleys are represented as rectangles. To get a better grasp on the depositional regime across geologic time and how climate has affected it, the results from seismic horizons of interest are presented below.

5.2 Sedimentation in the Pleistocene, Pliocene and Miocene

Five seismic horizons have been identified in the sediment packages that accumulated on the north flank of Carnegie Ridge. The following paragraphs provide an insight to sediment accumulation rates and thicknesses in these seismic sequences.

5.2.1 Seafloor to Q-84 (84 ka) from Subbottom Profiler Data

There is more data from the subbottom profiler than from the seismic reflection surveys because the subbottom profiler continues to record on both seismic reflection lines and transects between core sites. Using what we interpret to be an 84 ka horizon composed from the Los Chocoyos Ash Layer (Worzel, 1959; Drexler, et al., 1980), a Quaternary sediment package can be mapped across the study area (Figure 14, Figure 18). An equation for thickness from the seafloor to the Los Chocoyos Ash Layer, Q 84, is given by:

(2) Thickness of SF to Q 84 Horizon=((Q 84(s)-SF(s))/2)*V_c,

where **V_c=1530m/s** and **s=TWTT**

The highest amount of deposition occurs in the NW of the study area right along the equator, and on the sides of the Sand Dune Valley. The sediment accumulation ranges from 2.50m near the Sand Dune Valley's lower (NW) terminus to 9.50m along the sides of the valley and to the NW of the study area. These correspond to sedimentation rates of 3 cm/10^3yr near the base of Sand Dune Valley and up to 8 cm/10^3yr on the sides and in the NW part of the study area.

5.2.2 Site 1240 Subunit 1A: SF (Seafloor) to Horizon PL-1

Using PL-1 (1.7 Ma) and SF (Seafloor), the representative sedimentary package thickness was determined using a seismic velocity of 1545 m/s (Figure 19). A seismic velocity of 1545 m/s was used based on in-situ physical property measurements of V_p taken on Site 1240A. An equation for thickness from the seafloor to subunit IA as depicted by Horizon PL-1, is given by:

(3) Thickness of Subunit IA=((PL-1(s)-SF(s))/2)*V_c,

where **V_c=1545m/s** and **s=TWTT**

In the NW of the study area, this sediment unit ranges from 185 m to 115 m thick (Figure 19). In the middle of the survey area, packages start to rapidly decline with thicknesses being more constrained in their lateral distribution. These thicknesses range from 125 m to 50 m thick. In the SE of the survey area the packages are dramatically reduced in thickness to a range of 90 m to less than 50 m thick. The thickest package occurs along Line 2 in a basinal setting and has accumulated 185 m from the 1.7 Ma to present seafloor age. The thinnest package, where it is not been completely eroded away, has a thickness of less than 50m. These thickness correspond to accumulation rates of 11cm/10^3yr-7cm/10^3yr in the NW, 7cm/10^3yr-3cm/10^3yr mid-survey region and finally 5cm/10^3yr -2.5cm/10^3yr in the SE. From NW-SE the extent of this horizon to the seafloor becomes intermittent as a result of surface sediment erosion and dynamic sedimentation with closer proximity to the ridge.

5.2.3 Site 1240 Subunit 1B: Horizon PL-1 to Horizon PL-2

The thickness of subunit IB was calculated using the equations below:

(4) Thickness of SF to PL-2=((PL-2(s)-SF(s))/2)*V_c,

where **V_c=1550 m/s** and **s=TWTT**

(5) Thickness of Subunit IB= Equation (4) – Equation (3)

Subunit IB found between PL-2 (2 Ma) and PL-1 (1.7 Ma) is shown in Figure 20. In the NW part of the survey, sediment thickness between the two horizons seems to be constrained to measurements below 60 m. Mid-survey the sedimentary ooze thickness ranges from ~ 70 m to ~45 m. In the SE of the survey, the thickest accumulations are present and range from upwards of 92 m to ~50m. These thicknesses correspond to accumulation rates of 18 cm/10^3yr, 15 cm/10^3yr - 23 cm/10^3yr, 31 cm/10^3yr - 17 cm/10^3yr and reflect a much more rapid deposition of sediment than the upper Pleistocene unit.

5.2.4 Pl-2 to P-1

The horizons representative of the seismic sequence that spans a transition from the Pleistocene into the early Pleistocene are represented by Pl-2 (2 Ma) to P-1 (2.2 Ma) and shown in Figure 21. The thickness represented by this seismic sequence was calculated using the following equation:

(6) Thickness of SF to P-1=((P-1(s)-SF(s))/2)*V_c,

where **V_c=1555 m/s** and **s=TWTT**

(7) Thickness of PL-2 to P-1= Equation (6) – Equation (4)

P-1 has a very sinuous characteristic and is missing in some parts of the survey due to chaotic seismic intervals. In the NW part of the survey, sediment thickness between

the two horizons is at the thinnest and averages ~40m. Mid survey the thickness changes to ~125m-80m. In the SE of the survey area deep accumulations are found and the thickness fluctuates between 175m-80m. These correspond to accumulation rates of 20 cm/10^3yr, 80 cm/10^3yr to 40 cm/10^3yr, and finally 88 cm/10^3yr to 40 cm/10^3yr. This is markedly higher than levels in the later Pleistocene time period as shown through horizons, PL-1 and PL-2.

5.2.5 P-1 to LM-1

The horizons representative of fluctuations of $CaCO_3$ content, as correlated with Site's 157 and 846, reflect ages of 2.2 Ma and 5.3 Ma, respectively (Figure 22). Although there is no core or well control in the MV1014 survey area for this depth, using a faster V_p will likely yield more realistic thickness calculations because of the degree of induration of sediments at this depth. An equation for thickness is denoted by:

(8) Thickness of SF to LM-1=((LM-1(s)-SF(s))/2)*V_c,

where **V_c=1560 m/s** and **s=TWTT**

(9) Thickness of P-1 to LM-1= Equation (8) – Equation (6)

Package thickness could only be constrained to the mid survey and SE survey area. Mid survey, the thickness of this seismic sequence occurs at the thinnest sequence with thickness ranging from 16.25 m to 85 m. In the SE, the thickest package occurs with the sequence expanding into thicknesses of 185 m to 85m. These correlate to accumulation rates of a mere 5 m/10^6yr to 27 m/10^6yr, and 27 m/10^6yr to 60 m/10^6yr. A hiatus in deposition has been recorded in Site 157 occurring around the Late Miocene to Pliocene

(van Andel, 1973) which could explain a regional change in depositional regime or erosion being a dominant factor during this time.

5.2.6 Erosional Unconformity LM-1a

A horizon of high negative amplitude occurs around 100 m above basement throughout most of the survey area from mid-survey to the SE (Figure 11, 13). This horizon, as correlated with Site 157 and Transit Line 5, is an erosive unconformity and the sediments beneath are interpreted to be a chalky-chert sequence. This chert transition from a semi-lithified chalk is evident seismically by its characteristic strong trough reflector (Figure 12) and attenuation of seismic signal in stratum beneath it signifying a greatly lithified package. The transition into a cherty sequence is made more evident by the highly erosive surface. In the sediment section below the erosive unconformity, the cherty transitional layers are so lithified at times that distinguishing between them and the basaltic basement can be difficult due to their velocity similarity. Thickness of this transition (Figure 23) was calculated with the equation:

(10) Thickness of Cherty Sequence=((LM-1a(s)-AC(s))/2)*V_c,

where **V_c=2000 m/s** and **s=TWTT**

A V_p of 2000m/s was used based on typical chert velocities in the equatorial Pacific having a V_p around 2900m/s. The change in V_p from 2900 to a more conservative velocity of 2000 m/s is used due to the presence of a calcareous ooze and chalk matrix. Mid-survey area, the typical accumulation thicknesses from acoustic chert basement to top of the erosional unconformity, LM-1a, are around 100m with the lowest value around 15 m.

In the southeast of the survey area closest to Carnegie Ridge, the eroded sequence is much thicker and has a package thickness ranging from 75 m to 185 m on the sides of the SDV.

5.3 Occurrence of Erosion

Erosional episodes are common within the study area, and can be found because of horizon truncation and large-scale incision of valleys or current "channels" in the seismic profiles (Figure 10). Truncation of horizons is prevalent throughout the seismic sections in closest proximity to the ridge. Sediment surface truncation occurs from the middle to the southeastern portion of the survey area. Medium-scale erosional features occur where an east-west trending fault scarp has enhanced near-bottom currents (Figure 24). This channelization, via fault scarp, has provided a pathway for the near-bottom currents to gain enough velocity to downcut into a depositional center at the northern terminus of Sand Dune Valley. I propose the currents caused by the fault scarp have also aided if not are the main driving force in the excised Western Valley, Sand Dune Valley's smaller counterpart. Large-scale erosional features, such as the main valley, Sand Dune Valley, occur on the saddle region of the Carnegie Ridge and have possibly eroded up to 400m of sediment. Other large-scale erosional features, such as unconformities, are evident seismically throughout the survey area and appear to occur throughout the geologic record (Appendix B, Vertical Seismic Profiles).

Sand Dune Valley is the prominent erosional valley and encompasses a staggering 180 km^2 of area. Later in Section 6, I will estimate when erosion occurred and what volume of sediment has moved.

6. DISCUSSION

Sediment accumulation in the deep sea is controlled by sediment supply, dissolution and rates of erosion (Scholle, 1983). The depositional regime of the study area changes from a normal biogenic environment with pelagic drape in the NW to a complex regime further south marked with proposed basal diagenetic changes and various types of erosional episodes (Figure 10, Figure 24, and Figure 25). Closer to the Carnegie Ridge, five different environments have been identified illustrating the dynamic sedimentation near a deep-sea ridge (van Andel & Malfait, 1980). In the middle part of the survey, a SW-NE trending fault scarp dissects the survey area and creates the northernmost boundary for the Sand Dune Valley (Figure 2, Figure 24). Many have postulated a "sediment pool" for the eroded material from the valley north of this scarp but while we observe significant sediment in the basin on a total sediment isopach from seafloor to acoustic basement, we do not find sufficient sediment to account for that lost from Sand Dune Valley (Figure 9).

Many E-W trending channels, north of this scarp, dissect sediment and expose chalk substrata. Mass transport deposits containing unconformities clearly representing erosion, re-sedimentation and slumping occurrences also occur. In the middle of the survey region north of the Carnegie Ridge proper, with a basement age ~5-6 million years old, a changing thermal regime and more overburden results in the diagenesis of calcareous ooze and biogenic silica. Depth to the diagenetic transition tends to remain around 450 m but can vary as a function of time, overburden and geothermal regime. Previous surveys SOUTH TOW, COCOTOW, Leg 5, YALOC 69 and 71 have age-dated

piston and free-fall cores taken within the SDV and show the valley floor to be a semi-lithified chalky ooze that is Late Miocene in age.

Although the diagenetic seismic sequences are time transgressive, it is the diagenetic process forming chalk and then limestone or cherty sequences that sheds light on the timing of large-scale erosive processes within the Carnegie Ridge survey area. Sand Dune Valley exemplifies the large-scale erosion/dissolution prevalent in the area and reflects a sedimentary profile cut down to Miocene-aged chalk stratum with an unconformable limestone base. Using estimates of overburden required to cause the lithification to chalk (~200m; Mienert, 1984), estimates found at Sites 1238 and Sites 504, and diagenesis to chert (~450m), we can calculate an approximate time that erosion took place. It is evident that in order for diagenetic processes to proceed a certain amount of overburden must be present and this aids in age dating erosive episodes since diagenetic transition took place pre-erosion/dissolution. It should be noted that diagenesis to chert has been achieved at much shallower depths further north along the Costa Rica Rift at Site 504 (Figure 6).

We can combine this knowledge with data discovered from two previous surveys conducted by Lonsdale and Malfait in the 1970's where sediment recovered past the NW- SE trending fault scarp has exposed two unconformities (Figure 7, Figure 8). The unconformities of interest show two periods of missing sediment dated to mid Pliocene and Pleistocene. Combining this data with supplementary data collected in ODP cores and major geologic events during this time in the eastern Equatorial Pacific, we postulate that two highly erosive episodes are the main cause of the dynamic depositional

environment found with proximity to the Carnegie Ridge and created the Sand Dune Valley.

Erosion has evidently had a profound influence on deposition throughout the southern study area since sometime in the Late Miocene but there has potentially been at least two highly erosive events that have excavated out massive amounts of material from the Sand Dune Valley and Western Valley. I postulate that a first erosive event occurred around 4-5 million years ago during the early Pliocene eroding away up to 300m of sediment. Dissolution could have played some part in this process as much of the eroded sediment was highly lithified cherts and chalks. This sediment is proposed to have been redistributed laterally and to the north. This event correlates with the hiatus found at Site 157. This event dating to the mid Pliocene allows ample time (~7 million years after basement formed) for deposition of sediment within the Sand Dune Valley for overburden of ~400m to allow the ooze to lithify to a chalkier substrate and then reprecipitate into chert. This bodes well for our Pliocene to Miocene age model where the LM-1a horizon represents a lithified sequence that has been heavily eroded into at ages upwards of 9 Ma.

I further postulate that a second event took place during the late Pliocene to early Pleistocene, due to an erosional unconformity uncovered by Piston core 13(Figure 8) on COCOTOW survey lead by Peter Lonsdale, which further eroded up to 200m of sediment to the present day manganese-encrusted chalk floor of the SDV. Here the piston core recovered a thin veneer of Quaternary aged sediment over Pliocene aged strata. Figure 8 illustrates the dynamic structural influence on this area. It is evident that activation of normal faulting influenced this erosion, with the footwall providing protection from

erosive currents or spillover events primarily trending NW-SE. This same faulting regime, however, also facilitated erosion in an E-W trending fault scarp which is evident in Figure 24 and is the likely mechanism for the smaller incised Western Valley. The two events which possibly caused these highly erosive episodes are thought to be activation of the Galapagos Spreading Center ~4-5 million years ago, with subsequent normal faulting, and the final closing of the Isthmus of Panama restricting all communication between the equatorial Pacific and the Atlantic Ocean ~3 Ma, which could have intensified currents and affected primary production and perhaps changed CCD levels or onset dissolution events.

To further complicate the depositional history, the extremely large amount of sediment that was eroded during these episodes is not evident in any anomalously thick sediment packages found around the "sediment pool" or areas encompassing the valley. Thicker than average sediment packages do encompass the erosional valleys, but do not represent large scale re-depositional episodes required from the erosion of as much as 75km^3 of missing sediment (Figure 9). Previous surveys have placed current transport modes depositing sediment to the NW of the valley and the areas encompassing it, but no large-scale sediment deposit has been identified. Without precise dating of the deeply buried horizons using core control, we cannot postulate exactly where sediment deposition was primarily being directed. However, we can use the earlier dated horizons of interest that occur in the top of the section to propose recent (~2ma-present) sediment depositional regimes, and postulate depositional regimes in the basal section using the Horizon P-1 (2.2 Ma) and Horizon LM-1 (5.3 Ma) correlated with Site 846.

6.1 Sediment Supply and Depositional Trends

Trends in deposition can be postulated utilizing isopach maps created for each seismic sequence. This sheds light on major changes and shifts in deposition throughout the study area from the late Miocene to the present. By analyzing the geographical constraint on anomalous thicknesses within in each sequence a geological model can be developed that illustrates likely sources for the sediments and effects on deposition from erosion. Located in a region of equatorial upwelling and high productivity; pelagic snow should be a major component of sediment input; however, it is evident from erosion and lateral constraint on some seismic packages, indicated by pinch outs in the vertical seismic profiles, another source has also been influential, the Peru Basin to the south.

6.1.1 Seafloor to Q-84 (84 ka) from Subbottom Profiler Data

Although the Los Chocoyos ash layer (Figure 14) is a thin sediment layer (~10 cm thick) in the region of the Carnegie Saddle, the ash should be resolvable on seismic reflection profiles due to the difference in acoustic impedance between ash and calcareous ooze. Ash thickness, acoustic impedance differences, bioturbation, sedimentary processes and topography are all factors which may affect the detection of the seismic horizon on a 3.5 kHz record (Lin & Ledbetter, 1984). The ash layer that is thought to represent the Los Chocoyos eruption is found around 9 m below the sea floor in the northwestern portion of the Carnegie Ridge Survey. As the study area is traversed NW-SE the amount of sediment on top of the ash horizon decreases by a one third. This implies less availability of sediment in the SE of the study area or active reworking of sediment with transport occurring to the NW. The occurrence of thin packages above the

ash horizon in the SE of the study area with large piles to the east and west of Sand Dune Valley suggest displacement of sediment occurring to the sides of the valley since 84 ka to the present. Even though deep tow studies on the Sand Dune Valley have uncovered evidence of Quaternary sediment transport occurring to the NW in the valley (transverse Barchan dunes of relict foraminiferal sands) the occurrence of higher accumulation rates on the sides of the valley suggest a lateral transport mechanism from the southern Peru Basin via density-driven flows as well. This also likely suggests heightened productivity levels at the equator. Low sediment package thickness actually occurs past the northern terminus of the Sand Dune Valley suggesting this area is not a place of deposition during more geologically recent times. This could also demonstrate heightened bottom currents along the east-west trending fault scarp which is providing a bottom-current conduit to carve out the Western Valley.

6.1.2 SF (Seafloor) to Horizon PL-1

The isopach for Site 1240's Subunit 1A represented by the seafloor and MV1014's horizon PL-1 shows a drastic change from Quaternary sediment supply and deposition (Figure 19). Sediment supply seems to be primarily controlled by equatorial upwelling in the northwestern portion of the survey with little to no sediment supply from the southern Peru Basin. Approaching the ridge area of the study area, the package appears to only have substantial thicknesses in the depositional minibasins, with dramatically rduced package thickness occurring throughout the southern portion of the survey area. This demonstrates intensified, erosive currents closer to the mouth of the Sand Dune Valley during the late Pleistocene.

6.1.3 Horizon PL-1 to Horizon PL-2

From the isopach created in Kingdom Suite for Site 1240's subunit 1B, the most anomalous sediment accumulations occur in localized packages in the southwest and northwest but are mainly constrained to large packages along the eastern portion of the survey area (Figure 20). Overall sedimentation rates appear constant throughout the study area compared to other seismic sequences. Subunit IB from Site 1240, bound by horizons PL-1 and PL-2 indicates enhancement of equatorial upwelling and primary productivity between 1.7 Ma to 2.1 Ma most likely as a result of intensified oceanic circulation (Mix, et al., 2003). The focus of the anomalously thick package to the southeastern portion of the survey area also suggests an extra influence from the Peru Basin to the south.

6.1.4 PL-2 to P-1

As the sediment sequences get older, the packages start to be constrained geographically to the southernmost portion of the survey area with closer proximity to the ridge where crustal ages are greater. Here ridge dynamics are a dominant force in controlling environment of deposition. In this early Pleistocene to Pliocene seismic sequence, which is represented by horizon PL-2 to P-1, the thickest areas of sediment deposition occur at the northern terminus of the Sand Dune Valley and along the eastern side of the Sand Dune Valley (Figure 21). This likely demonstrates sediment supply influence from the Peru Basin to the south and/or redistribution of sediment via density-driven flows from the Peru Basin. This sheds light on a second major erosive period during the Pleistocene. An unconformity was also uncovered northward of the northern terminus of the Sand Dune Valley, where the entire mid to late Pleistocene is missing.

This suggests that Pliocene to Pleistocene sediment supply is a factor of spill-over events from the southern Peru Basin carving out sediments in the Sand Dune Valley and then redistributing the sediments laterally and into the terminus which was postulated to be the "sediment pool". Complicating the matter is the unconformity showing a drastic erosive episode initiating during the mid to late Pleistocene most likely in an east-west trend which catalyzed the excavation of the Western Valley as it lies in close proximity to the fault scarp.

6.1.5 P-1 to LM-1

In the seismic sequence representative of an early Pliocene to late Miocene package, the deposition of sediments has shifted from a depositional center at the northern terminus of the Sand Dune Valley to the sides of the Sand Dune Valley and Western Valley suggesting sediment supply from the southern Peru Basin and/or redistribution of sediment laterally (Figure 22). This seismic sequence demonstrates pinch-outs and angled bedding characteristic of a major shift in depositional regime from pelagic to onlap, suggesting intensified bottom currents and lateral transport mechanisms.

6.1.6 LM-1 to LM-1a

The seismic sequence representative of a late Miocene sequence continues to be constrained to the southernmost portion of the survey area where crustal ages are appropriately old enough. The thickest accumulations continue to persist on the sides of the valleys indicating lateral transport of sediment via density-driven currents from the Peru Basin to the south.

6.1.7 LM-1a to Acoustic Basement (AC)

The oldest seismic sequence in the survey area is represented by a prominent, chaotically unconformable surface. The seismic sequence is very close to basaltic basement and likely is composed of cherty chalk or extremely lithified chalk at this depth. Due to major erosive periods, it has been exposed along the Sand Dune Valley floor and remains at a consistent thickness where it is present (Figure 23). The seismic reflections that are visible in this hard substrate are parallel to semi-parallel, illustrating probable accumulation from pelagic snow before the onset of erosive forces sometime in the late Miocene to early Pliocene. The sediment supply is most likely a result of equatorial upwelling and not sourced from the southern Peru Basin.

6.2 Erosion

Erosion is an important regime in deposition and reconstruction of depositional environments and sedimentation in the geologic past for the area encompassing the Carnegie Ridge. The following examines erosion local to the area from small-scale to large and from the initiation of sedimentation to the present.

6.2.1 Large-scale Erosion: Evolution of the Sand Dune Valley

Placing a time scale on the erosion responsible for carving out the topography in the survey area presents a challenge but can be done with different proxies and the use of cores obtained during ODP/DSDP expeditions. We can constrain onset of erosion by analyzing diagenetic processes of the sedimentary stratum and identifying unconformities in core samples. The lithification of ooze to chalk requires a minimum amount of overburden and the diagenetic process which forms a limestone/chert transition occurs

throughout the study area. Using the geothermal regime indicative to the region and approximating a minimum amount of sediment required for a semi-lithified transition into chalk (~200m) and diagenetic transition into chert (~400m), we can calculate an approximate age of onset of erosion.

The floor of Sand Dune Valley is exposed manganese-encrusted, semi-lithified chalk from the late Miocene underlain by what was interpreted to be cherty limestone at the base (Figure 8; Lonsdale & Malfait, 1974). They noted that the acoustic basement was very smooth, like the cherty limestone acoustic basement found at Site 157 (van Andel & Heath, 1973) and unlike typical basalt basement on Carnegie Ridge (e.g., the transition from rough to smooth acoustic basement along Line 10 as Sand Dune Valley is approached; Appendix B, Vertical Seismic Profiles). The presence of cherty limestone means that the sediments have experienced significant burial and chemical diagenesis.

In order for this transition from siliceous-calcareous ooze to chalk to limestone/chert to occur the sediment package must be exposed to overburden/lithostatic pressure, time and an elevated geothermal regime. Previous studies conducted in the equatorial Pacific concluded that 400m of overburden typically must be present for the ooze-limestone transition in the Panama Basin (Mienert, 1984; Beiersdorf & Natland, 2007). However, DSDP Leg 16 Site 157, and Leg 69 Site 504 and 505 have recovered the complete sediment column to basement and found that this transition occurs with varying depths in the Panama Basin and that 400m of overburden is not required if a high geothermal regime is present (Mienert, 1984; Beiersdorf & Natland, 2007; van Andel & Heath, 1973; Mayer, et al., 1992). According to Beiersdorf et al., (2007), in areas with

a high geothermal gradient, e.g. Site 504, the transition into a lithified chalk occurred around 130 mbsf whereas the transition occurred deeper in areas with a lower geothermal gradient, at depths around 210m (Site 505). A lower geothermal gradient may be caused by the presence of varying topography and basement fluid flow processes (Beiersdorf & Natland, 2007) in a region of generally elevated heat flow caused by mid-ocean ridge volcanism. Site 157, which occurs on the southern flank of the ridge, records the lithification into chalk around 240 m and diagenesis into a cherty substrate at 345m (van Andel & Heath, 1973). This fits well with current controls on the seismic sequences within the MV1014 survey where seismic sequences below LM-1 reflect pronounced signal strength and most likely reflect lithification to chalk as well as a highly eroded hardground represented by LM-1a which is interpreted to be a chalky chert or limstone.

Using sediment accumulation rates constrained biostratigraphically through Site 157 and Site 846, presented earlier, we can date the down-cutting that created Sand Dune Valley. To further constrain the large-scale erosion of the valley, we can calculate a proposed volume of sediment that was eroded using a marine erosion equation with phi=0.5 for foraminiferal sand, which is generated from the original foram-rich ooze, to calculate the minimum time allotted for large-scale removal of this sediment. The proposed volume of sediment eroded is 75 km^3 with a minimum time of ~6 Ma. So large-scale erosion must have commenced circa 5 Ma with perhaps a second erosive event occurring around 3 Ma. It must be noted that at least ~200m (Figure 25) of sediment has been eroded away from the valley which is highly stratified, consolidated and requires a much greater force to entrain. Figure 25 illustrates a proposed reconstruction of likely

erosive episodes and demonstrates pre-erosion thickness of the total sediment column for lithification and diagenetic processes. It would be irrational to assume that some type of dissolution was not occurring synchronously to enable this large-scale erosional feature. Corrosive bottom water spilling over from the southward Peru Basin must be the catalyst. The large-scale erosive episodes appear to be intermittent in character, with periods of deposition occurring in-between.

6.2.2 Medium-scale Erosion: E-W Trending Channels

Figure 24 shows detail from line 4, taken down the axis of Sand Dune Valley, and shows not only the smooth topography which underlies Sand Dune Valley, but also a major erosional feature perpendicular to it. There is a major fault scarp marking the northern terminus of Sand Dune Valley, the subsequent faulting that took place created a step-like, blocky appearance trending downward to the NW. Subsequently, these fault scarps created channels for any type of E-W trending currents in the area and have been dissecting the biogenic sedimentary packages, causing further re-deposition of material. This is also responsible for the excavation of the Western Valley as described above.

6.2.3 Small-scale Erosion: Sediment Surface Truncation

Sediment surface truncation occurring to the right of volcanic edifices (Figure 24) are most likely the result of channeling and near-bottom intensification of currents. Sediment surface truncation that is not a function of a channeling current around an edifice, demonstrates no trends and shows the haphazard currents recorded in previous surveys which have no preferential direction and show no signs of periodicity.

6.2.4 Nature of Hiatuses

Hiatuses have been recorded throughout the basin and are constrained in the DSDP core 157, and ODP cores 1238 and 1239. DSDP core Site 157 records a hiatus around the late Miocene to early Pliocene boundary where accumulation rates were dramatically reduced to 1m/my (van Andel, 1973). ODP Leg 202 Sites 1238 and 1239 record a hiatus occurring during the mid-Miocene where accumulation rates plummeted from 30m/my to 1m/my (Mix, et al., 2003). The occurrences of the hiatuses in deposition suggest that subbottom current activity was likely high pre 8 Ma.

6.3 Constraining Erosive Events

Possible causes of erosive events have been considered and are proposed to be a function of one or more of the following: major and localized occurrences during the Miocene to present influencing tectonic activity and topography, and fluctuations of the carbonate compensation depth. Each one will be investigated respectively.

6.3.1 Major Occurrences during the Miocene to Present

In the eastern equatorial Pacific, periods of higher sediment accumulation rates occur during the late Miocene and early Pliocene with moderate accumulation rates found during the late Pliocene (Shackleton, 1995). This decrease in the calcium carbonate flux has been attributed to oceanographic changes linked to tectonic activity in the Panamanian seaway (Pisias & Prell, 1985). During the Miocene a “carbonate crash” occurred throughout the equatorial Pacific from around 11.2-8.6 Ma (Lyle, et al., 1995). This could coincide with the missing sediment at Site 157 where up to ~6-7 million years of sediment could be missing. At Sites 1238 and 1239, there was little or no deposition before 7 Ma.

It has been hypothesized that early stages of the closing of the Isthmus of Panama could be the catalyst for the crash (Tiedmann, et al., 2007), as well as shoaling of the CCD and changes in deepwater circulation. Tectonic changes initiated by the ridge jump and closing of the Panamanian seaway also heavily influence sediment supply and deposition and are likely a more substantial candidate due to the depths of deposition.

6.3.2 Fluctuations in the Carbonate Compensation Depth (CCD)

Variations in sedimentation rates can largely be due to the degree of carbonate dissolution or the carbonate compensation depth (CCD) versus rate of sediment supply (Scholle, 1983). Deep ocean nannofossil assemblage change, abundance and preservation are also controlled by the CCD (Flores, et al., 1995). Lyle et al., (1995) as well as many others have postulated that the carbonate crash discussed above could be a result of a shoaling of the CCD and changes in deepwater circulation. This could have a drastic effect on sediment accumulations. A global sea level drop during the mid to late Miocene is believed to have deepened the CCD and enhanced carbonate preservation (Jiang, et al., 2007). This works well with our current model where ample sediment was accumulating with enough overburden to permit lithification to chalks and cherts at depth. A shoaling of the CCD after this could explain some sort of dissolution component needed to entrain the highly lithified basal sections. According to the tectonic reconstruction by Harpp et al. (2004), modified from Meschede & Barckhausen (2000), the Carnegie Ridge has stayed at a consistent latitude and it is not believed to have undergone sub-aerial exposure so a shoaling of the CCD could explain our mechanism needed for erosion on a large-scale.

6.3.3 Topographical Constraint on Deposition

Figure 26 is a geological model on the topographical influence on sediment within the survey area with proximity to the Carnegie Ridge and the fault scarp. The sedimentary columns have been removed to demonstrate channelization from volcanic edifices throughout the region. It is postulated that erosive spill over events initiate from Peru Basin to the south and transport sediments laterally. Sediments still entrained in the water column come into contact with the volcanic pinnacles and are redirected back to the sides. Other sediments are finally deposited into the sediment pool created by the fault scarp, but not until more geologically recently since it is believed that initiation of the scarp did not proceed until the ridge jump occurred ~5Ma with subsequent normal faulting as a result. This evidence is also provided by the isopach from PL-2 to P-1 showing a focus in the "sediment pool" region only during this time and not later.

7. CONCLUSION

The Carnegie Ridge and Panama Basin prove to be a dynamic marine environment dominated by a bathymetrically high ridge with various volcanic pinnacles, basinal settings and massive erosion, probable dissolution and redeposition of sediment. The MV1014 cruise acquired geochemical, geological and geophysical data using multichannel 2-D seismic and 3.5 kHz subbottom profiler, swathmap bathymetry, coring, and water casts to investigate biogenic sedimentary deposition in the Panama Basin and erosion from Carnegie Ridge. Through 2-D seismic assessment and the development of age models, it has been determined that two massively erosive episodes carved out the present landscape during the early Pliocene (~5 Ma) and the late Pliocene to early Pleistocene (~3-2 Ma).

REFERENCES

Beiersdorf, H. & Natland, J., 2007. Sedimentary and diagenetic processes in the central Panama Basin since the Late Miocene: The lithology and composition of sediments from Deep Sea Drilling Project Site 504 and 505.. *Proceedings of the Deep Sea Drilling Program, Initial Reports*, Volume 69.

Bloomer, S., Mayer, L. & Moore, T., 1995. Seismic stratigraphy of the eastern Equatorial Pacific Ocean: paleoceanographic implications. *Proceedings of the Ocean Drilling Program, Scientific Results*, Volume 138.

de la Torre, G., 2005. The crustal structure of Carnegie Ridge inferred from gravity and seismic data. *Master's Thesis.* Texas A&M University. College Station, Texas:

Drexler, J., Rose, W., Sparks, R. & Ledbetter, M., 1980. The Los Chocoyos Ash, Guatemala: A Major Stratigraphic Marker in Middle America and in Three Ocean Basins. *Quaternary Research,* Volume 13, pp. 327-345.

Flores, J., Sierro, F. & Raffi, I., 1995. Evolution of the Calcareous Nannofossil Assemblage as a Response to the Paleoceanographic Changes in the Eastern Equatorial Pacific Ocean from 4 to 2 Ma (Leg 138, Sites 849 and 852). *Proceedings of the Ocean Drilling Program, Scientific Results*, Volume 138.

Francois, R., Frank, M., Rutgers van der Loeff, M. & Bacon, M., 2004. 230Th normalization: An essential tool for interpreting sedimentary fluxes during the late Quaternary. *Paleoceanography,* Issue 19.

Gartner, S., 1973. Nannofossil age determinations, DSDP Leg 16. *Deep Sea Drilling Program Reports and Publications, Leg 16 Laboratory Studies*, pp. 883-889.

Hamilton, E., 1976. Variations of density and porosity with depth in deep-sea sediments. *Journal of Sedimentary Petrology,* 46(1-2), pp. 280-300.

Harpp, K., Wanless, V., Otto, R. & Hoernle, K., 2004. The Cocos and Carnegie Aseismic Ridges: a Trace Element Record of Long-Term Plume-Spreading Center Interaction.. *Journal of Petrology,* 46(1), pp. 109-133.

Hey, R., 1977. Tectonic evolution of the cocos-Nazca Spreading Center. *Geological Society of America Bulletin*, Volume 88, pp. 1404-1420.

Janik, A., Liberty, L. & Lyle, M., 2004. Seismic expression of Pleistocene paleoceanographic changes in the California Borderland from digitally acquired 3.5 kHz subbottom profiles and Ocean Drilling Program Leg 167 drilling. *Journal of Geophyscial Research,* Volume 109.

Jiang, S., Wise, S. & Wang, Y., 2007. Cause of the Middle/Late Miocene Carbonate Crash: Dissolution or Low Productivity?. *Proceedings of the Ocean Drilling Program, Scientific Results,* Volume 206, pp. 1-24.

Liao, Y. & Lyle, M., 2014. Late Miocene to Pleistocene sedimentation and sediment transport on the Cocos Ridge, eastern tropical Pacific Ocean. *Marine Geology,* Volume 355, pp. 1-14.

Lin, T. & Ledbetter, M., 1984. Distribution of volcanic ash horizons in the eastern equatorial Pacific. *Marine Geology,* Volume 59, pp. 251-269.

Lonsdale, P., 1977. Inflow of bottom water to the Panama Basin. *Deep Sea Research,* Volume 84, pp. 1065-1101.

Lonsdale, P., 1980. Manganese-nodule bedforms and thermohaline density flows in a deep-sea valley on Carnegie Rdige, Panama Basin. *Journal of Sedimentary Petrology,* 50(4), pp. 1033-1048.

Lonsdale, P. & Klitgord, K., 1978. Structure and tectonic history of the eastern Panama Basin. *Geological Society of America,* Volume 89, pp. 981-999.

Lonsdale, P. & Malfait, B., 1974. Abyssal dunes of foraminiferal sand on the Carnegie Ridge. *Geological Society of America Bulletin,* Volume 85, pp. 1697-1712.

Lyle, M., Dadey, K. & Farrell, J., 1995. The late Miocene (11-8Ma) Eastern Pacific carbonate crash: evidence for reorganization of deep-water circulation by the closure of the Panama gateway. *Proceedings of the Ocean Drilling Program, Scientific Results,* Volume 138.

Lyle, M., Koizumi, I., Delaney, M. & Barron, J., 2000. The sedimentary record of the California Current system, middle Miocene to Holocene: a synthesis of Leg 167 results. *Proceedings of the Ocean Drilling Program, Scientific Results,* Volume 167, pp. 341-376.

Lyle, M. et al., 2005. Do geochemical estimates of sediment focusing pass the sediment test in the equatorial Pacific?. *Paleoceanography,* Volume 20, pp. 1-12.

Malfait, B., 1974. The Carnegie Ridge at 86°W: Structure, sedimentation and near-bottom observations. *PhD Dissertation,* Oregon State University. Corvallis, Oregon. pp. 1-131.

Mayer, L., Pisias, N. & Janecek, T., 1992. Site 846. *Proceedings of the Ocean Drilling Program, Initial Reports*, Volume 138.

Mayer, L., Shipley, T. & Winterer, E., 1986. Equatorial Pacific seismic reflectors as indicators of global oceanographic events. *Science,* Volume 233, pp. 761-764.

Meschede, M. & Barckhausen, U., 2000. Plate Tectonic Evolution of the Cocos-Nazca Spreading Center. *Proceedings of the Ocean Drilling Program, Scientific Results* , Volume 170.

Mienert, J., 1984. The importance of carbonate content in the acoustic stratigraphy of Panama Basin. *Marine Geology,* Volume 54, pp. 237-247.

Mix, A., Blum, P. & Tiedemann, R., 2003. Site 1240. *Proceedings of the Ocean Drilling Program, Initial Reports*, Volume 202, pp. 1-82.

Mix, A., Tiedemann, R. & Blum, P., 2003. Site 1238. *Proceedings of the Ocean Drilling Program, Initial Reports.*, Volume 202, pp. 1-101.

Mix, A., Tiedemann, R. & Blum, P., 2003. Site 1239. *Proceedings of the Ocean Drilling Program, Initial Reports.*, Volume 202, pp. 1-93.

Moore, T., Heath, G. & Kowsmann, R., 1973. Biogenic sediments of the Panama Basin. *Journal of Geology,* 81(4).

Pisias, N. & Prell, W., 1985. Changes in calcium carbonate accumulation in the equatorial Pacific during the Late Cenozoic; evidence from HPC Site 572. *Geophysics,* Volume 32, pp. 443-454.

Plank, J., Zanevald, R. & Pak, H., 1973. Distribution of Suspended Matter in the Panama Basin. *Journal of Geophysical Research,* 78(30).

Sallares, V. & Charvis, P., 2003. Crustal thickness constraints on the geodynamic evolution of the Galapagos Volcanic Province. *Earth and Planetary Science Letters,* Volume 214, pp. 545-559.

Scholle, P., 1983. Pelagic Environments, Carbonate Depositional Environments.. *AAPG Memoir,* Volume 33, pp. 619-692.

Shackleton, N., 1995. A new late Neogene time scale. Application to the Leg 138 Sites. *Proceedings of the Ocean Drilling Program, Scientific Results,* Volume 138.

Singh, A., Marcantonio, F. & Lyle, M., 2011. Sediment focusing in the Panama Basin, eastern Equatorial Pacific. *Earth and Planetary Science Letters,* Volume 309, pp. 33-44.

Tiedmann, R., Mix, A., Richter, C. & Ruddiman, W., 2007. Leg 202. *Proceedings of the Ocean Drilling Project, Scientific Results*, pp. 1-56.

van Andel, T., 1973. *Tectonics and sedimentation in the Panama Basin: geologic results of Leg 16.*, Washington: US Government Printing Office.

van Andel, T. & Heath, G., 1973. DSDP 16, Site 157. *Initial Reports of the DSDP*, Volume 16, pp. 53-150.

van Andel, T. et al., 1971. Tectonics of the Panama Basin, eastern Equatorial Pacific. *Geological Society of America Bulletin*, Issue 82, pp. 1489-1508.

van Andel, T. & Malfait, B., 1980. A modern oceanic hardground on the Carnegie Ridge in the eastern Equatorial Pacific. *Sedimentology*, Volume 27, pp. 467-496.

Werner, R., Hoernle, K., Barckchausen, U. & Hauff, F., 2003. Geodynamic evolution of the Galapagos system (Central East Pacific) over the past 20 m.y.. Constraints from morphology, geochemistry, and magnetic anomlaies.. *Geochem. Geophys. Geosyst.*, 4(12), p. 1108.

Worzel, J., 1959. Extensive deep-sea sub-bottom reflections identified as white ash. *National Academy of Science Proceedings*, Volume 45, pp. 349-355.

APPENDIX A

FIGURES

This appendix contains figures to be used in conjunction with the text.

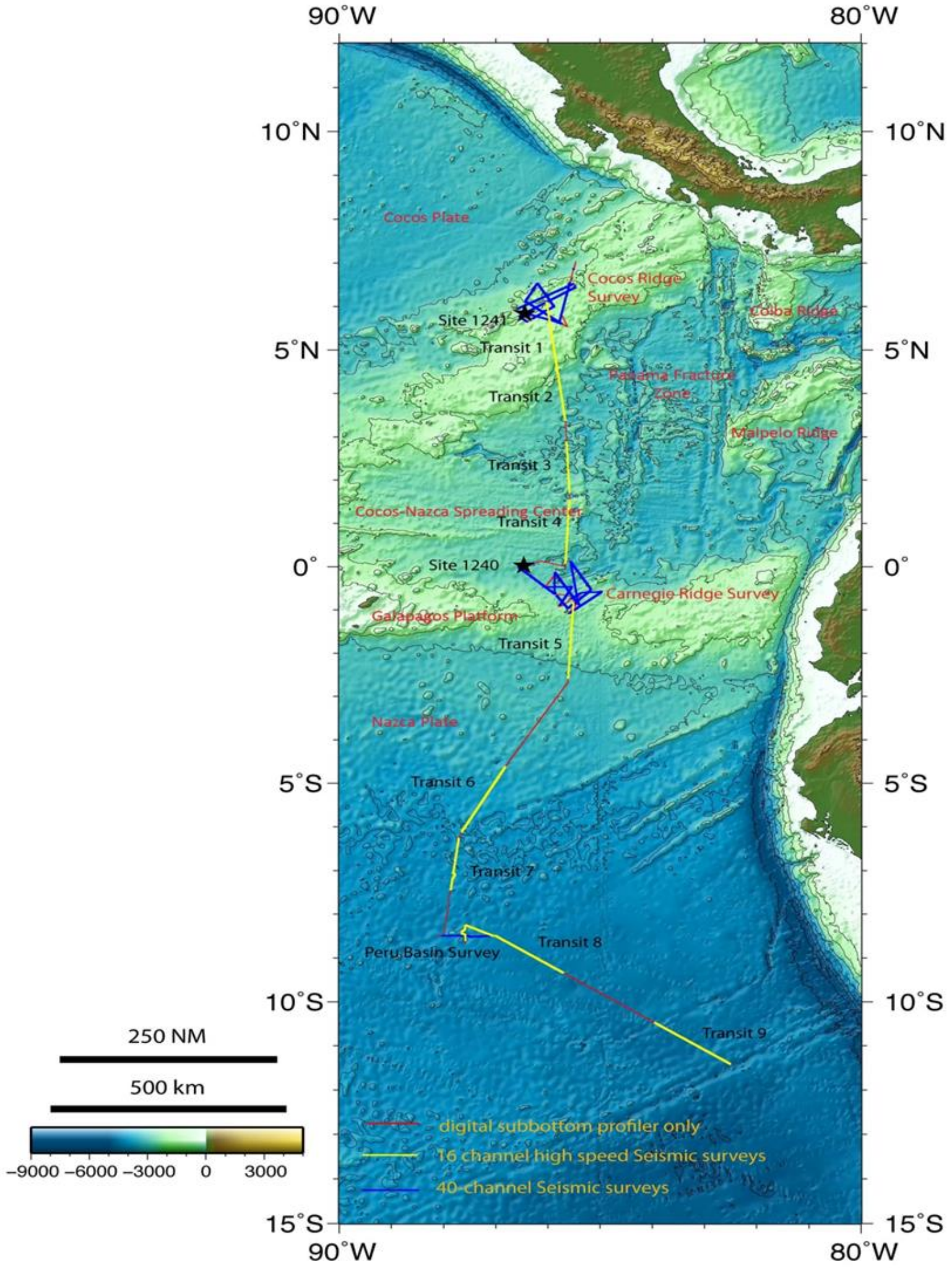

Figure 1. MV1014 Panama Basin Cruise
Map of MV1014 survey areas extending along the coasts of Central and South America. Primary focus areas are the Cocos Ridge, Carnegie Ridge and Peru Basin.

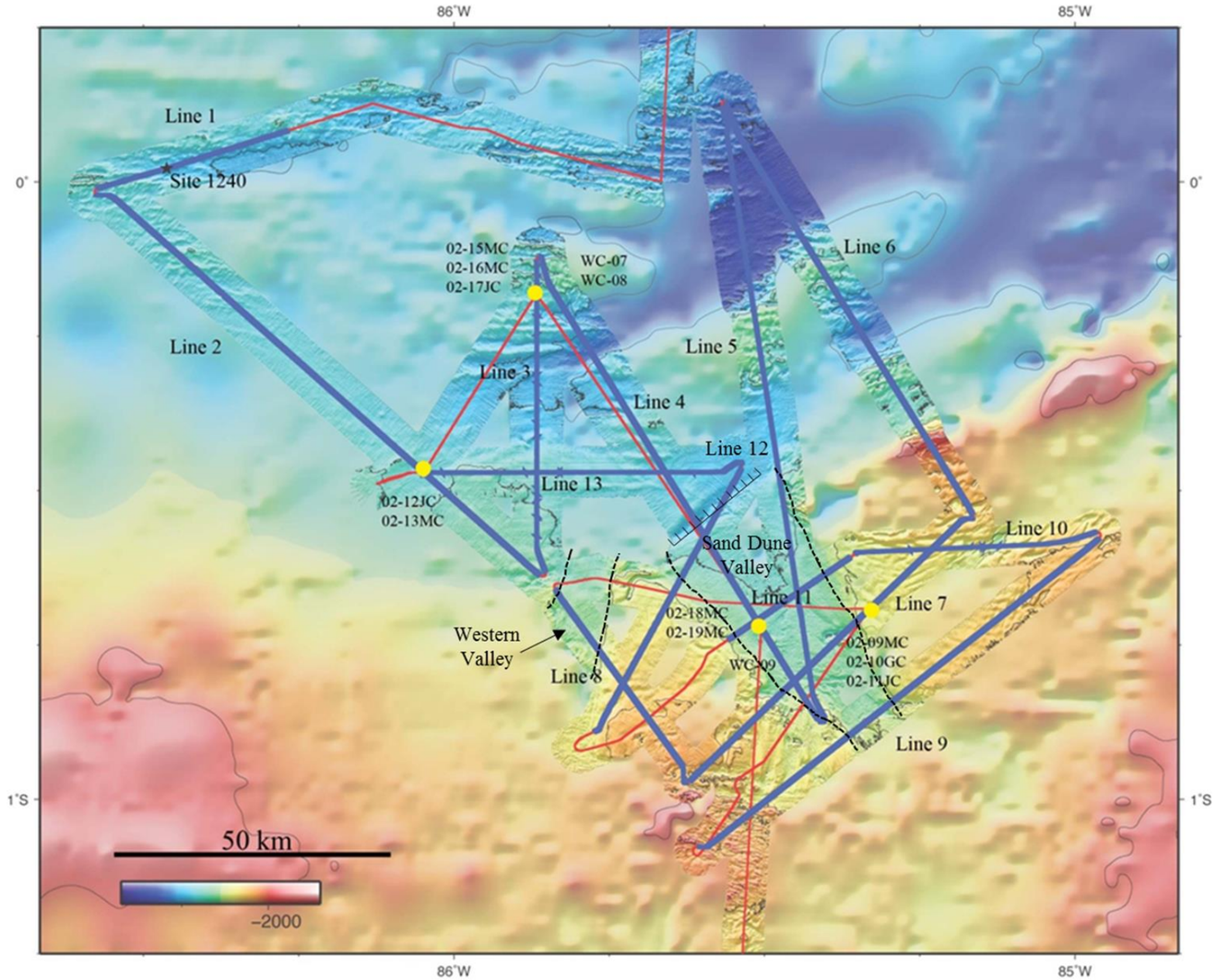

Figure 2. Carnegie Ridge Survey Area
Map of Carnegie Ridge survey area consisting of 13 tracklines, jumbo core sites 11,12 and 17, gravity core site 10, multi-core sites 9, 13, 15, 16, 18 and 19, and water cast sites 7, 8 and 9. Trackline 1 records seismic through previous ODP Leg 202 core site 1240A. Blue lines show where seismic reflection data were collected along with subbottom profiler data. Red lines indicate where only subbottom profiler data were collected.

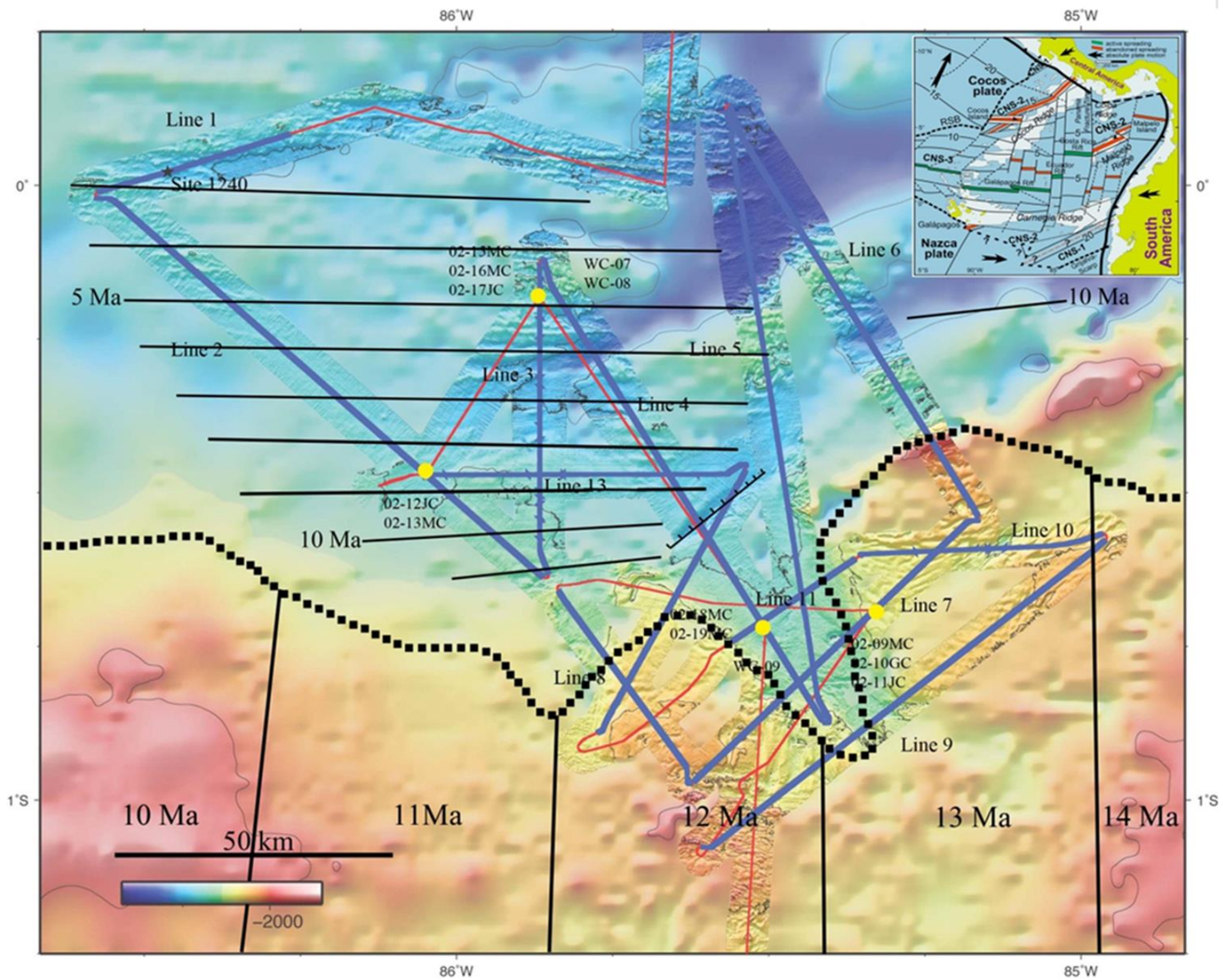

Figure 3. Crustal Ages
Carnegie Ridge crustal ages derived from inset of plate tectonic evolution of the Cocos-Nazca spreading center taken from Meschede, and Barckhausen, (2000) and ridge crustal ages from de la Torre's thesis (2005) "The Crustal Structure of Carnegie Ridge Inferred from Gravity and Seismic Data".

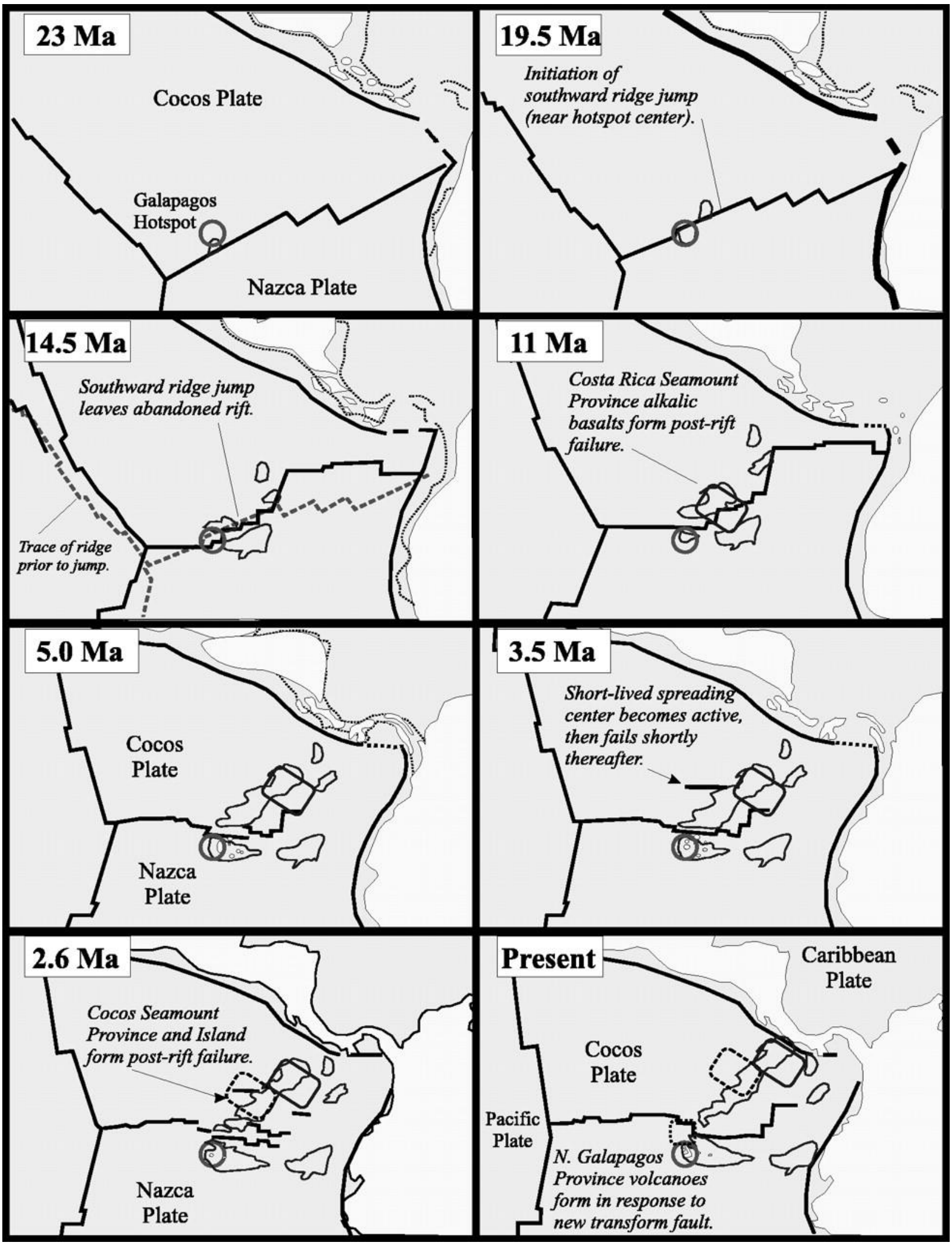

Figure 4. Evolution of the Carnegie Ridge
Tectonic evolution from Harpp (2005), modified from Meschede and Barkhausen (2000) and Werner (2003) evolution of the Carnegie, Malpelo and Cocos Ridges as a result of the Galapagos Hot Spot interacting with the Cocos-Nazca spreading center. The saddle region or mouth of the SDV has been dated at 12.9 Ma (Sallares and Charvis, 2003).

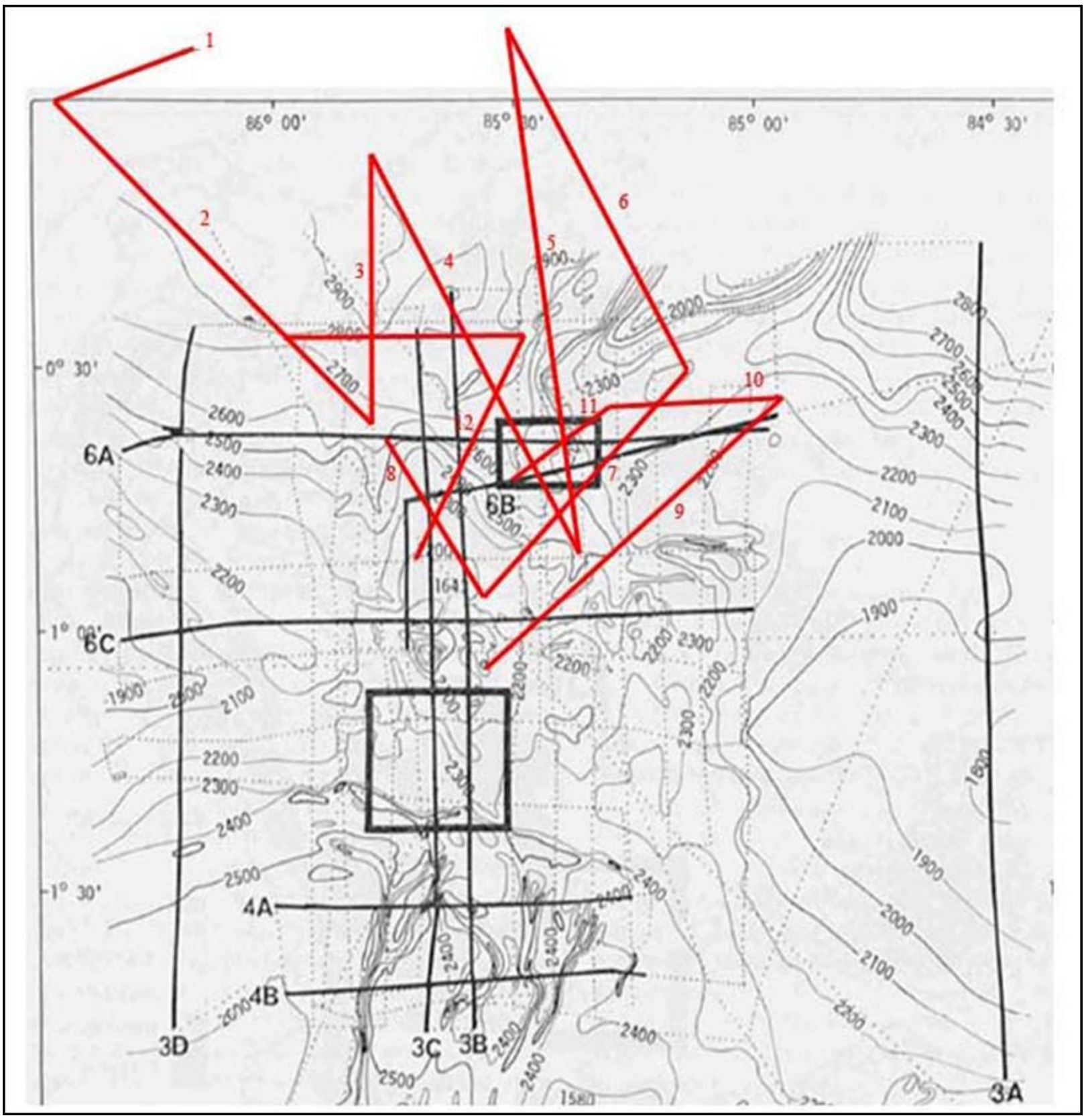

Figure 5. Trackline Overlay Map
MV1014 Survey in red overlain on previous study area by Malfait and van Andel in the 70's to show extent of study area and previous work.

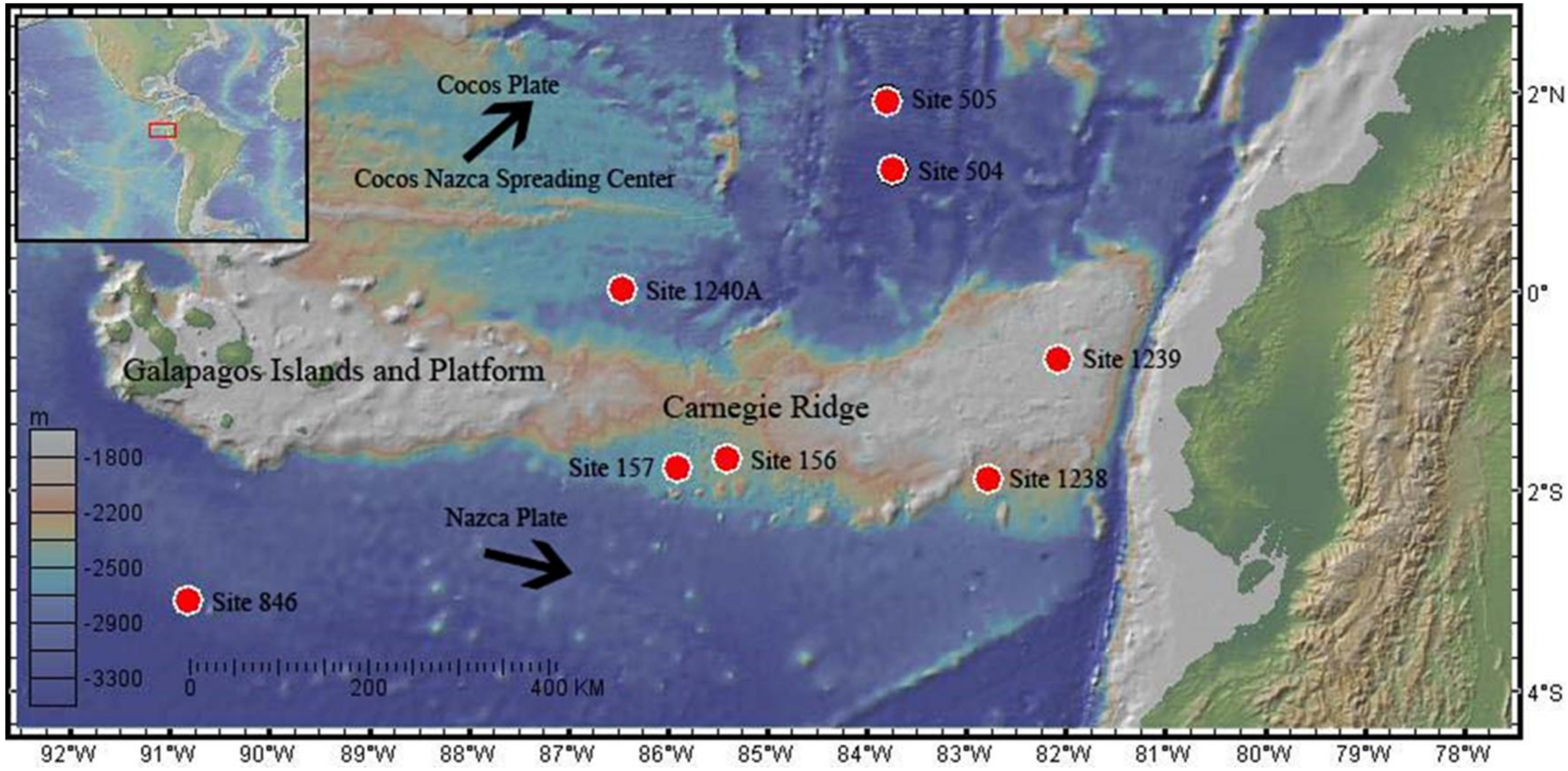

Figure 6. Core Site Map
DSDP Leg 16 Sites 156, 157; DSDP Legs 68 and 69 Sites 504, 505; ODP Leg 138 Site 846; ODP Leg 202 Sites 1238, 1239, 1240A. Core sites were used as a basis for geologic framework, age model and diagenetic model. Relative plate motions are shown with arrows.

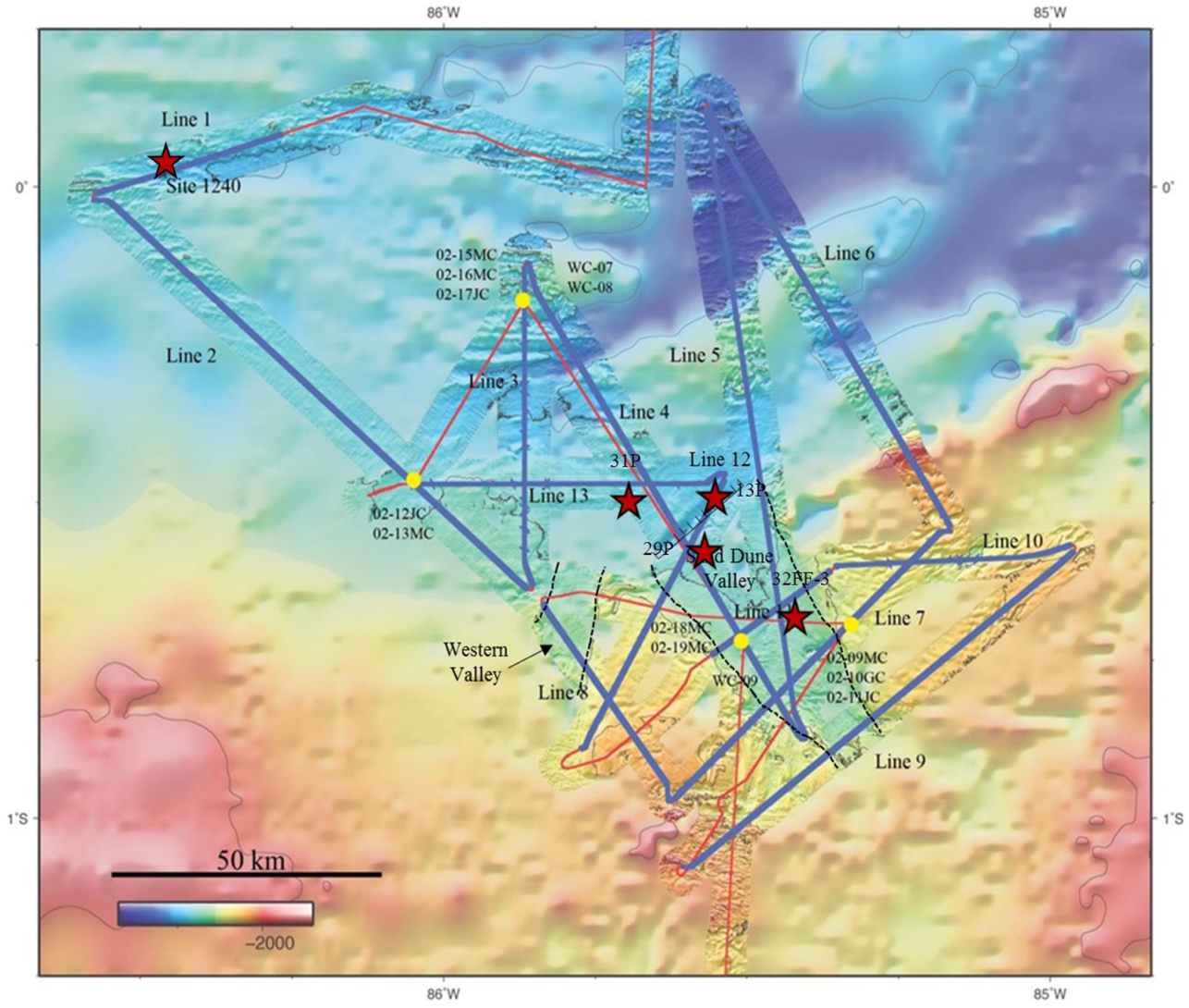

Figure 7. Core Sites in Survey Area
Carnegie Ridge study area with addition of ODP, DSDP, Yaloc-71 free fall cores and COCOTOW/SOUTHTOW piston cores used to create age models, record unconformities, and age the SDV floor. ODP Leg 138 Site 846 is not shown (previously shown in Figure 6), but was used to create the Pliocene-Miocene age model for older seismic reflectors of importance.

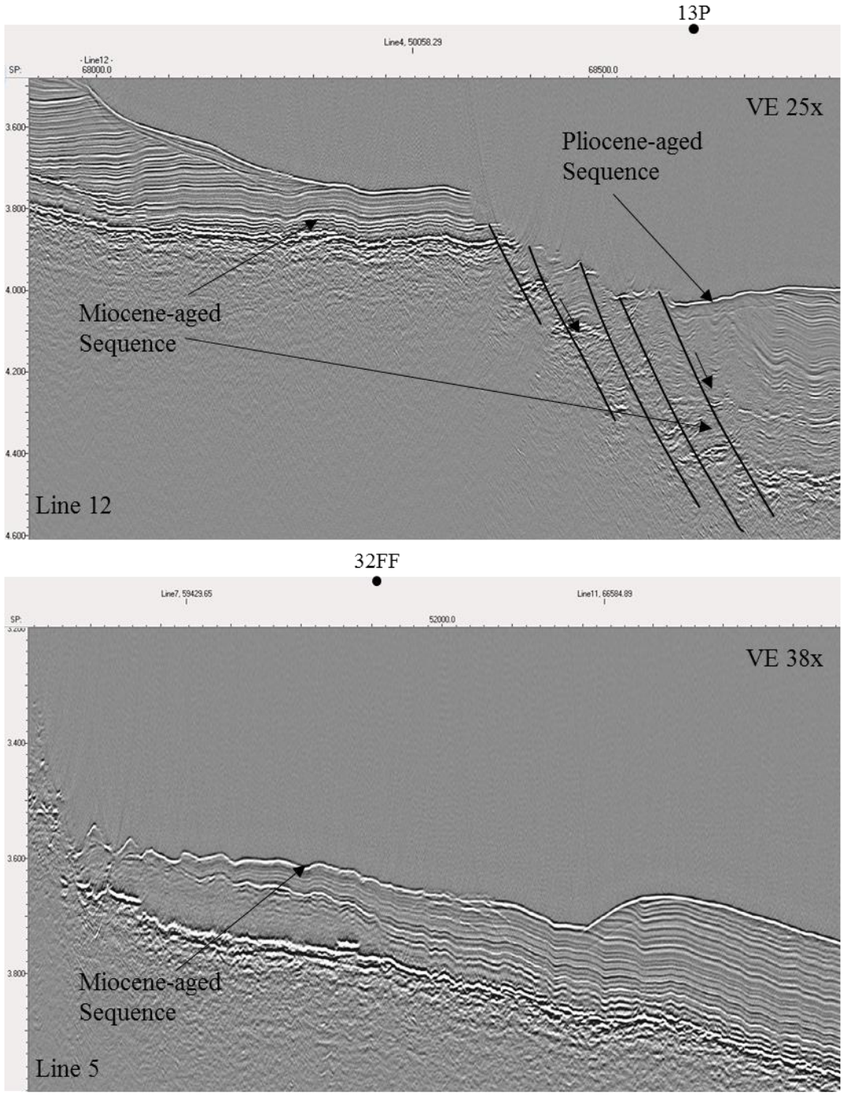

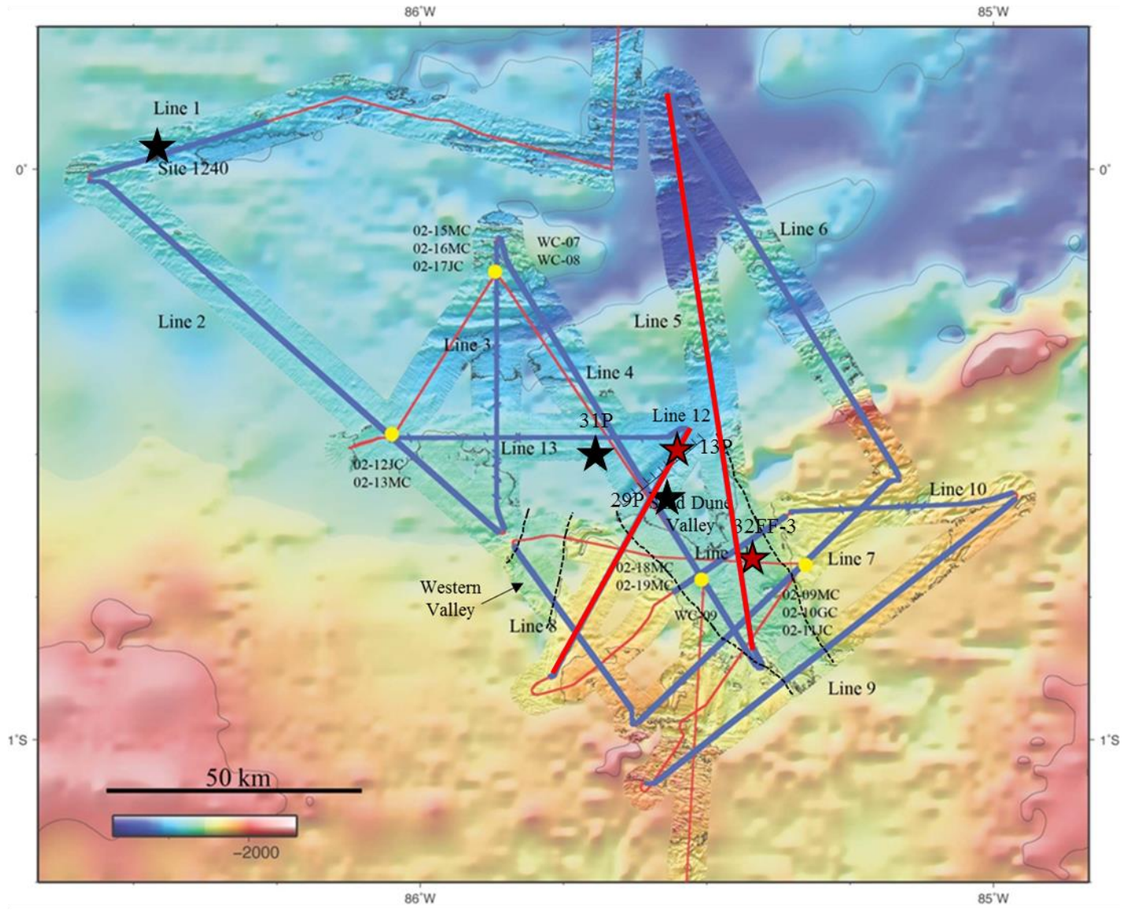

Figure 8. Unconformities Recovered in Survey Area/ Tracklines 12 and 5
Figure shows seismic reflection profiles demonstrating unconformities recovered during COCOTOW (Piston Core 13P, Line 12) and YALOC-71 (Free-Fall Cores Y71-3-32FF3/FF4, Line 5).

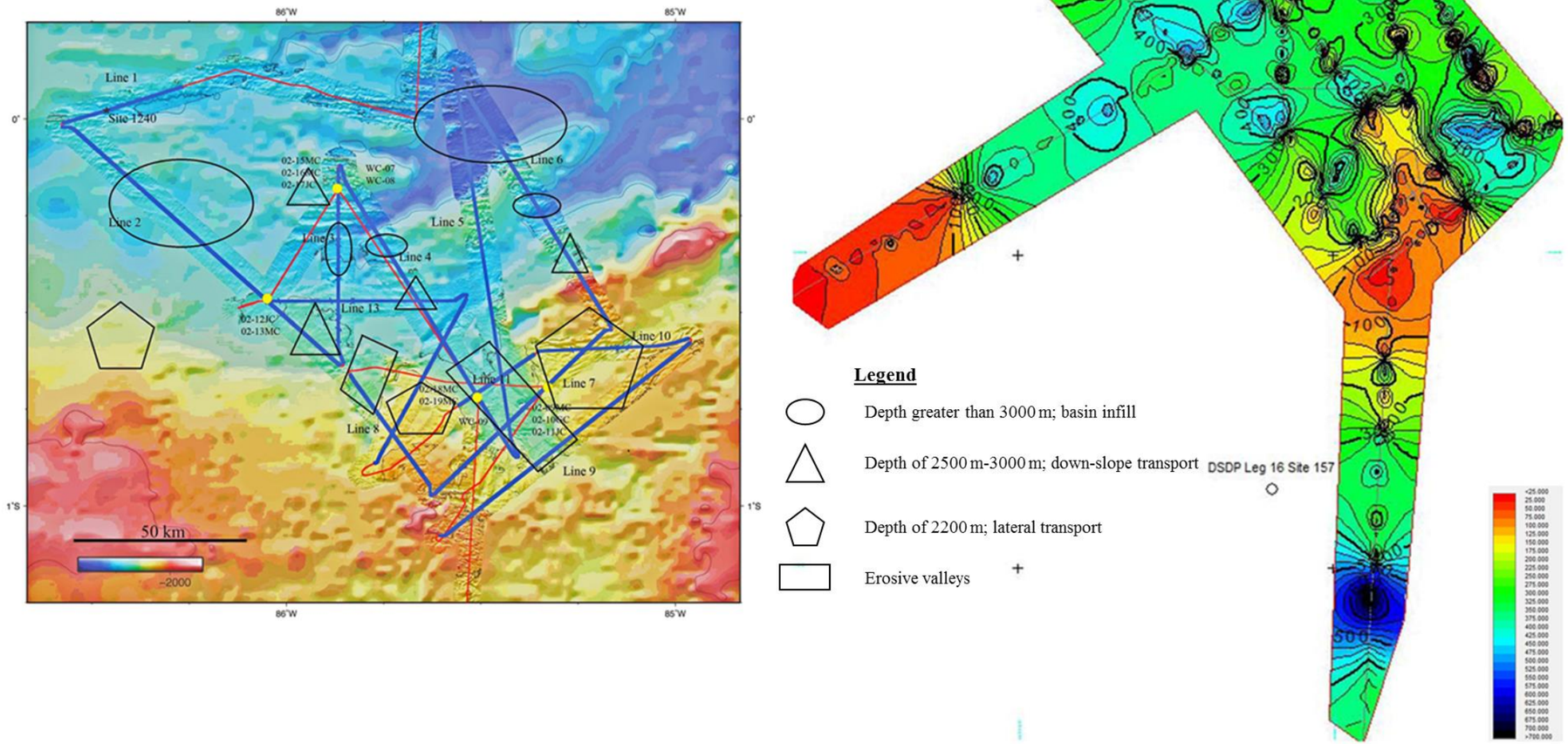

Figure 9. Depositional/Erosional Trends in Carnegie Ridge Study Area
Isopach created in Kingdom Suite of total sediment thickness (m) using a constant seismic velocity of 1600m/s juxtaposed with a bathymetric map to highlight features such as the ridge, valleys and abyssal hills. Sand Dune Valley and Western Valley are shown as rectangles. Slightly thicker sediments are found at the terminal points of both valleys; however, total sediment accumulations do not add up to an adequate amount for what is proposed to have been eroded.

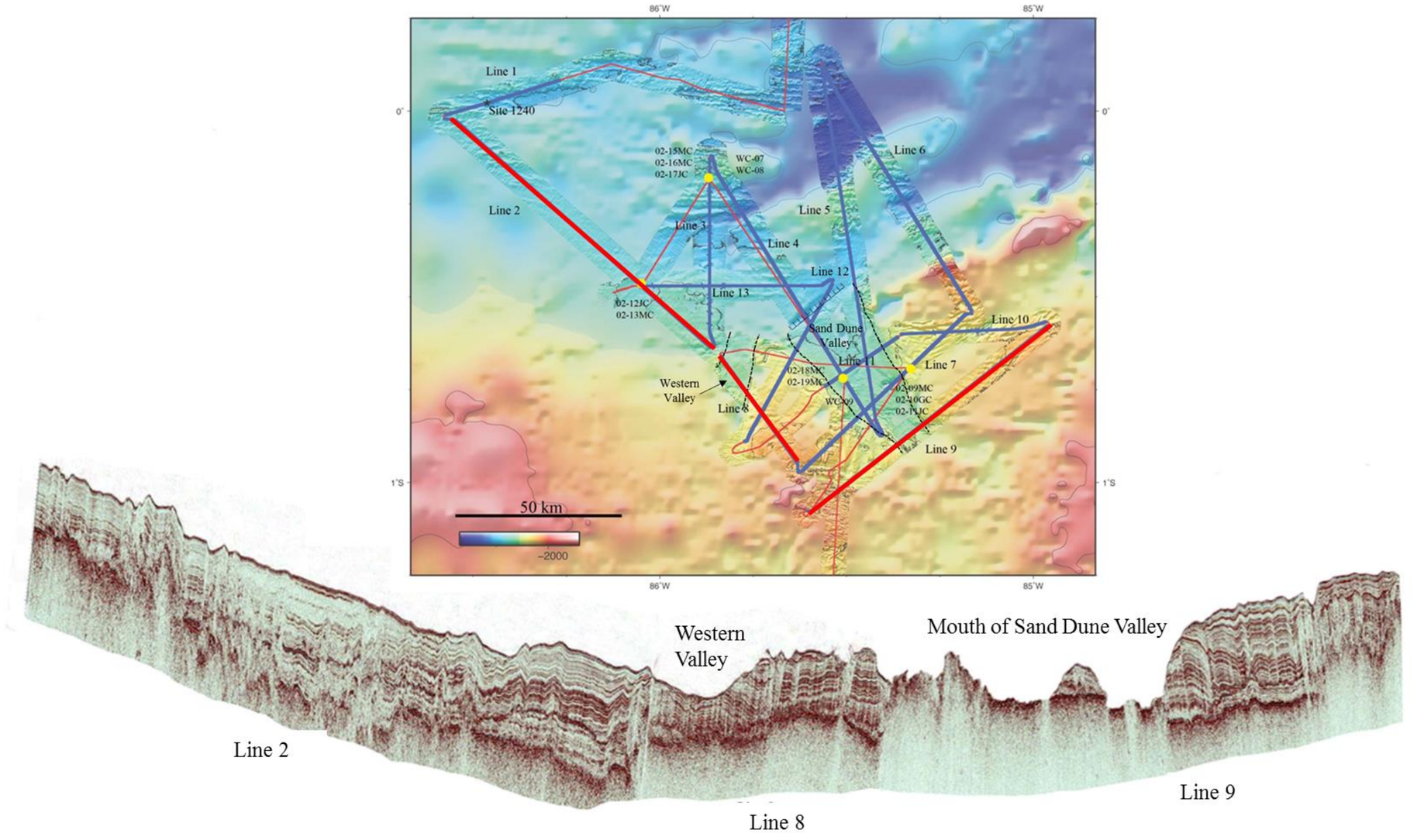

Figure 10. NW-SE Profile of Sediments; Lines 2, 8 and 9
Combined vertical seismic profiles illustrating the change in depositional and erosional regime in the MV1014 Panama Basin survey area from NW-SE.

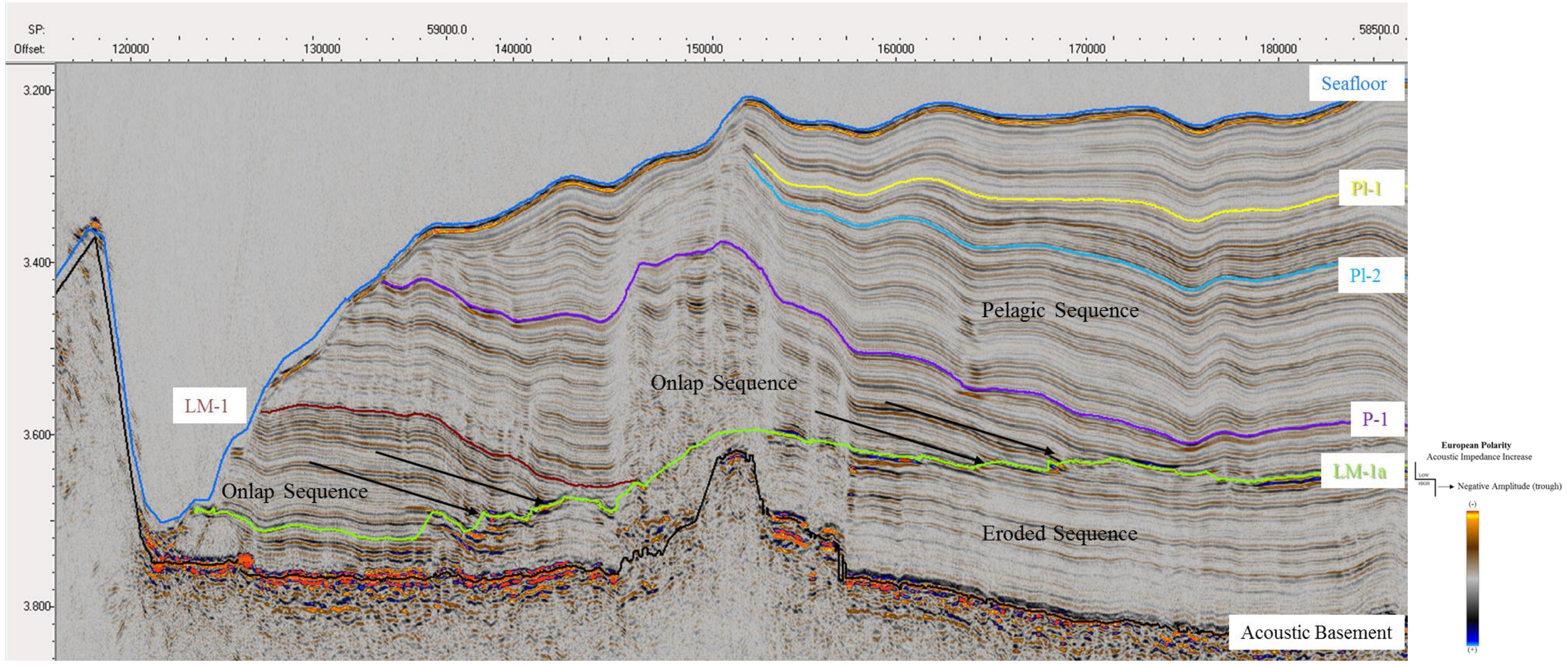

Figure 11. 3-D Seismic Horizons, Line 7
Seismic horizons picked in the Carnegie Ridge Survey Area: Seafloor (blue), PL-1 (yellow), PL-2 (light blue), P-1 (Violet), LM-1 (maroon), LM-1a (lime green) and Acoustic Basment (black). Naming conventions of horizons are indicative of proposed age of seismic sequence; i.e., PL=Pleistocene, P=Pliocene, LM=Late Miocene. Bedding in the seismic sequences illustrate normal pelagic drape in the Late Miocene, followed by a period of erosion (LM-1a), an influx of sediment from the Peru Basin to the south with onlap occurring until sometime in the Pliocene (P-1), and then a return to pelagic drape during the Pleistocene.

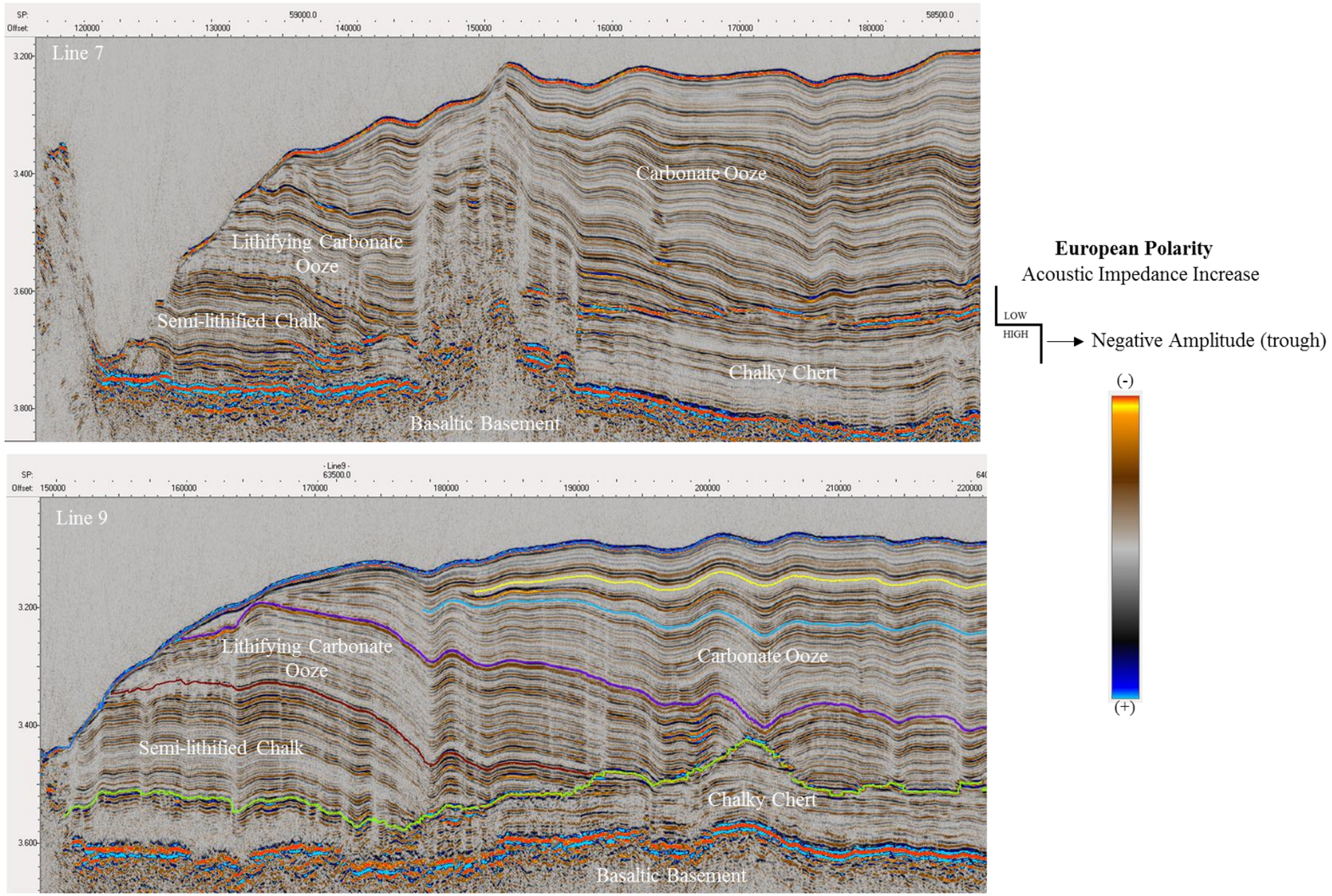

Figure 12. Proposed Diagenetic Lithological Sequences
Seismic profiles of lines 7 and 9 demonstrating seismic characteristics indicative of calcareous ooze to chalk to limestone transformation common to the CR study area. Each horizon varies in depth throughout the study area as formation is dependent upon overburden, time and geothermal regime. Deep tow and various cores have penetrated basement within the Panama Basin and show that these horizons possibly could be more pronounced as a result of diagenesis.

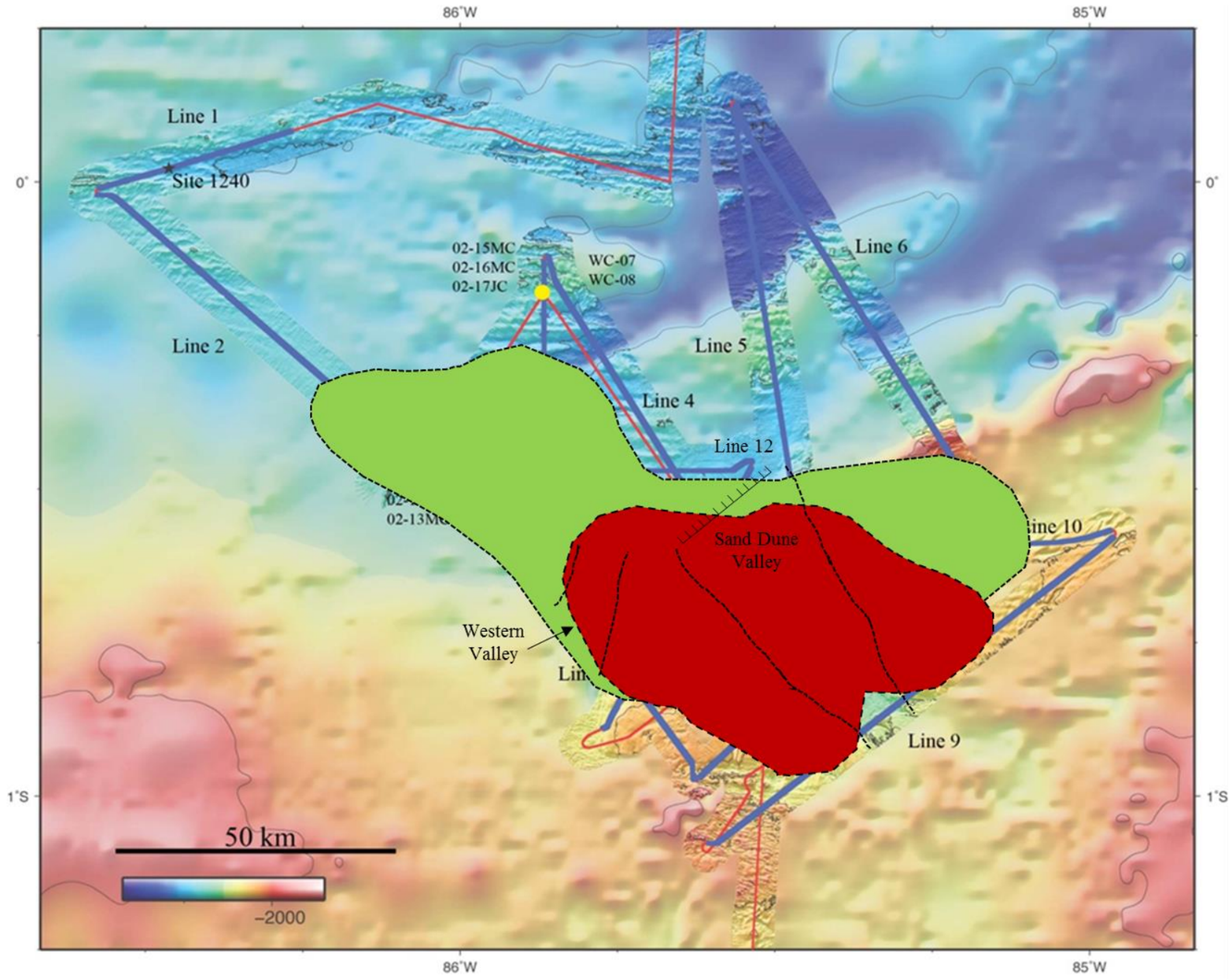

Figure 13. Seismic Sequences with Physical and Chemical Traits of Diagenesis
Bathymetric map of Carnegie Ridge with overlay of two polygons demonstrating the depositional extent of seismic sequences indicative of physical and chemical diagenesis. Free-fall cores and two deep-tow surveys have revealed the presence of chalk and cherty chalk along exposed outcrops around the fault scarp and along the valley floors of the Sand Dune Valley.

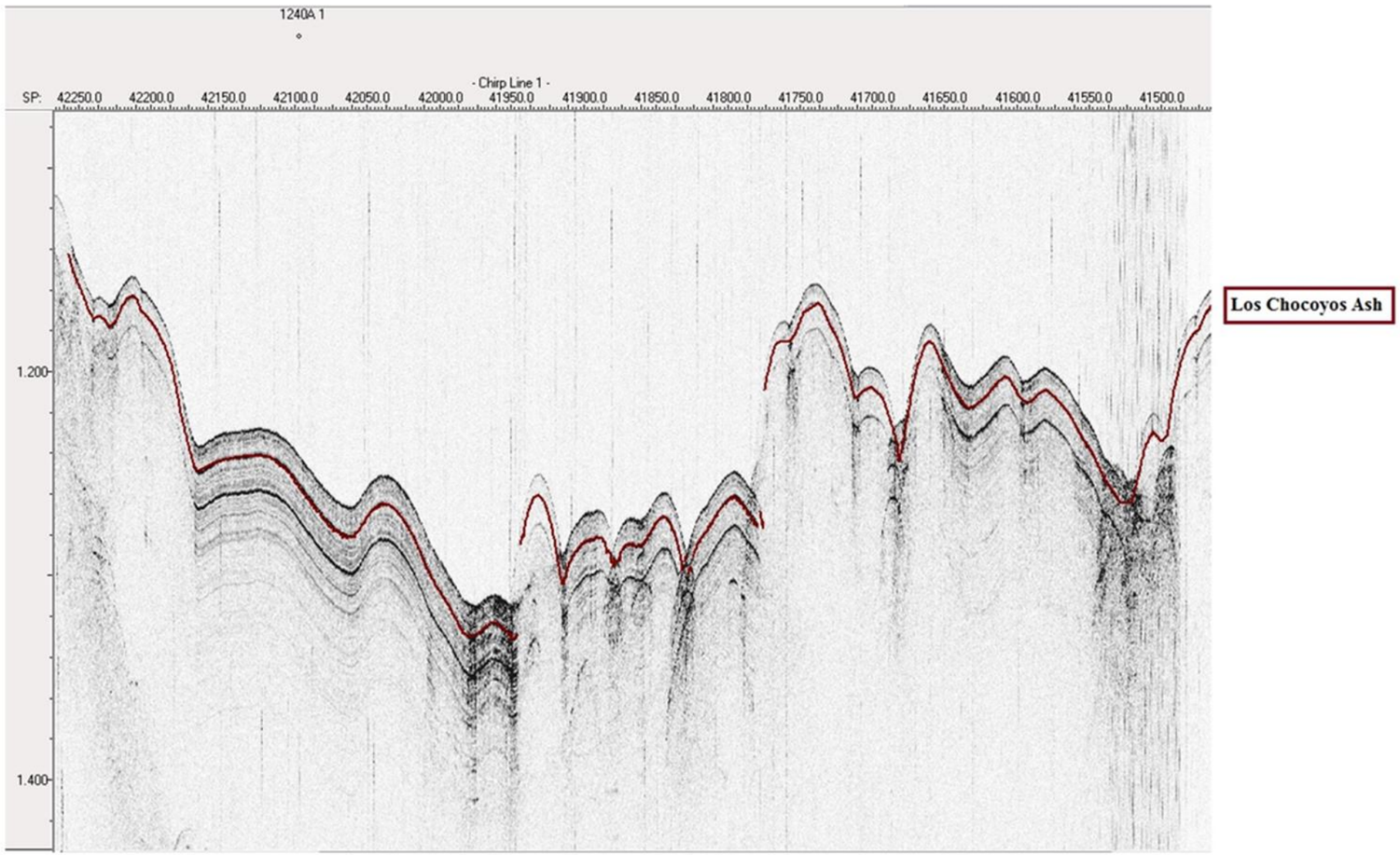

Figure 14. Los Chocoyos Ash Layer.
3.5 kHz profile showing 84,000 Ka Horizon Q-84 thought to be Los Chocoyos ash layer "D" present in the equatorial Pacific. The identification of the ash layer was used to postulate Quaternary sediment transport mechanisms.

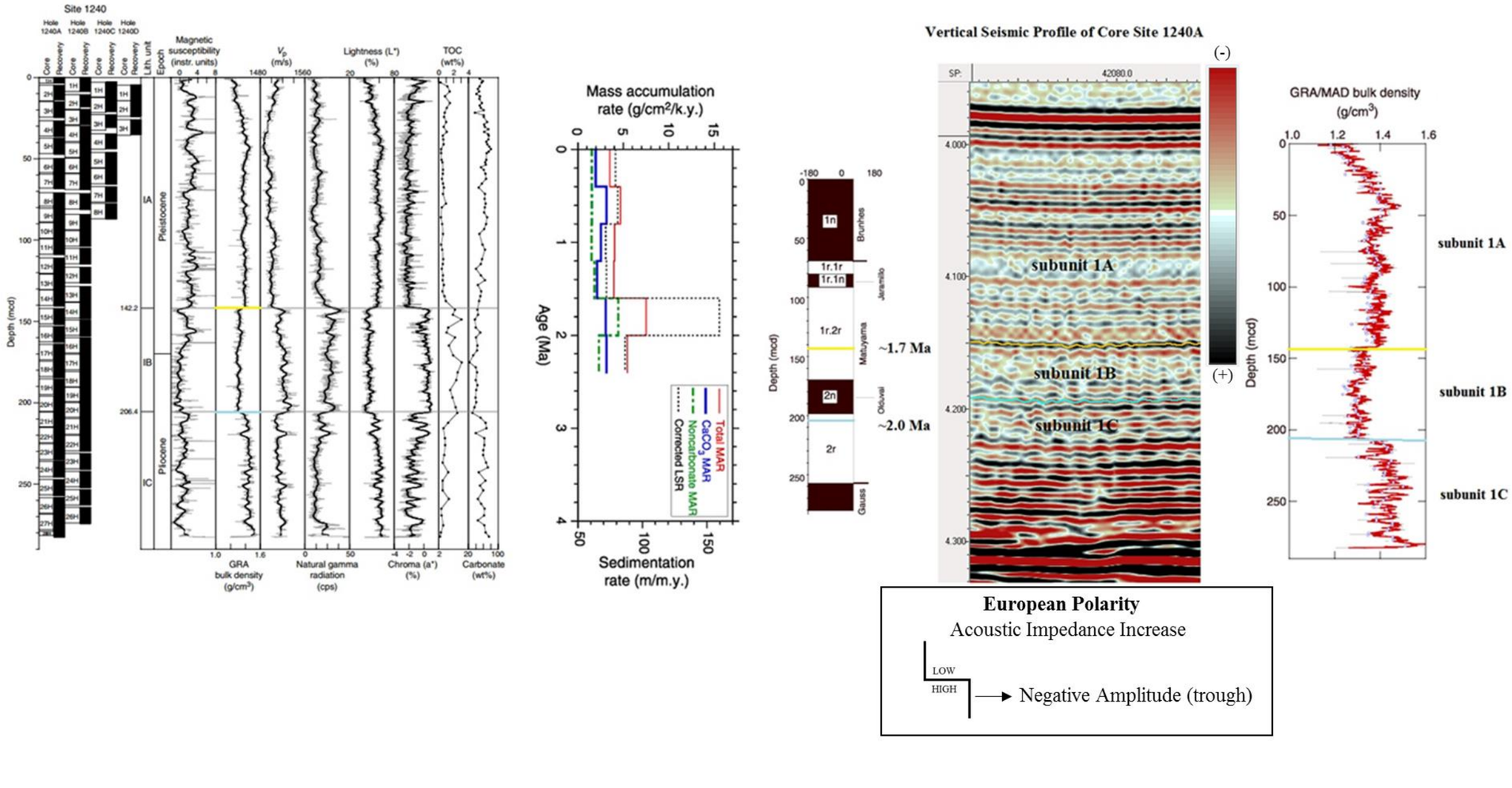

Figure 15. Pleistocene Age Model
Age model rendered from ODP Core Site 1240A and bulk density data, to date 1.7 Ma Horizon PL-1 and 2.0 Ma PL-2 to represent the Pleistocene depositional regime.

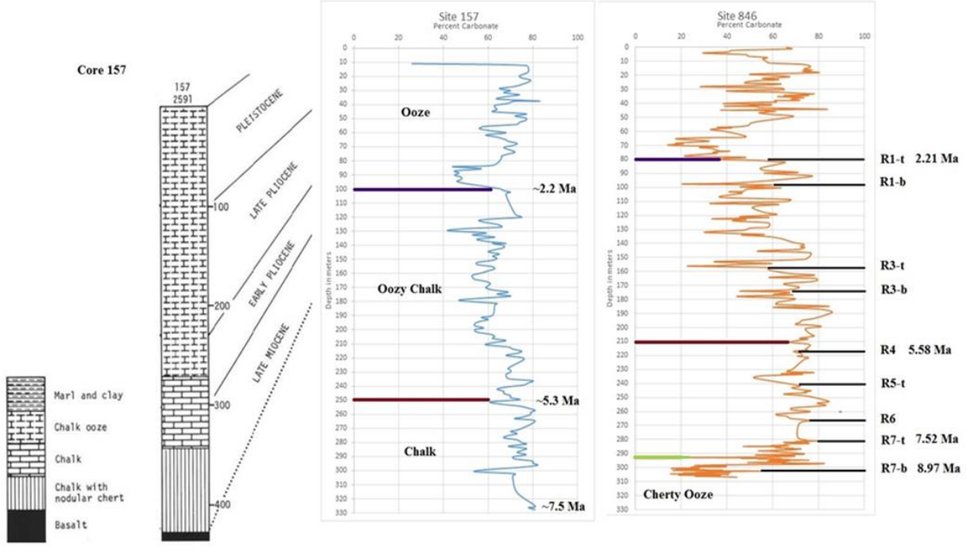

DSDP Leg 16 Site 157

ODP Leg 138 Site 846

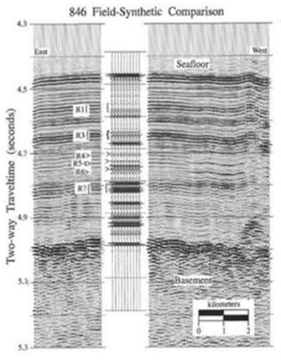

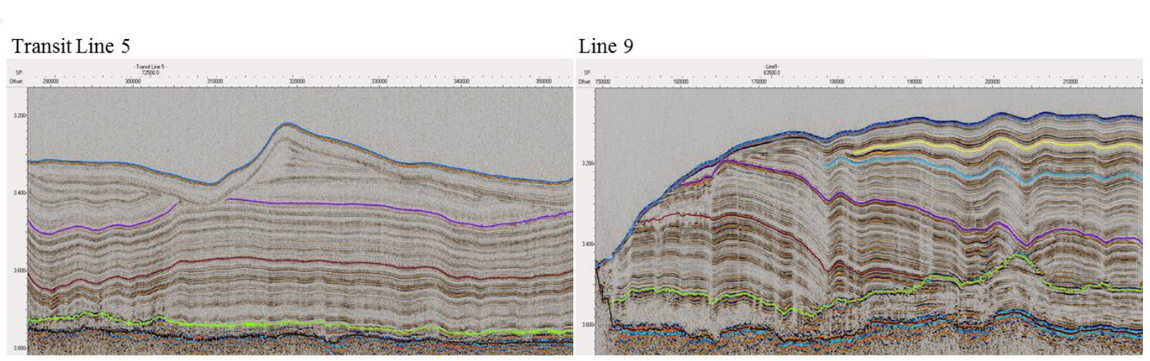

Figure 16. Pleistocene-Miocene Age Model
The use of DSDP Site 157 and ODP Site 846 allowed correlation of our seismic sections to previously constructed seismic stratigraphy (Bloomer et al., 1995) caused by variability in carbonate content. Poor basal faunal preservation in Site 157 results in bottom section omission after 330 mbsf, leaving Site 846 for approximate dating of LM-1a horizon that correlates to the R-7 sequence in 846. We can trace these horizons P-1 (purple), LM-1 (maroon), LM-1a(orange) in the Carnegie Ridge survey to constrain the age of erosional downcutting and sediment redistribution. Seismic sequences show characteristics of induration and chemical reprecipitation basaly in section creating heightened reflectors. The diagenetic transformation requires a minimum amount of overburden and time which was used as a proxy when considering deposition that must be in place before erosion ensued.

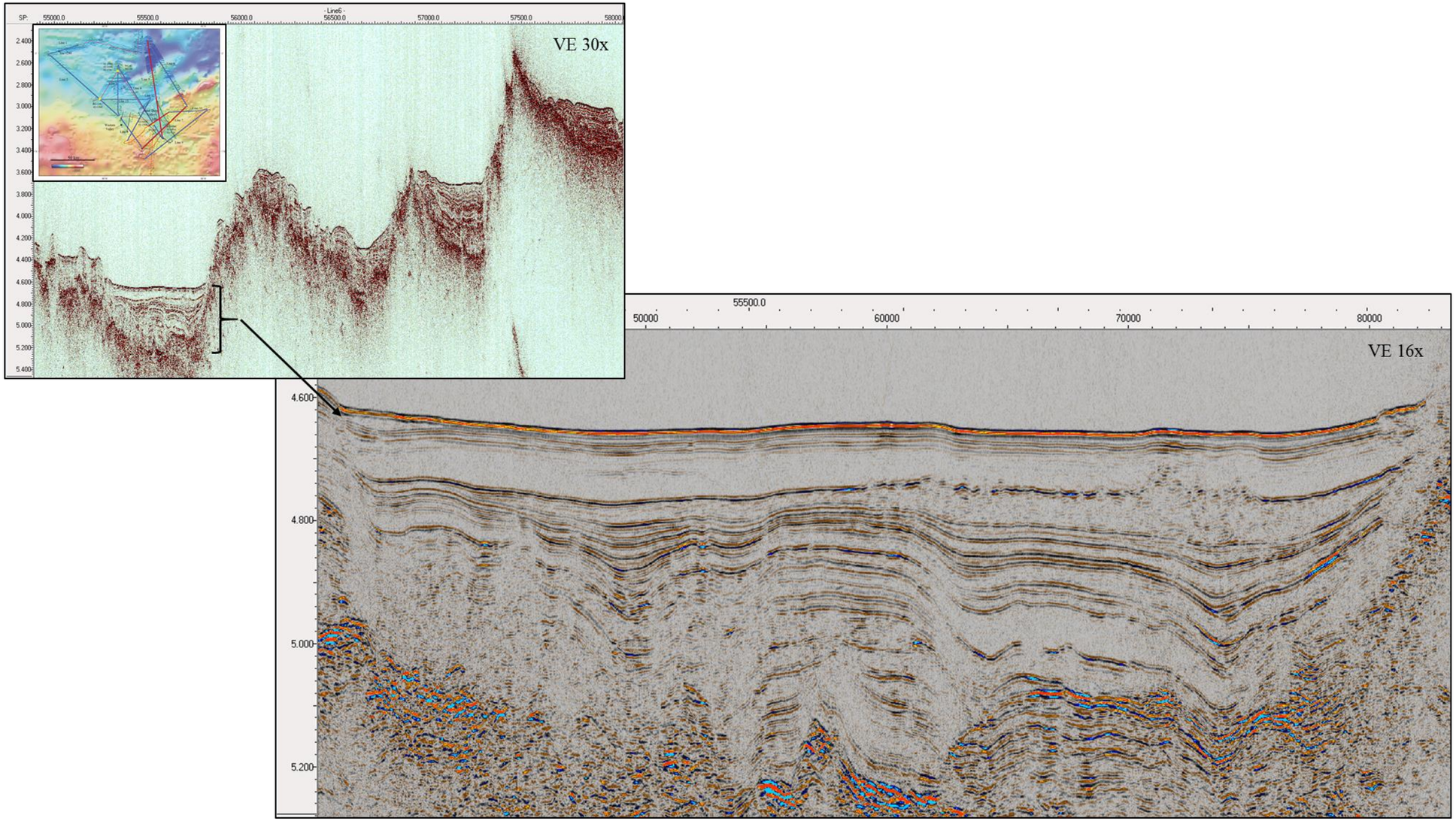

Figure 17. Topographically Created Minibasins, Line 6
Minibasins common to the Carnegie Ridge area from the presence of multiple volcanic pinnacles allowing trapping of sediment. A closer look at one of the infilled basins illustrates the topographical influence on slump deposits characterized seismically by a chaotic to amorphous reflection. These slump deposits appear to be repetitive and followed by periods of pelagic drape.

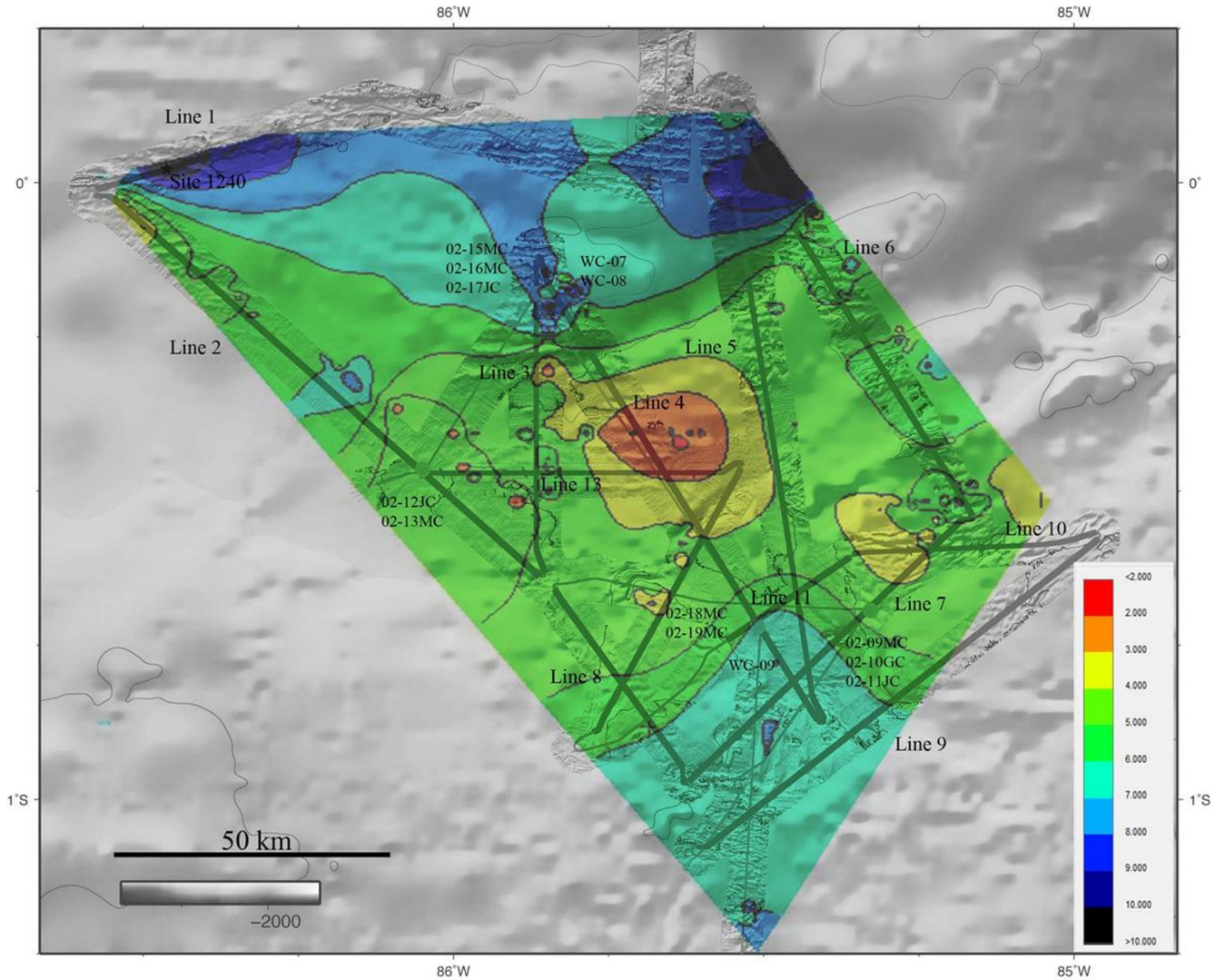

Figure 18. Quaternary Depositional Trends
Isopach map of depositional regime from 84,000 Ka Horizon, Q 84, to current day (seafloor). Contours are in 1 m intervals. Highest amount of depositional trend occurs in the north and on the sides of the SDV.

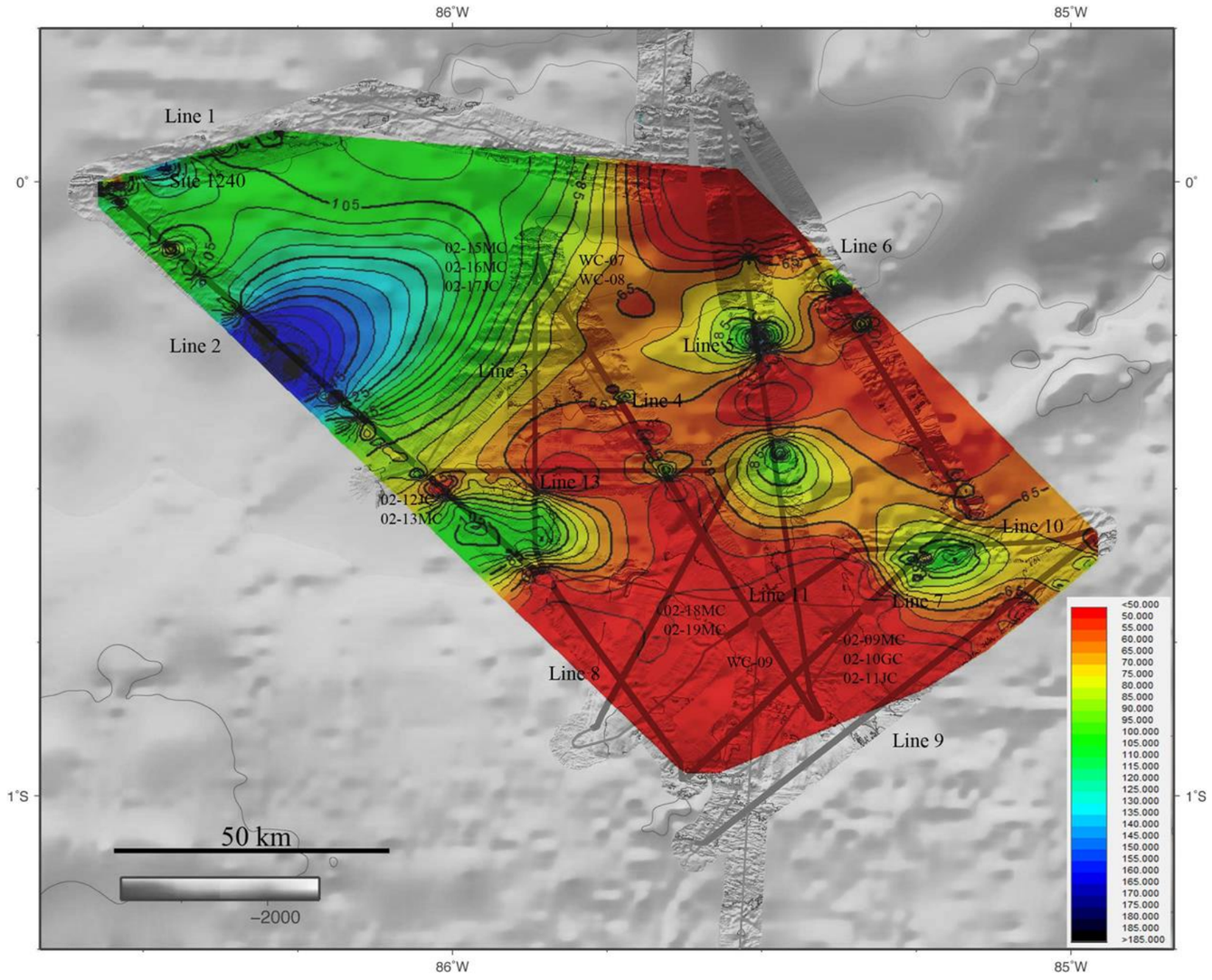

Figure 19. 1.7 Ma Depositional Trends
Isopach map of depositional regime from 1.78Ma Horizon to current day (seafloor). Contours are in 5m intervals. The greatest amount of sediment occurs in the NW of the study area and decreases by half in the SE.

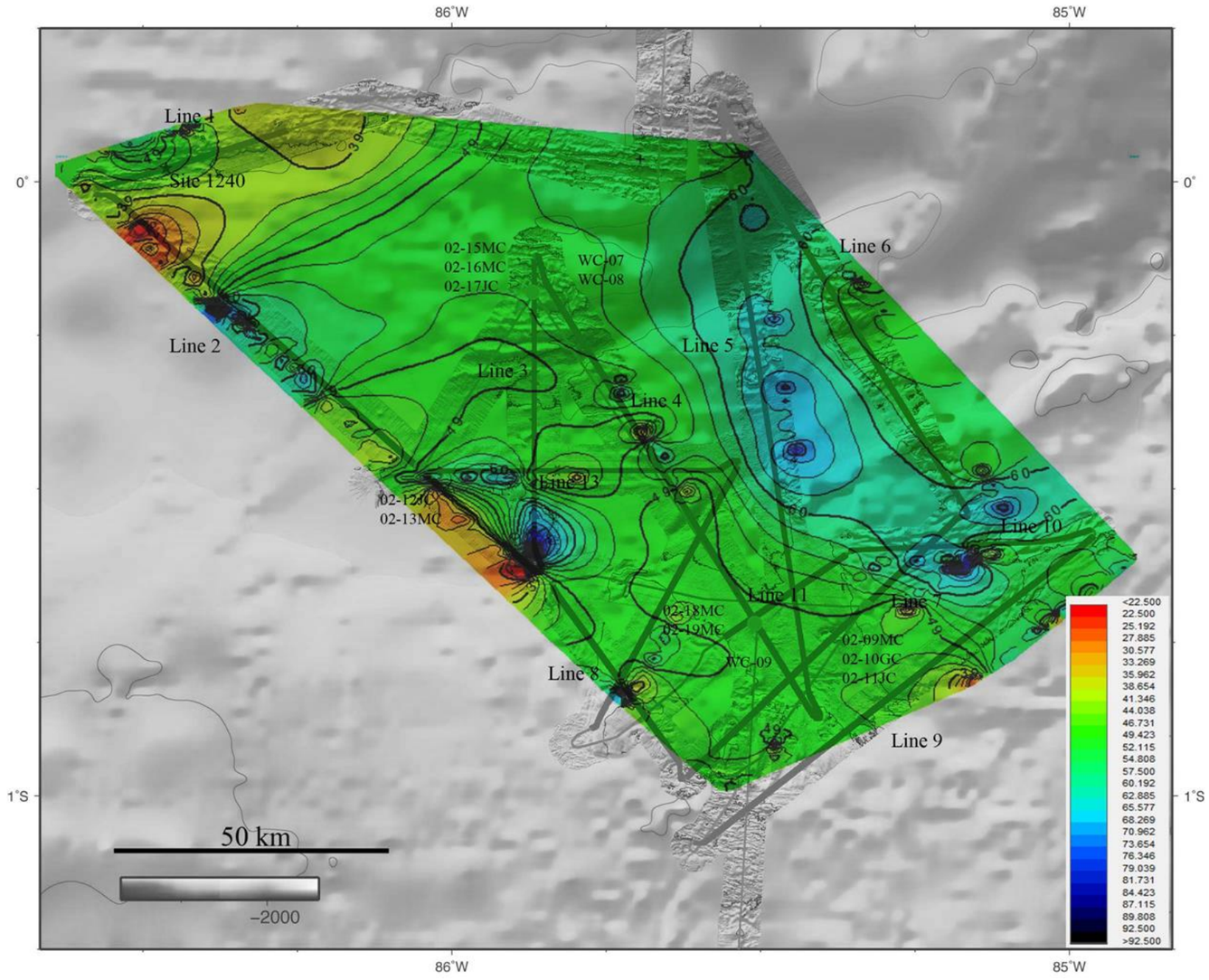

Figure 20. 2 Ma to 1.7 Ma Depositional Trends, Horizons PL-1 and PL-2
Isopach map of depositional regime from 1.945 Ma Horizon to 1.178 Ma Horizon. Contours are in ~2.50m intervals. The greatest amount of sediment occurs around the sides of the Sand Dune Valley. Overall sedimentation rates appear to be more constant throughout the study area.

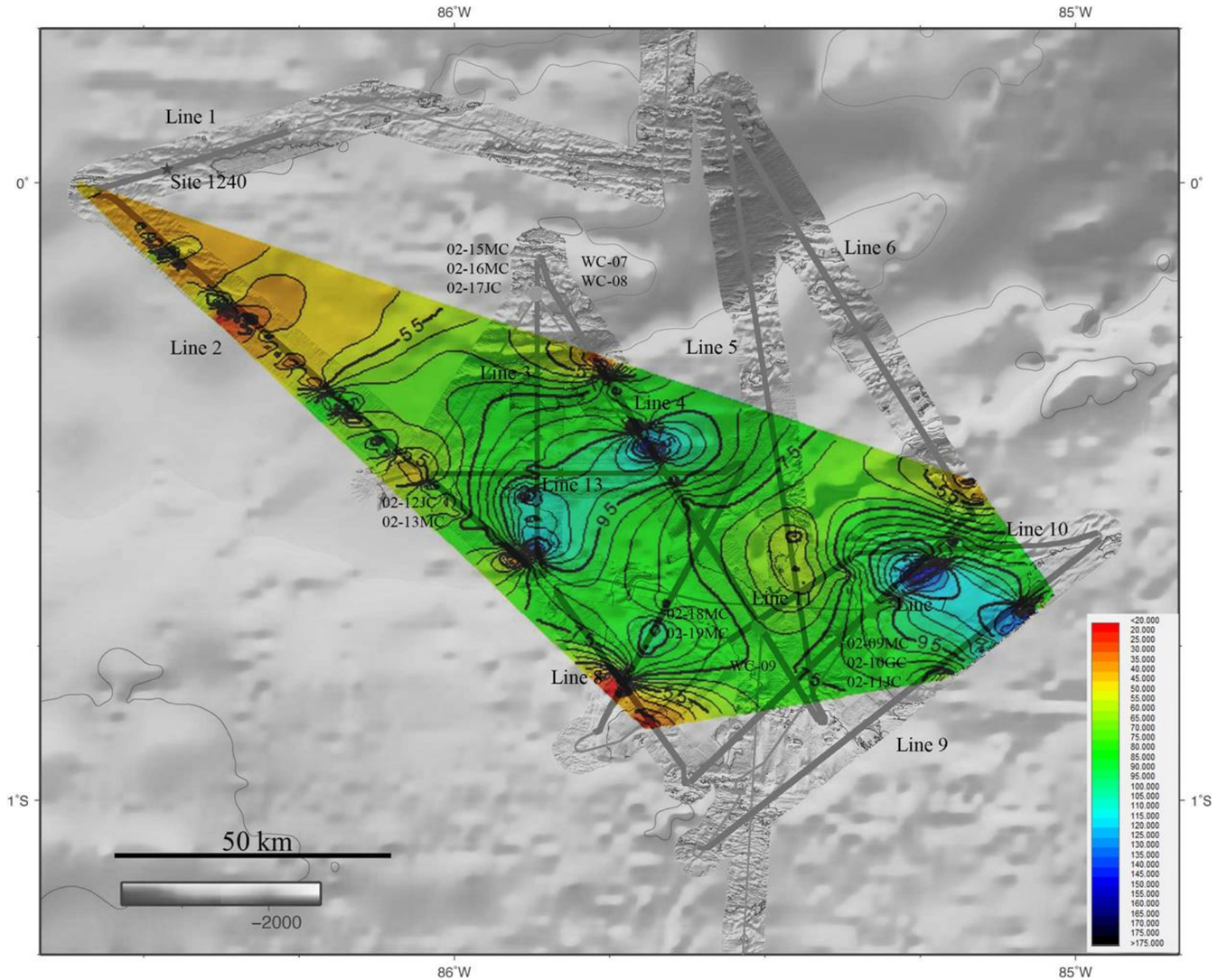

Figure 21. 2.2 Ma to 2.0 Ma Depositional Trends, Horizons P-1 and PL-2
Contours are in 5 m intervals. Thickest sediment packages occur in proximity to the northern terminus of the Sand Dune Valley (see Figure 24), which is proposed to be a sediment collection area, and on the southeastern side of the valley demonstrating lateral transport modes from Peru Basin to the south redistributing sediment.

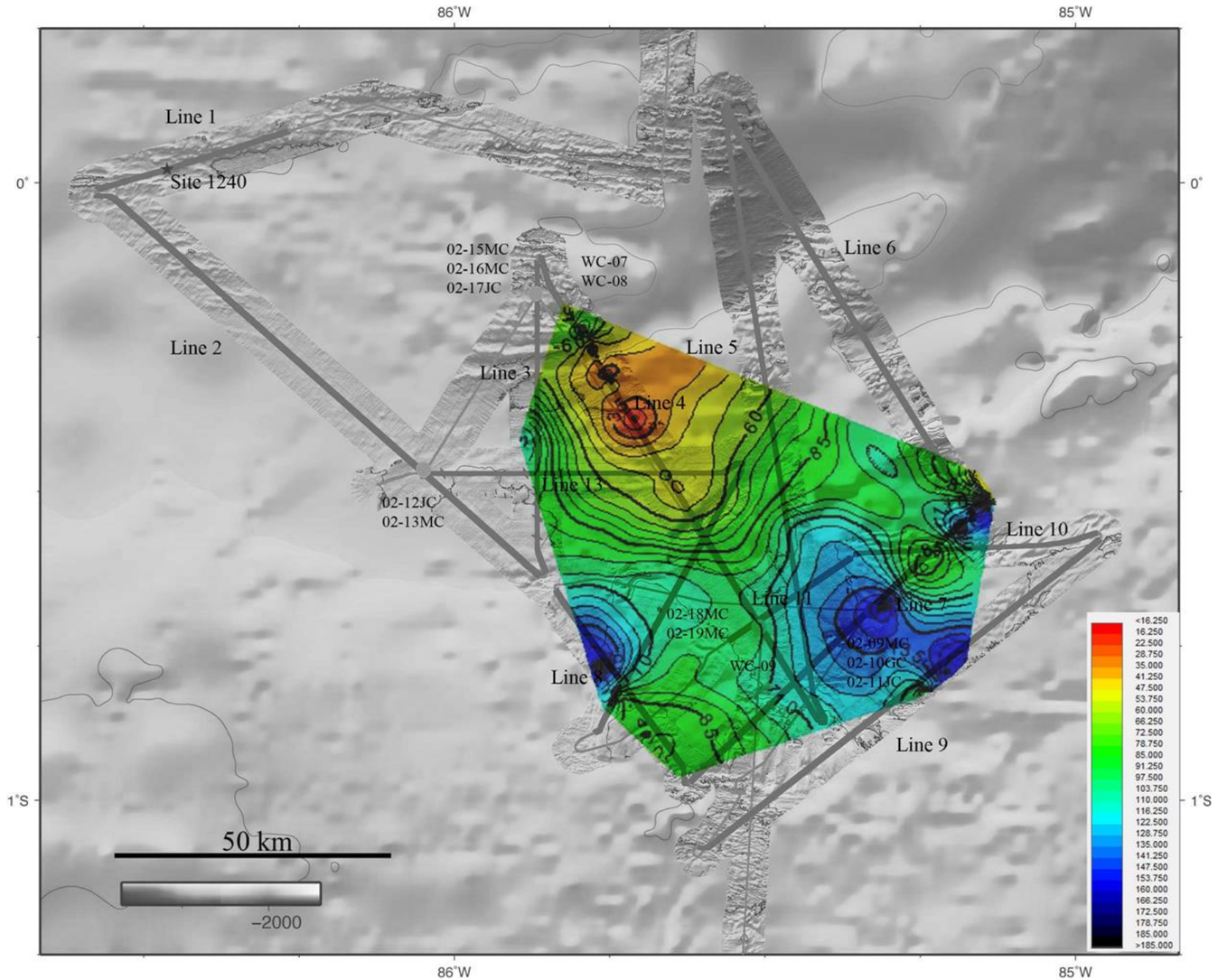

Figure 22. 5.3 Ma to 2.2 Ma Depositional Trends, Horizons LM-1 and P-1
Isopach map of depositional regime from 5.3 Ma Horizon to 2.2 Ma Horizon. Contour are in ~6.25m intervals. Thickest accumulation resides on the sides of the valleys suggesting a lateral transport mechanism and/or redistribution.

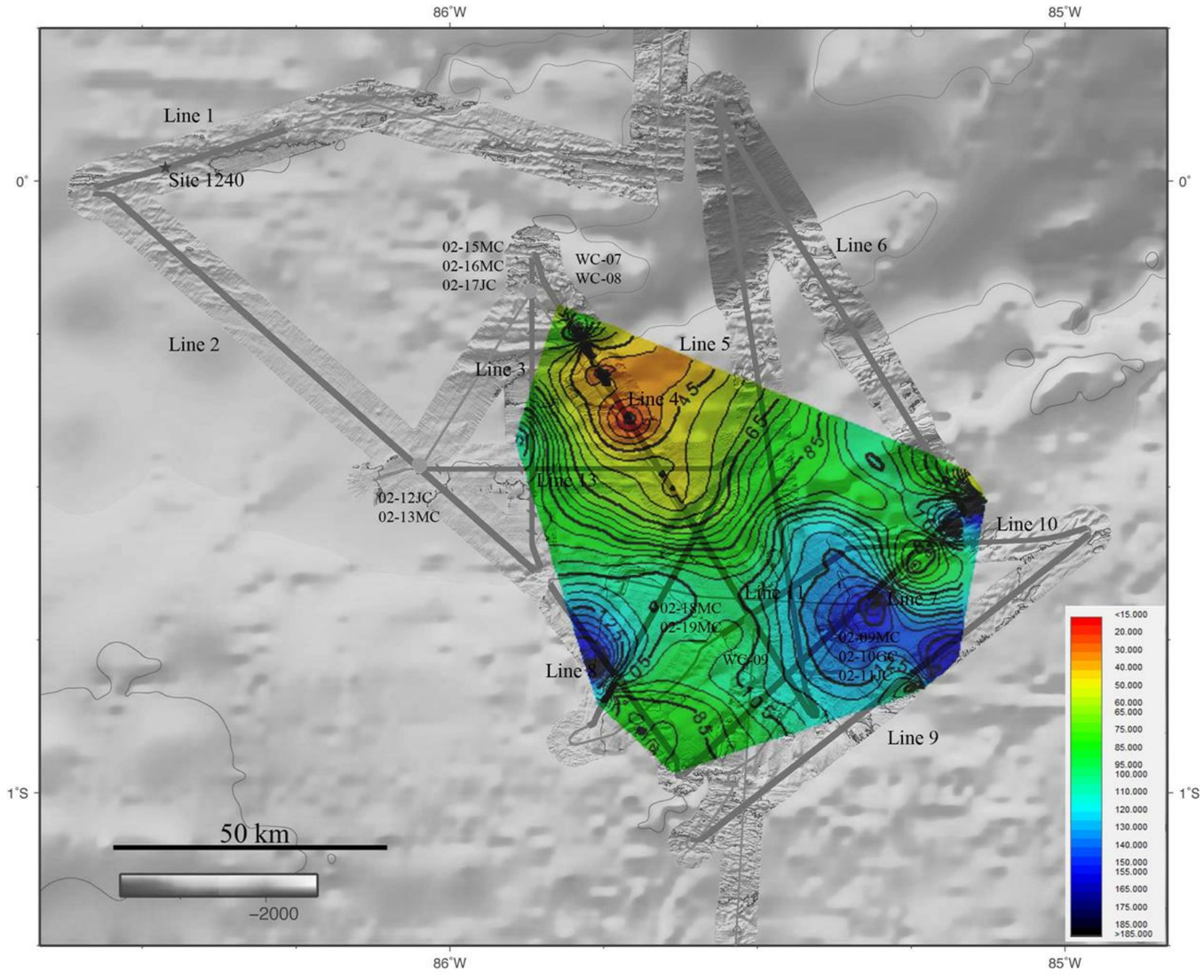

Figure 23. Thickness of Erosional Cherty Chalk Sequence
Contours are in 5m intervals. This erosive unconformity fluctuates in thickness due to differences in erosion and lateral extent of the package northward. It is thickest in the south where crustal ages are old enough.

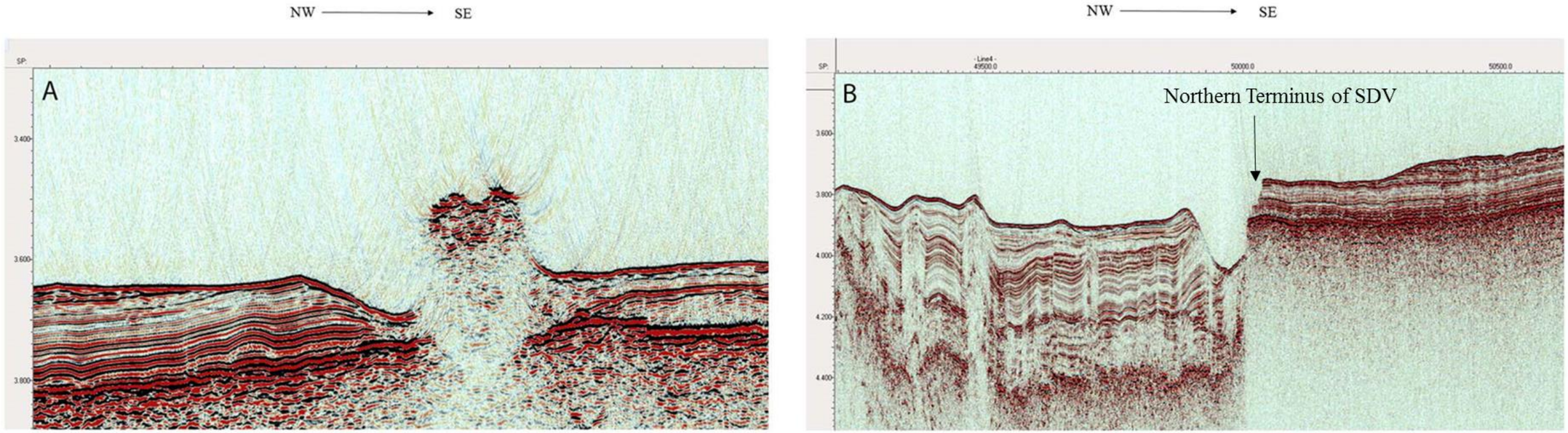

Figure 24. Medium and Small-Scale Erosional Types

A. Small-scale erosional features common to Carnegie Ridge area. Erosion stems from currents created by volcanic edifices.
B. Medium-scale carving of an E-W trending trough at a fault scarp. The fault scarp marks the northern terminus of the Sand Dune Valley.

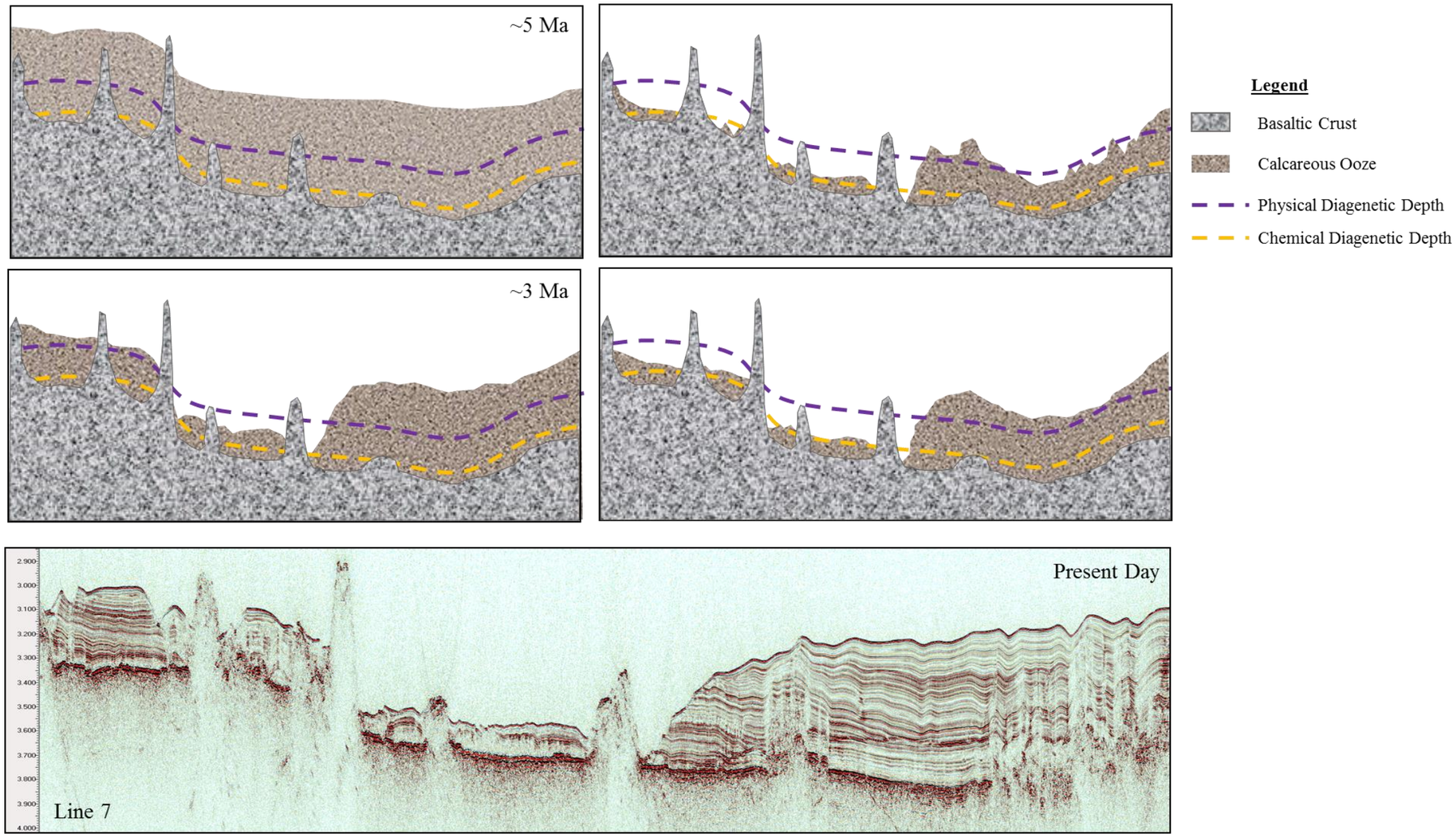

Figure 25. Geological Reconstruction of the Mouth of Sand Dune Valley
Free-fall cores and deep-tow surveys have found the presence of chalk and cherty sequences in and around Sand Dune Valley. Chalk and chert are both a result of diagenesis; chalk requiring an amount of overburden for compaction, and chert requiring overburden and a geothermal component for a chemical transformation. This geologic model reconstructs the amount of overburden required for the initial transformations to chalk and chert to have taken place and employs two erosive periods, evident from the basal, highly erosive chalky-chert package and another unconformity found higher in section.

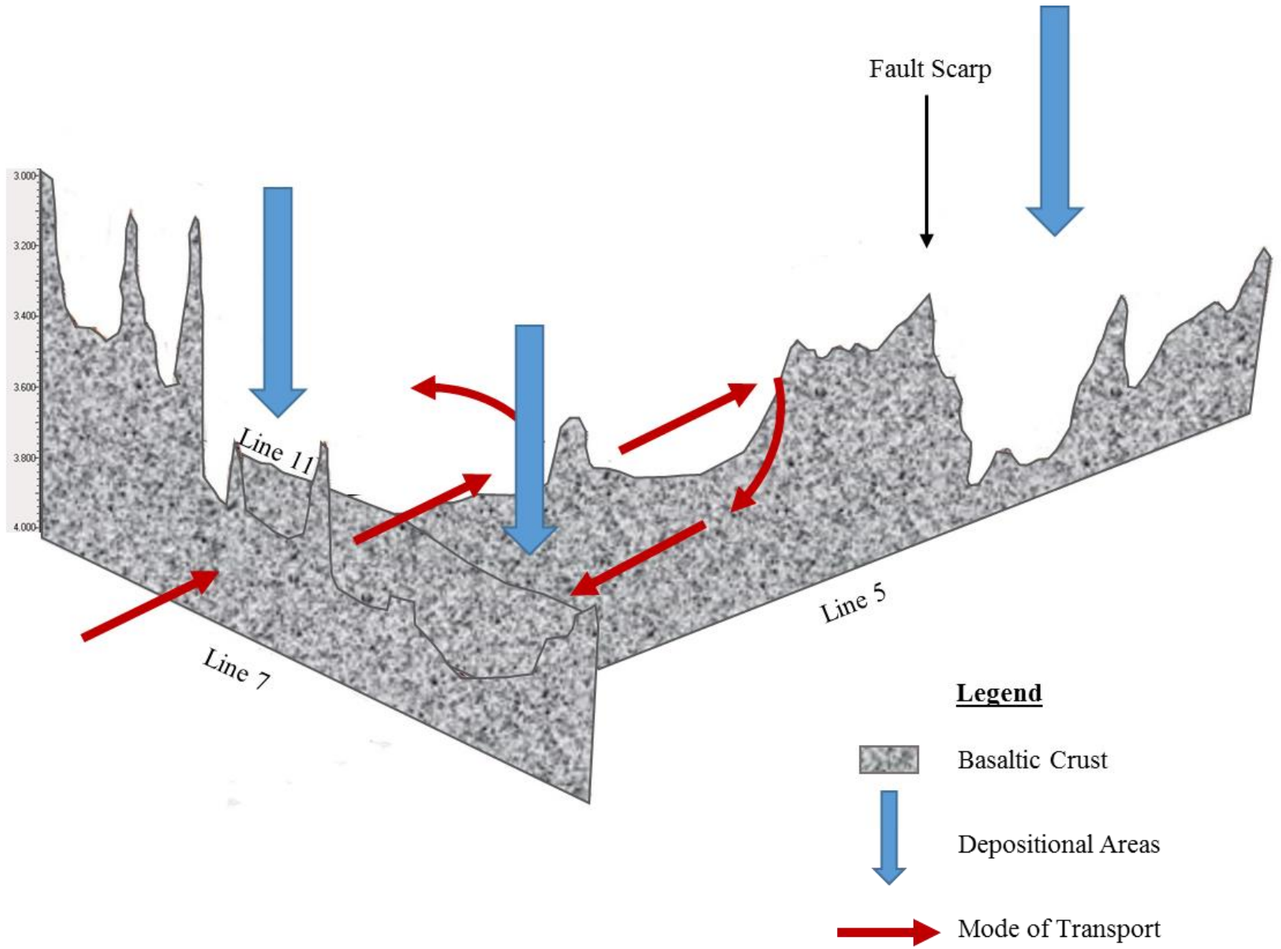

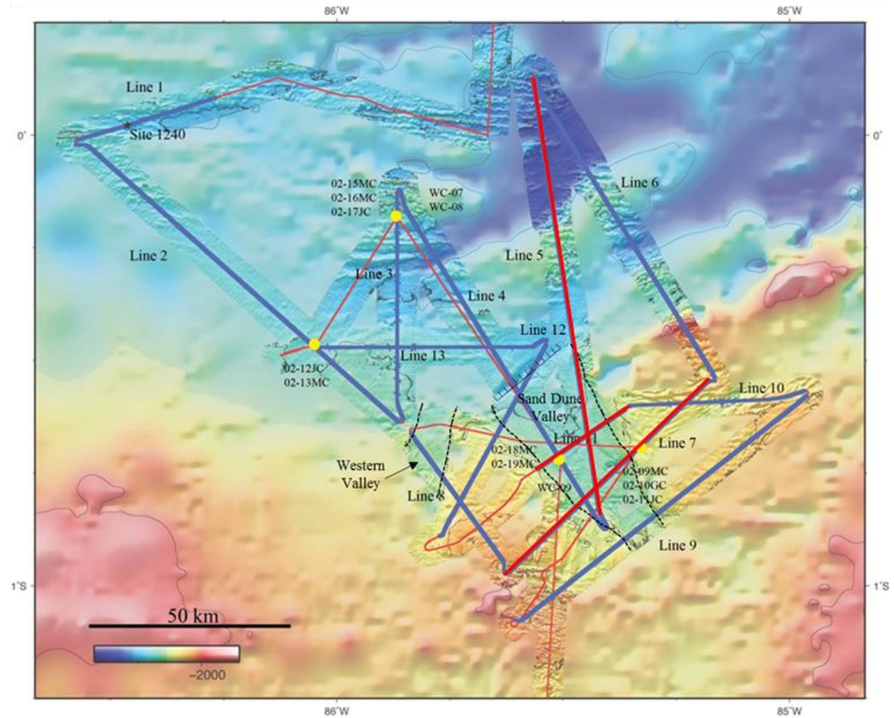

Figure 26. Depositional Model
Depositional model demonstrating topography's influence on sediment accumulation. Volcanic edifices enable redirection of sediments and relief for basin sediment infill. Areas with the thickest packages of sediment are shown with blue arrows. Red arrows show modes of sediment transport into Panama Basin from the Peru Basin to the south.

APPENDIX B

VERTICAL SEISMIC PROFILES

W ⟶ E

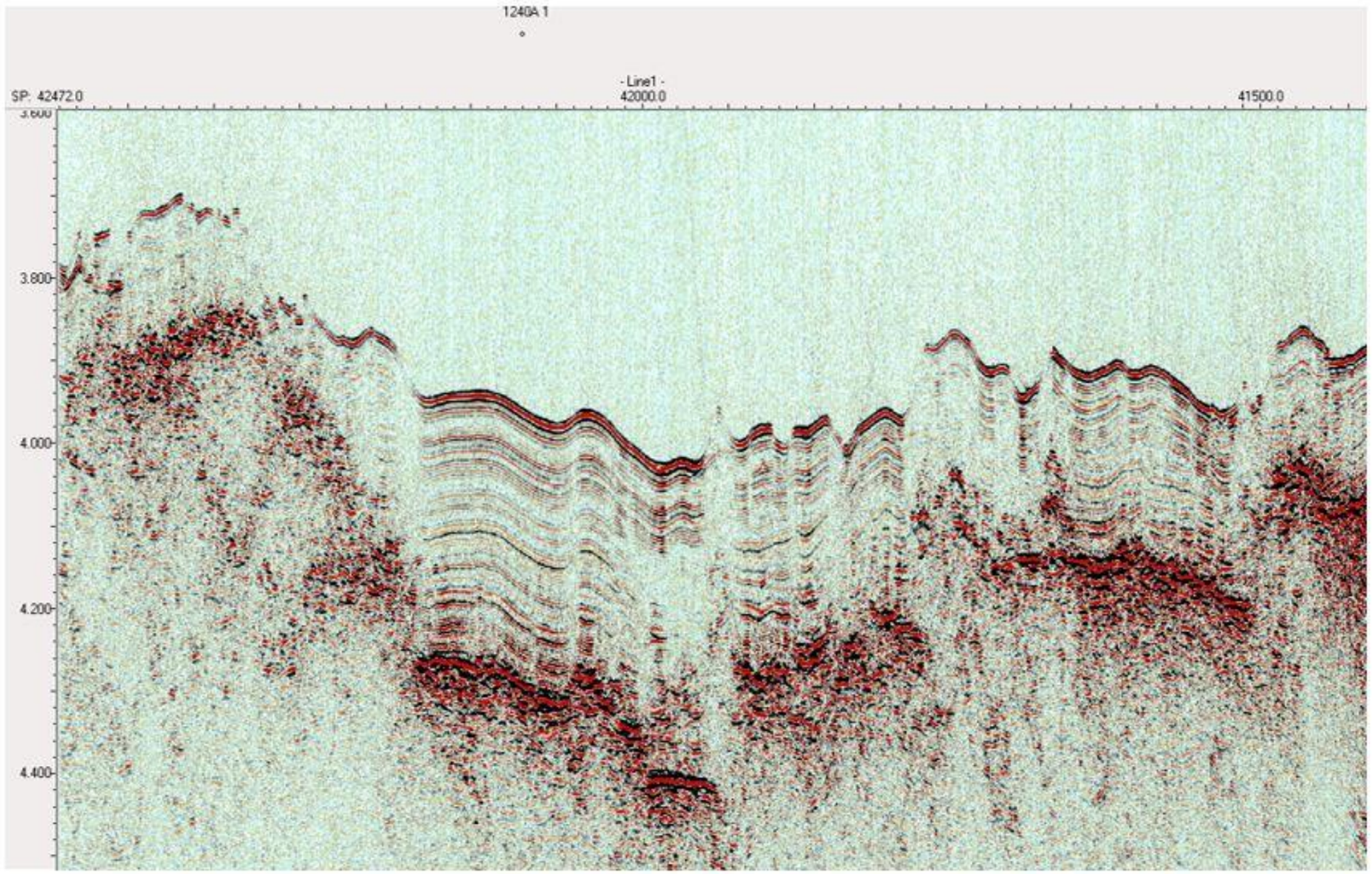

Line 1; Site of 1240A; 30 x Vertical Exaggeration

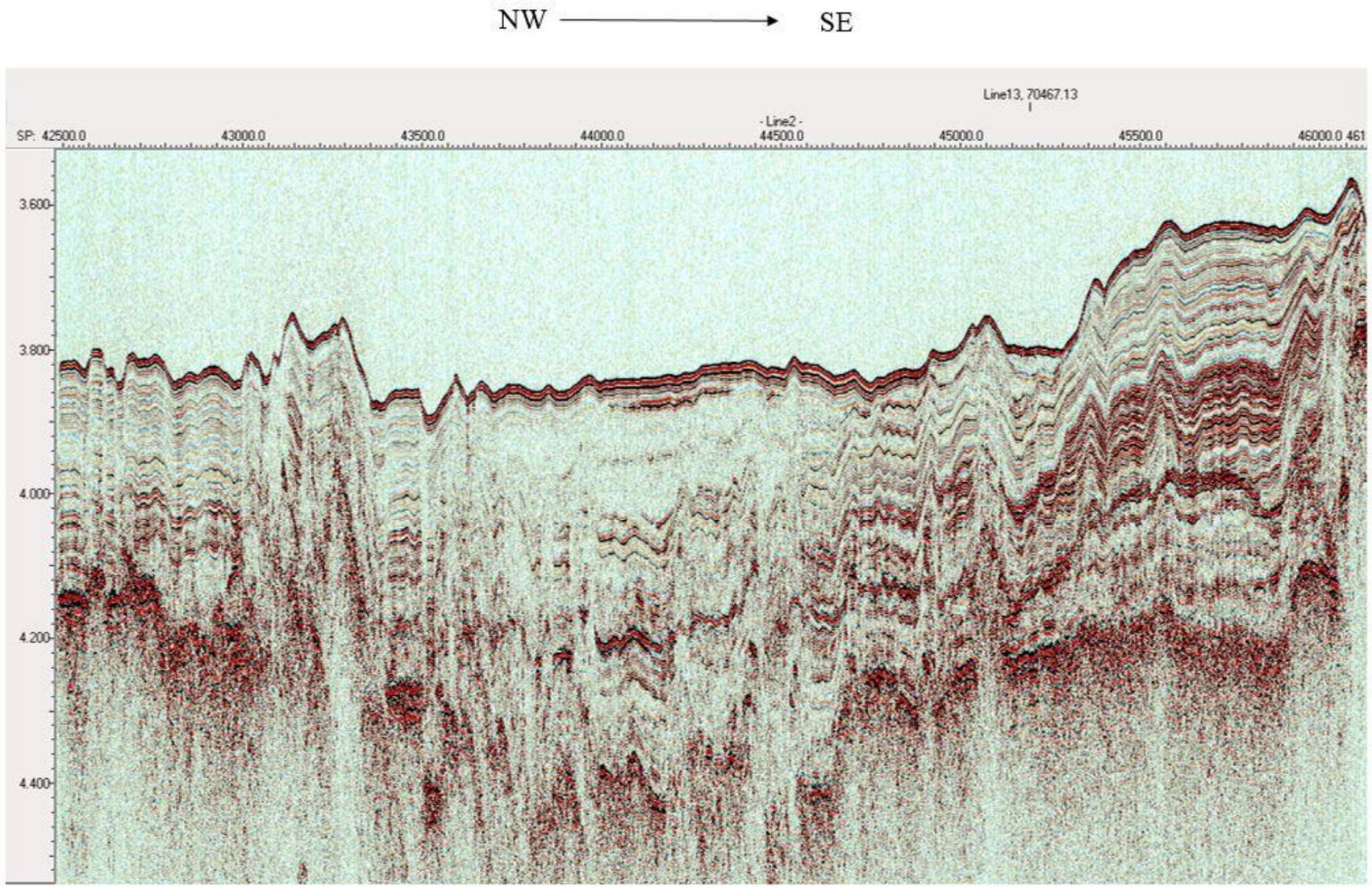

Line 2; 95 x Vertical Exaggeration

SW ⟶ NE

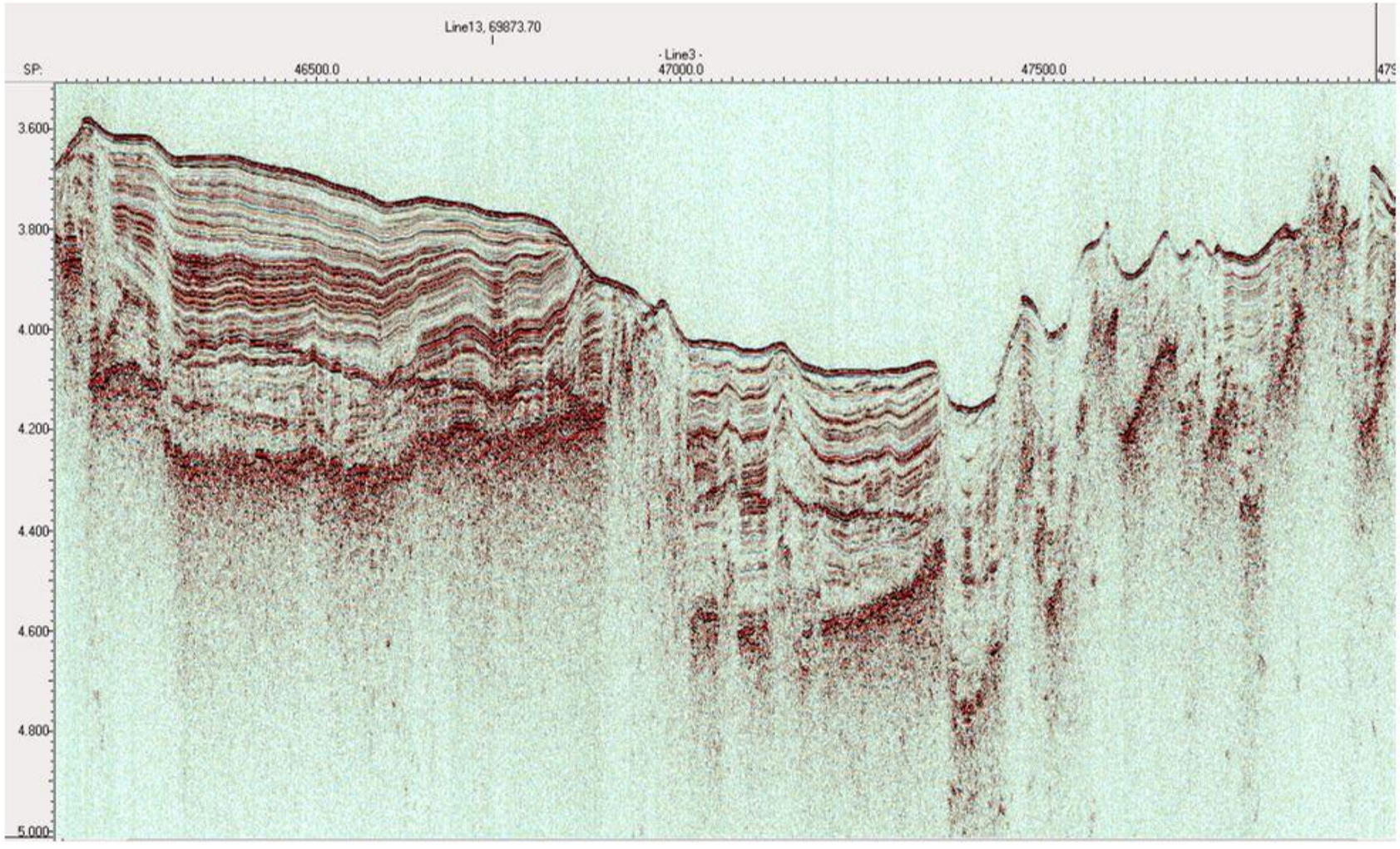

Line 3; 40 x Vertical Exaggeration

NW ⟶ SE

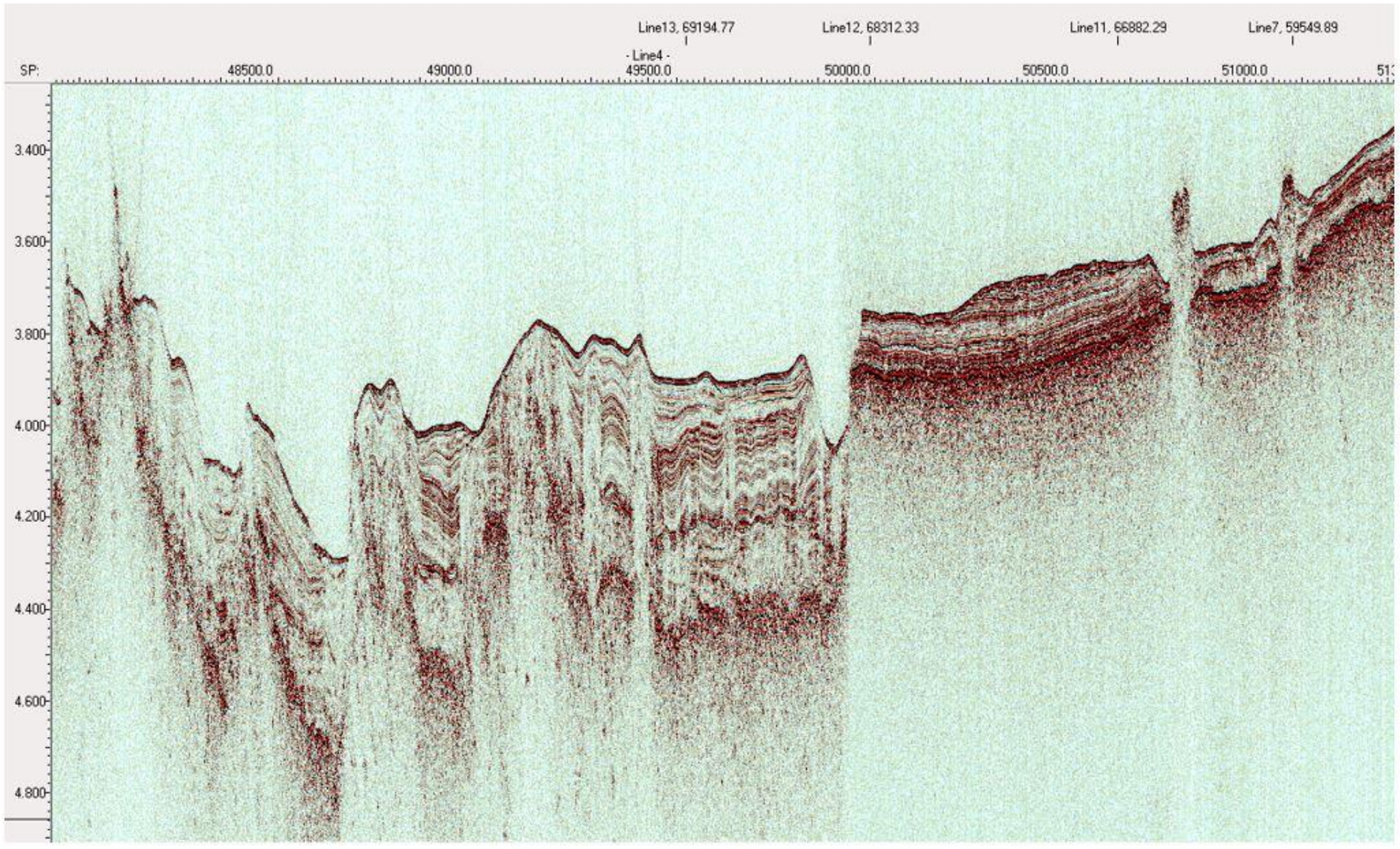

Line 4; 40 x Vertical Exaggeration

SW ⟶ NE

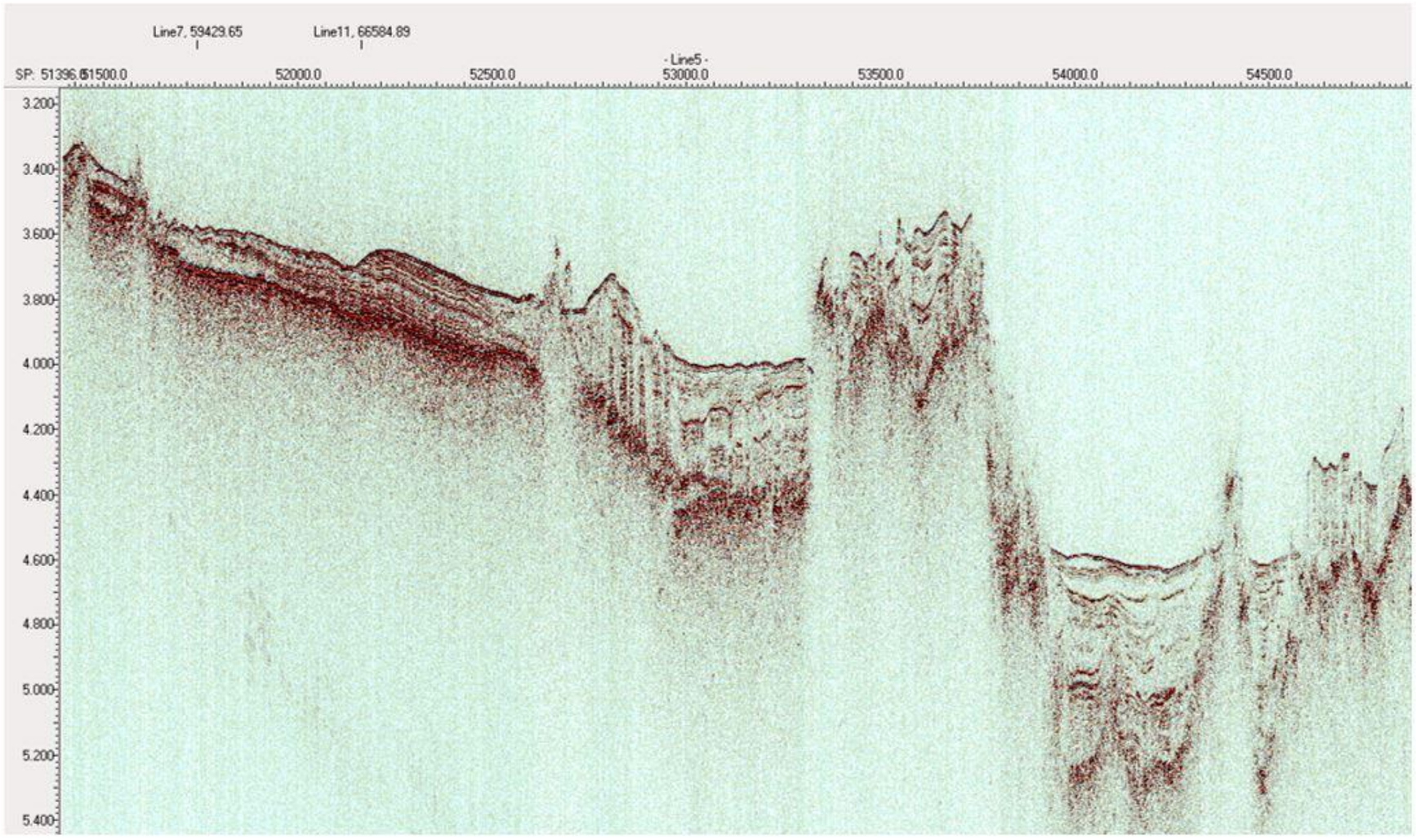

Line 5; 40 x Vertical Exaggeration

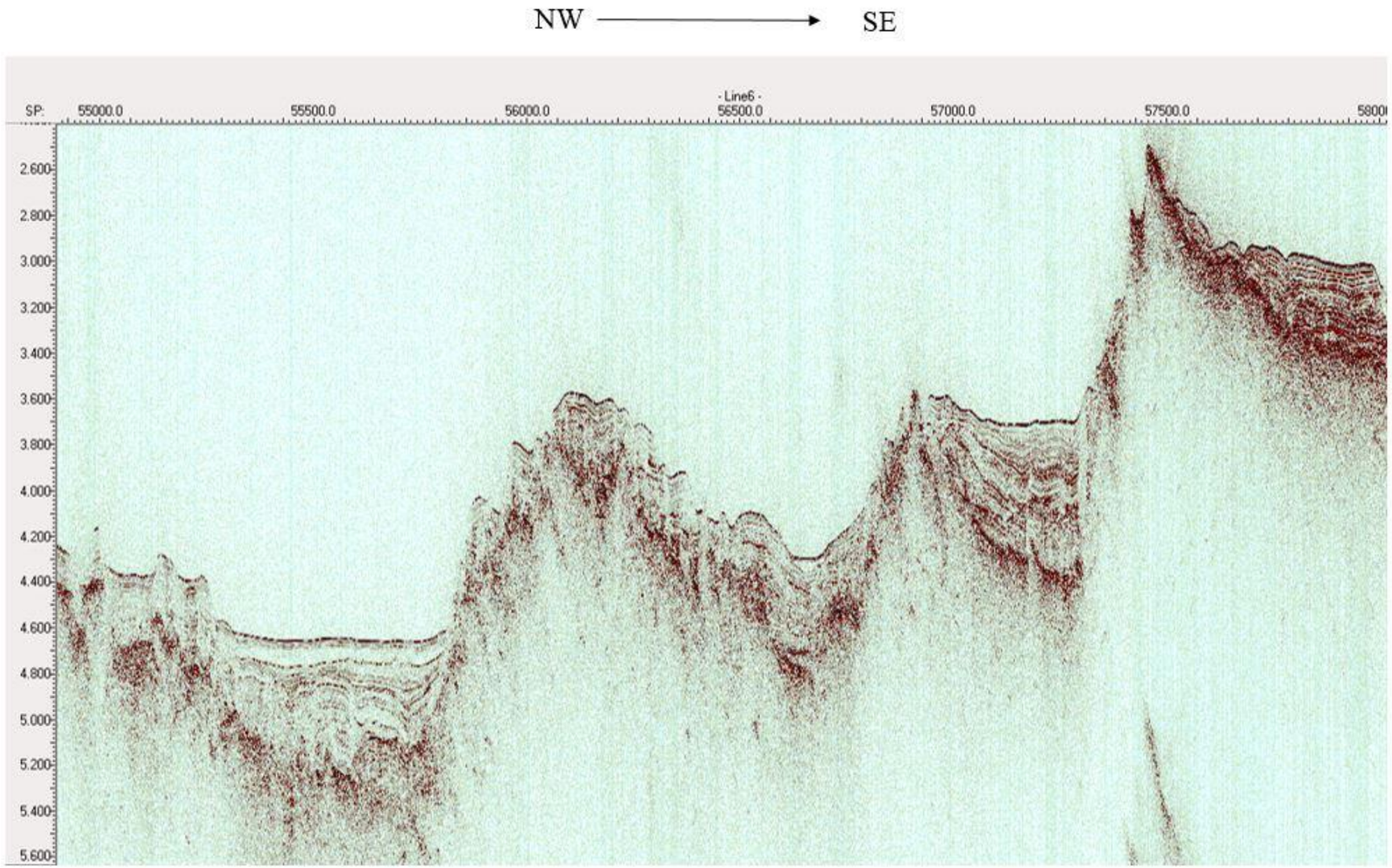

Line 6; 40 x Vertical Exaggeration

W ⟶ E

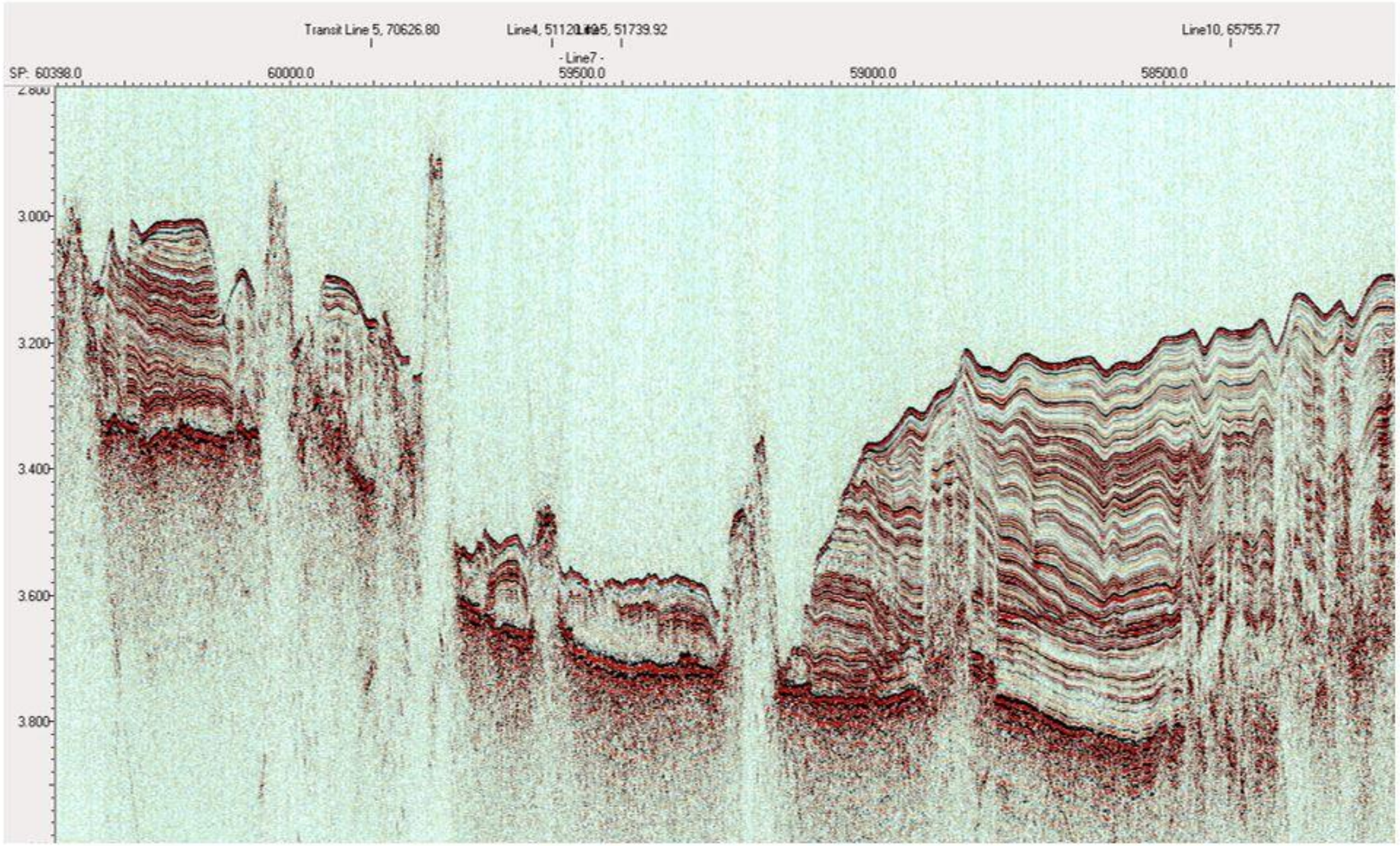

Line 7; 60 x Vertical Exaggeration

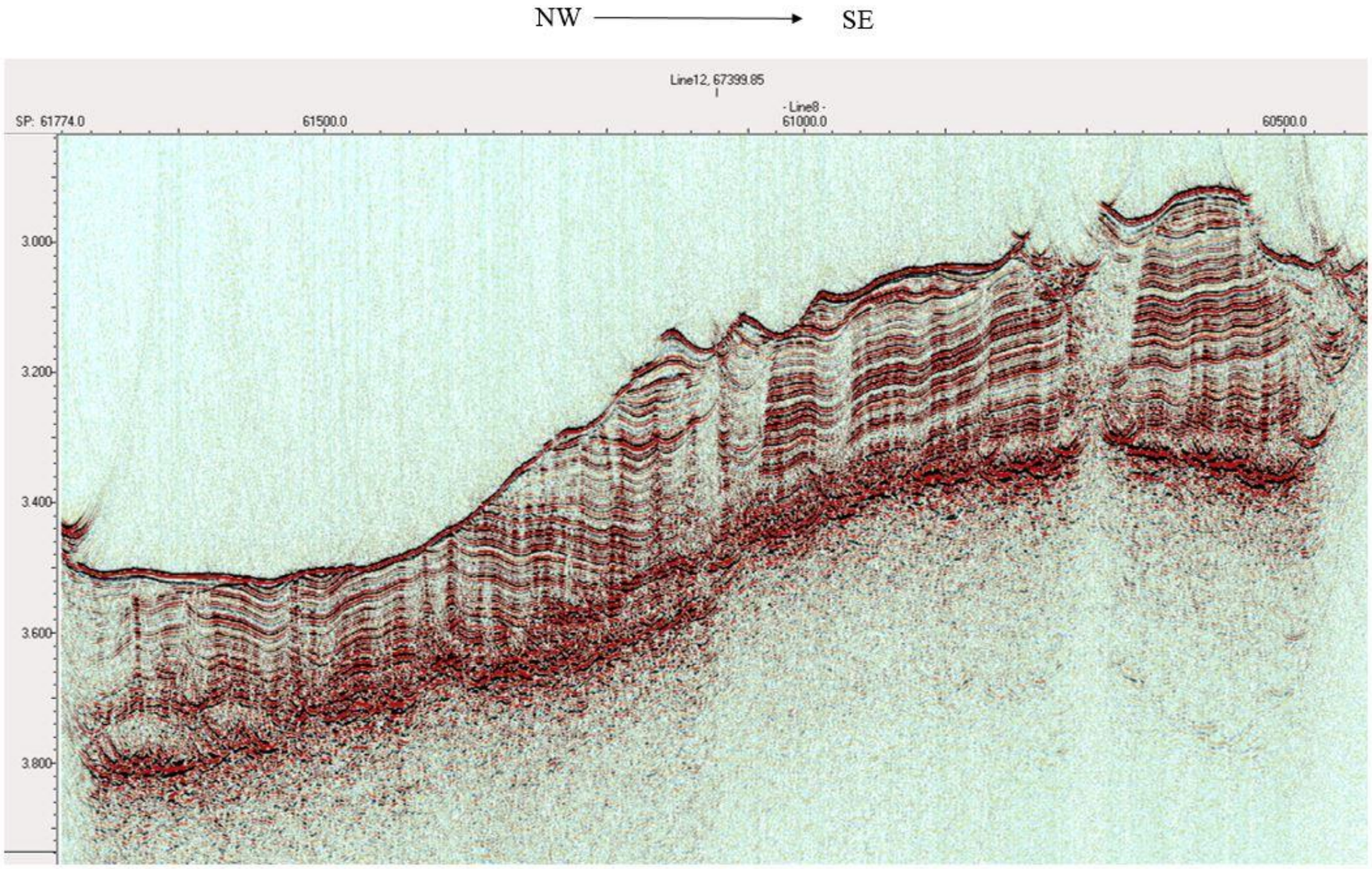

Line 8; 45 x Vertical Exaggeration

W ⟶ E

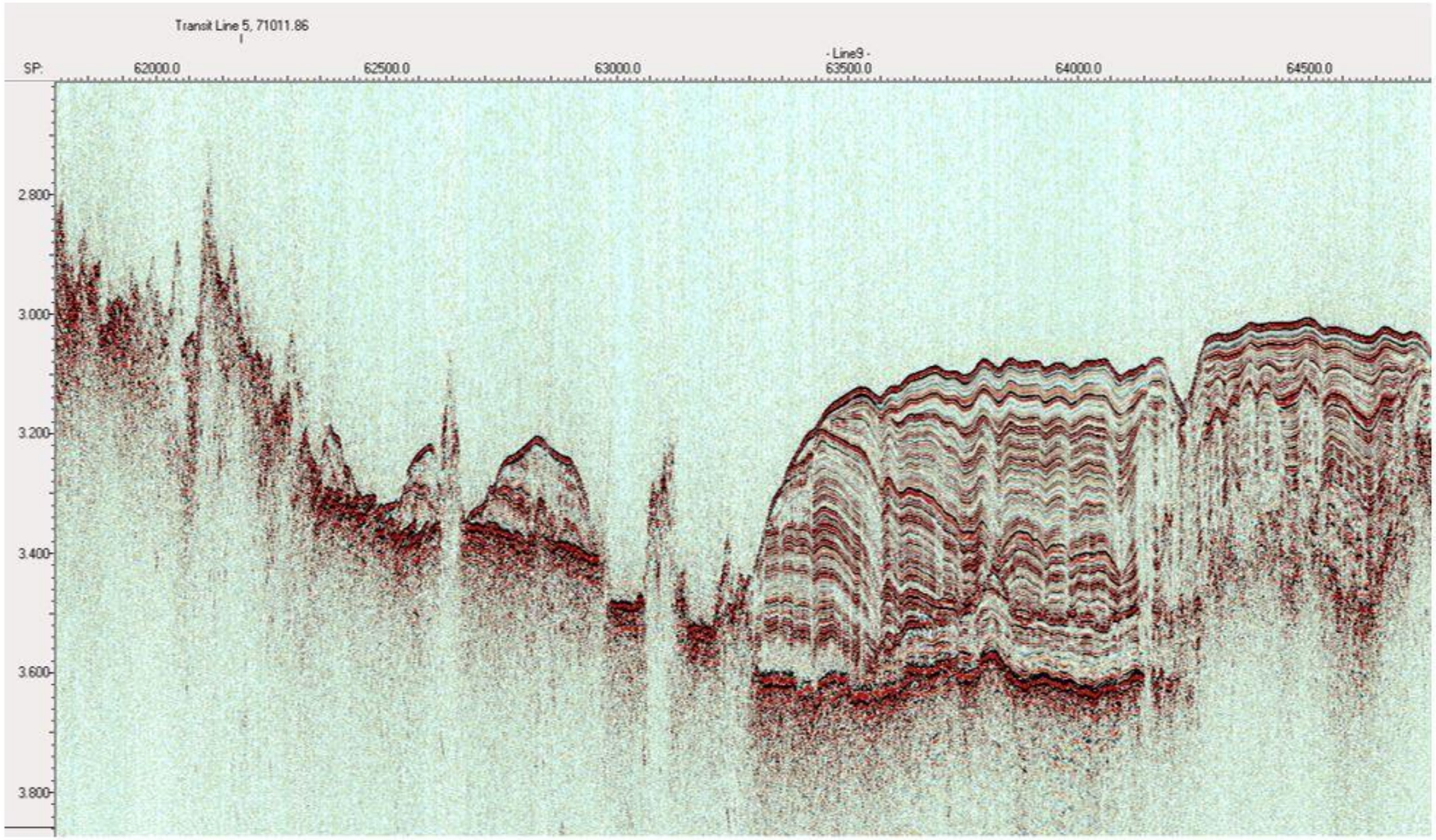

Line 9; 40 x Vertical Exaggeration

W ⟶ E

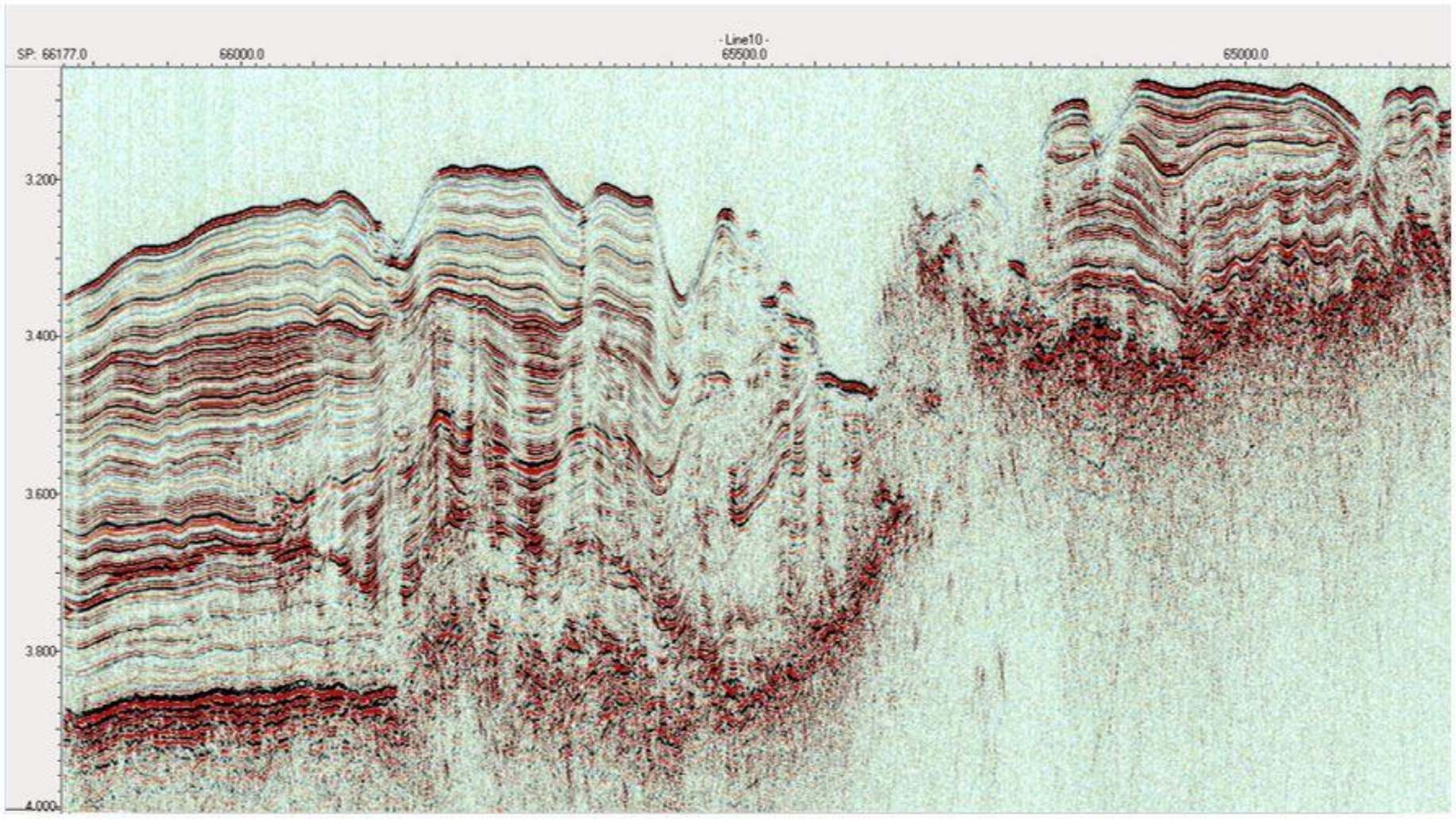

Line 10; 35 x Vertical Exaggeration

W ⟶ E

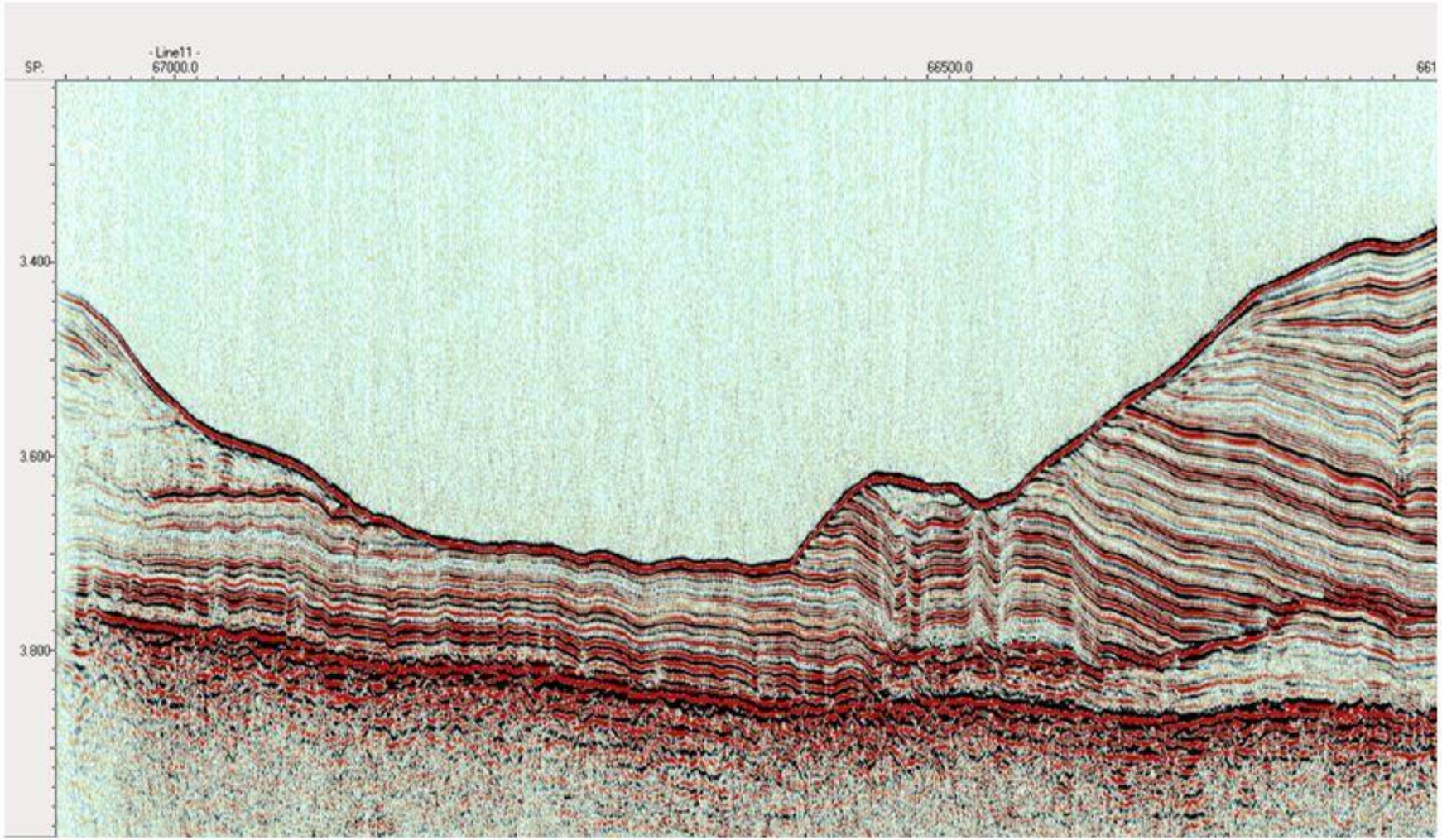

Line 11; 40 x Vertical Exaggeration

SW ⟶ NE

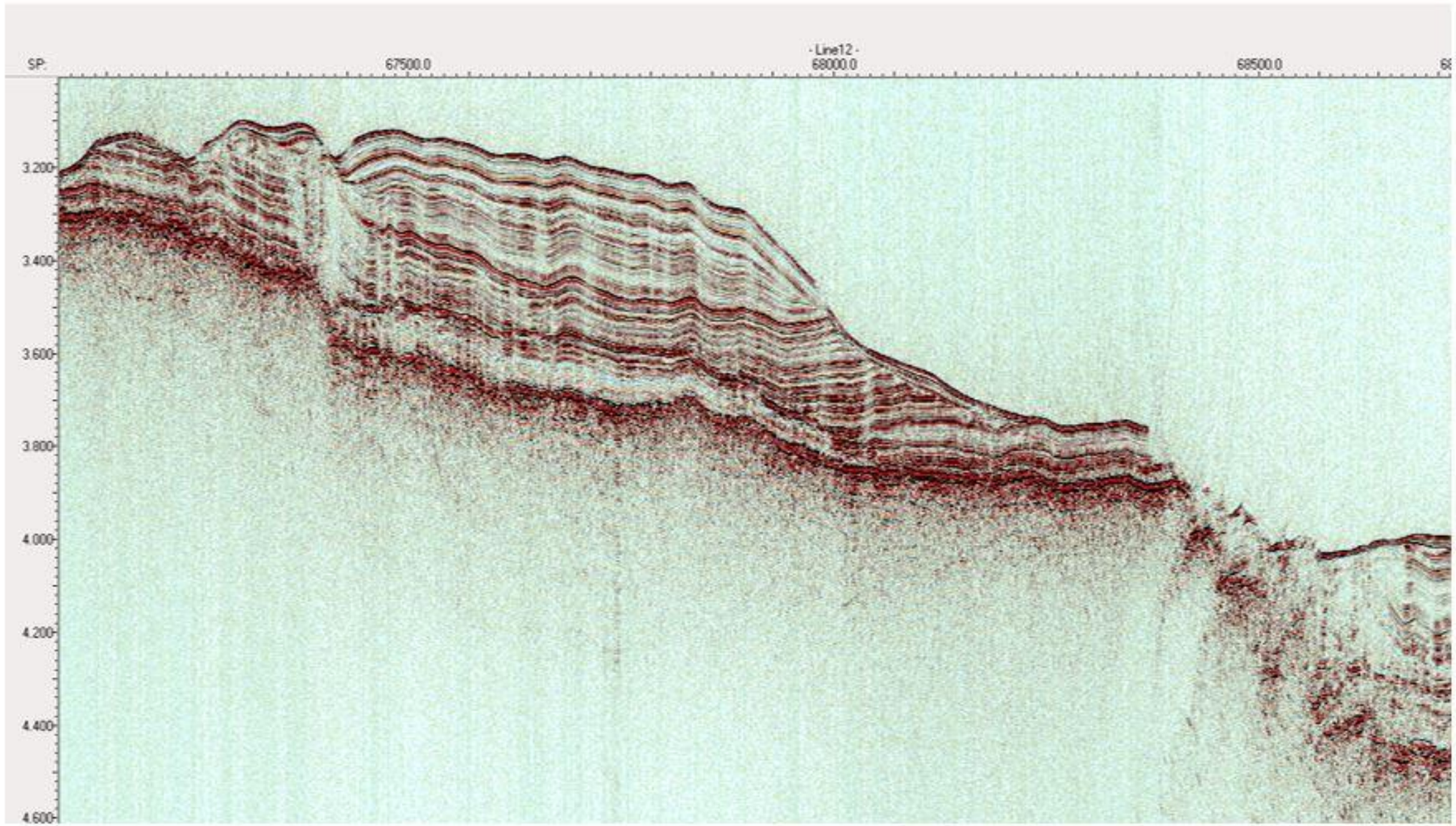

Line 12; 35 x Vertical Exaggeration

W ⟶ E

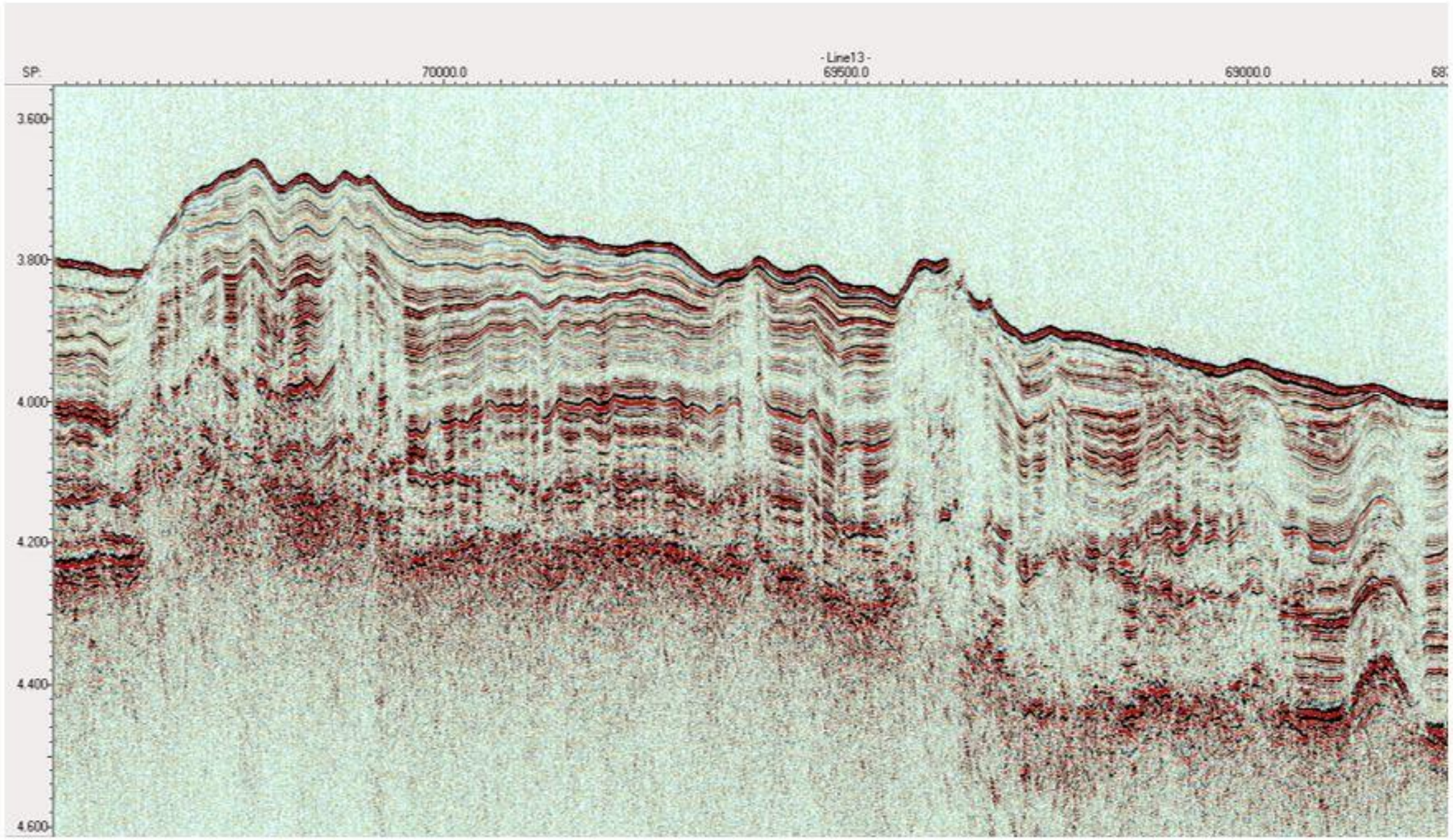

Line 13; 35 x Vertical Exaggeration

NE ⟶ SW

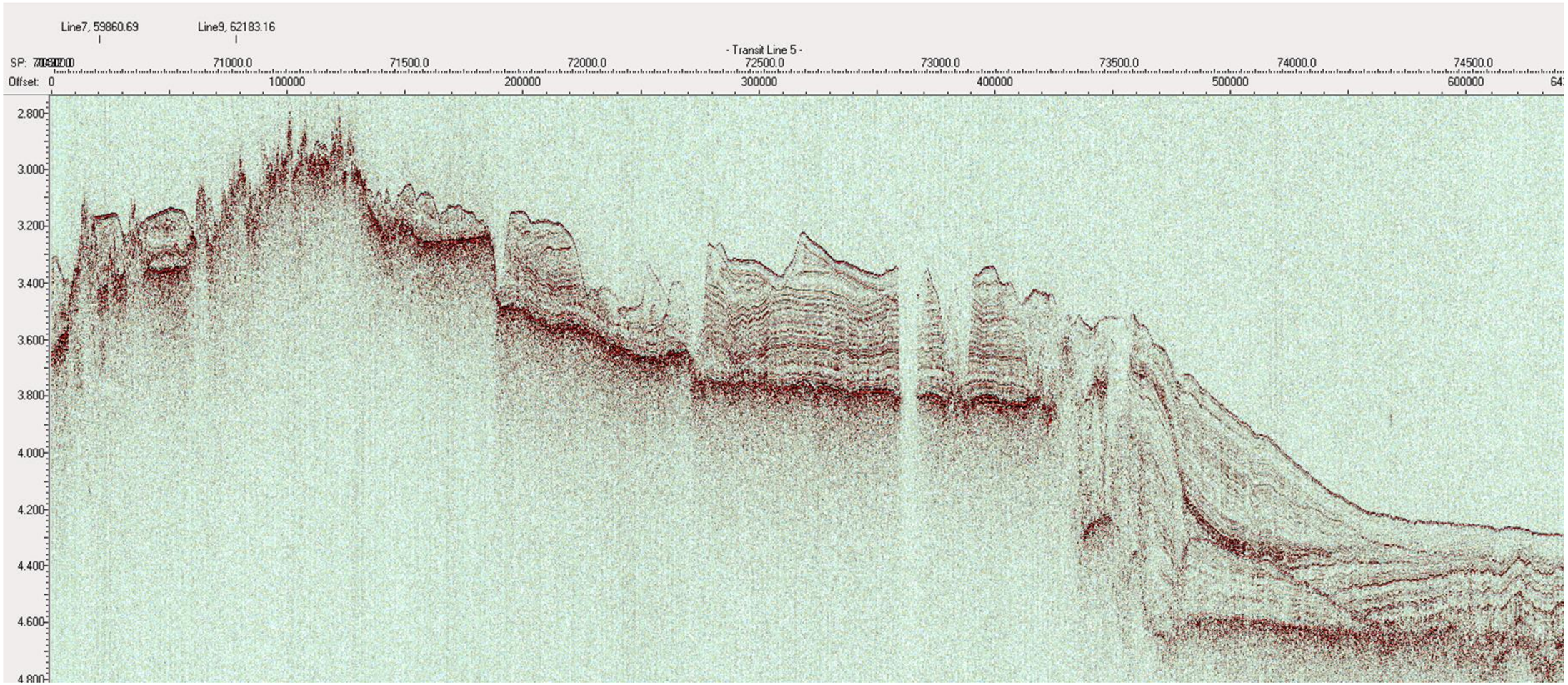

Transit Line 5; 90 x Vertical Exaggeration

APPENDIX C

TABLES

Table 1. Polarity Chron Boundaries and Biostratigraphical Constraints

Nannofossil	Polarity Chron	Approximate Age
LO Discoaster hamatus	**CN8a**	**9.635**
LO Catinaster calyculus		**9.641**
FO Discoaster neohamatus		**10.45**
FO Discoaster hamatus	**CN7**	**10.476**

Table 2. Comparison of Site 846 Horizons to Carnegie Ridge Horizons

EEP Seismic Horizon at Site 846 (Bloomer et al., 1995)	Approximate Age (Ma)	Carnegie Ridge Seismic Horizon	Approximate Age (Ma)
R1-b	**2.20**	**P-1**	**~2.20**
R4	**5.30**	**LM-1**	**~5.30**
R7-b	**8.97**	**LM-1a**	**~8.90**

APPENDIX D

DIGITAL FILES

This appendix contains data files for the horizons picked in Kingdom Suite. The horizons are presented in ASCII form as, X, Y, Time. Because of the length of the files, the first page of the table for each horizon at Tracklines 1, 2 and 3 is only presented for the Seafloor, PL-1, PL-2 and the Acoustic Basement. For deeper horizons, P-1, LM-1 and LM-1a, the first page of the table for each horizon at Tracklines 7, 8 and 9 are presented due to depositional constraints.

Line 1 Seafloor			Line 2 Seafloor			Line 3 Seafloor		
X	Y	Time	X	Y	Time	X	Y	Time
1907998.96	32838538.97	3.86	1794779.28	32803702.78	3.78	2059289.36	32579186.01	3.67
1907982.73	32838532.43	3.86	1794763.12	32803681.53	3.79	2059279.39	32579209.14	3.67
1907966.50	32838525.89	3.86	1794747.39	32803660.88	3.79	2059269.13	32579232.93	3.67
1907950.27	32838519.36	3.86	1794731.23	32803639.64	3.79	2059259.16	32579256.06	3.67
1907934.03	32838512.82	3.86	1794715.50	32803618.98	3.79	2059248.71	32579281.26	3.67
1907917.80	32838506.28	3.86	1794699.34	32803597.74	3.79	2059237.27	32579310.23	3.67
1907901.57	32838499.75	3.86	1794683.61	32803577.08	3.79	2059226.13	32579338.42	3.67
1907885.34	32838493.21	3.86	1794667.45	32803555.84	3.79	2059215.00	32579366.61	3.67
1907869.11	32838486.67	3.86	1794652.93	32803533.10	3.79	2059203.55	32579395.60	3.67
1907852.88	32838480.14	3.86	1794638.22	32803509.33	3.79	2059192.42	32579423.79	3.67
1907836.64	32838473.60	3.86	1794623.52	32803485.56	3.79	2059181.29	32579451.98	3.67
1907819.99	32838467.30	3.87	1794609.22	32803462.44	3.79	2059170.13	32579480.81	3.67
1907801.47	32838462.07	3.87	1794594.52	32803438.67	3.79	2059160.15	32579508.35	3.67
1907782.95	32838456.84	3.87	1794580.22	32803415.55	3.79	2059150.18	32579535.89	3.67
1907764.42	32838451.61	3.87	1794565.51	32803391.78	3.79	2059139.92	32579564.20	3.67
1907746.77	32838446.15	3.87	1794551.21	32803368.66	3.79	2059128.90	32579591.74	3.67
1907729.76	32838440.52	3.87	1794536.51	32803344.89	3.79	2059117.31	32579619.28	3.67
1907712.75	32838434.89	3.87	1794522.21	32803321.77	3.79	2059105.40	32579647.60	3.67
1907695.74	32838429.26	3.87	1794507.65	32803297.70	3.79	2059093.77	32579675.11	3.67
1907678.83	32838422.36	3.87	1794494.22	32803271.22	3.79	2059081.48	32579702.15	3.67
1907661.93	32838415.42	3.87	1794481.16	32803245.48	3.80	2059068.84	32579729.95	3.67
1907645.02	32838408.48	3.87	1794467.74	32803219.01	3.80	2059056.55	32579756.99	3.67
1907627.49	32838401.61	3.87	1794457.58	32803195.78	3.81	2059045.67	32579784.12	3.66
1907608.86	32838394.88	3.87	1794449.72	32803174.12	3.81	2059036.39	32579811.36	3.66
1907590.24	32838388.14	3.87	1794442.08	32803153.06	3.82	2059026.86	32579839.37	3.66
1907571.61	32838381.40	3.87	1794434.30	32803131.03	3.82	2059017.60	32579866.61	3.66
1907556.58	32838374.28	3.87	1794511.81	32802589.12	3.81	2059007.71	32579894.11	3.66
1907542.70	32838367.04	3.87	1794590.77	32802040.26	3.82	2058997.46	32579922.42	3.66
1907528.83	32838359.80	3.87	1794671.84	32801476.96	3.82	2058987.49	32579949.96	3.66
1907514.73	32838352.76	3.87	1794727.48	32801130.49	3.82	2058977.51	32579977.50	3.66
1907499.35	32838346.82	3.87	1794745.71	32801112.52	3.82	2058967.26	32580005.82	3.66
1907483.96	32838340.89	3.87	1794763.34	32801095.86	3.82	2058957.28	32580033.36	3.66
1907468.58	32838334.96	3.87	1794781.47	32801078.72	3.82	2058947.31	32580060.90	3.66
1907450.91	32838329.08	3.87	1794799.10	32801062.06	3.82	2058936.50	32580089.21	3.66
1907432.28	32838323.55	3.87	1794817.23	32801044.92	3.82	2058925.74	32580116.75	3.66
1907413.65	32838318.02	3.87	1794835.37	32801027.78	3.82	2058914.99	32580144.29	3.65
1907395.03	32838312.49	3.87	1794854.03	32801011.21	3.82	2058903.93	32580172.61	3.65
1907376.88	32838306.48	3.87	1794876.86	32800994.48	3.82	2058893.18	32580200.15	3.65
1907358.76	32838300.44	3.87	1794899.06	32800978.22	3.82	2058882.42	32580227.69	3.65
1907340.64	32838294.41	3.87	1794921.89	32800961.50	3.82	2058871.36	32580256.01	3.65
1907322.52	32838288.37	3.87	1794944.12	32800947.14	3.82	2058860.61	32580283.55	3.65
1907304.40	32838282.34	3.88	1794967.01	32800933.43	3.82	2058849.85	32580311.09	3.65
1907286.28	32838276.31	3.88	1794989.26	32800920.11	3.82	2058838.80	32580339.40	3.65
1907268.16	32838270.27	3.88	1795012.14	32800906.41	3.82	2058828.04	32580366.94	3.65
1907250.87	32838263.33	3.88	1795035.02	32800892.71	3.82	2058817.29	32580394.48	3.65
1907233.86	32838256.09	3.88	1795057.28	32800879.39	3.82	2058806.23	32580422.80	3.65
1907216.85	32838248.85	3.88	1795080.15	32800865.70	3.82	2058795.47	32580450.34	3.65

Line 1 PL-1			Line 2 PL-1			Line 3 PL-1		
X	Y	Time	X	Y	Time	X	Y	Time
1907998.96	32838538.97	3.97	1794779.28	32803702.78	3.99	2059226.13	32579338.42	3.69
1907982.73	32838532.43	3.97	1794763.12	32803681.53	3.99	2059215.00	32579366.61	3.69
1907966.50	32838525.89	3.97	1794747.39	32803660.88	3.99	2059203.55	32579395.60	3.69
1907950.27	32838519.36	3.97	1794731.23	32803639.64	3.99	2059192.42	32579423.79	3.69
1907934.03	32838512.82	3.97	1794715.50	32803618.98	3.99	2059181.29	32579451.98	3.69
1907917.80	32838506.28	3.97	1794699.34	32803597.74	3.99	2059170.13	32579480.81	3.69
1907901.57	32838499.75	3.97	1794683.61	32803577.08	3.99	2059160.15	32579508.35	3.69
1907885.34	32838493.21	3.97	1794667.45	32803555.84	3.99	2059150.18	32579535.89	3.69
1907869.11	32838486.67	3.97	1794652.93	32803533.10	3.99	2059139.92	32579564.20	3.69
1907852.88	32838480.14	3.97	1794638.22	32803509.33	3.99	2059128.90	32579591.74	3.69
1907836.64	32838473.60	3.97	1794623.52	32803485.56	3.99	2059117.31	32579619.28	3.69
1907819.99	32838467.30	3.97	1794609.22	32803462.44	3.98	2059105.40	32579647.60	3.69
1907801.47	32838462.07	3.97	1794594.52	32803438.67	3.98	2059093.77	32579675.11	3.69
1907782.95	32838456.84	3.97	1794580.22	32803415.55	3.98	2059081.48	32579702.15	3.69
1907764.42	32838451.61	3.97	1794565.51	32803391.78	3.98	2059068.84	32579729.95	3.68
1907746.77	32838446.15	3.97	1794551.21	32803368.66	3.98	2059056.55	32579756.99	3.68
1907729.76	32838440.52	3.98	1794536.51	32803344.89	3.98	2059045.67	32579784.12	3.68
1907712.75	32838434.89	3.98	1794522.21	32803321.77	3.98	2059036.39	32579811.36	3.68
1907695.74	32838429.26	3.98	1794507.65	32803297.70	3.98	2059026.86	32579839.37	3.68
1907678.83	32838422.36	3.98	1794494.22	32803271.22	3.98	2059017.60	32579866.61	3.68
1907661.93	32838415.42	3.98	1794481.16	32803245.48	3.98	2059007.71	32579894.11	3.68
1907645.02	32838408.48	3.98	1794467.74	32803219.01	3.98	2058997.46	32579922.42	3.68
1907627.49	32838401.61	3.98	1794457.58	32803195.78	3.98	2058987.49	32579949.96	3.68
1907608.86	32838394.88	3.98	1794449.72	32803174.12	3.98	2058977.51	32579977.50	3.68
1907590.24	32838388.14	3.98	1794442.08	32803153.06	3.98	2058967.26	32580005.82	3.68
1907571.61	32838381.40	3.98	1794434.30	32803131.03	3.98	2058957.28	32580033.36	3.68
1907556.58	32838374.28	3.98	1794511.81	32802589.12	3.98	2058947.31	32580060.90	3.68
1907542.70	32838367.04	3.98	1794590.77	32802040.26	3.98	2058936.50	32580089.21	3.68
1907528.83	32838359.80	3.98	1794671.84	32801476.96	3.98	2058925.74	32580116.75	3.68
1907514.73	32838352.76	3.98	1794727.48	32801130.49	3.98	2058914.99	32580144.29	3.68
1907499.35	32838346.82	3.98	1794745.71	32801112.52	3.97	2058903.93	32580172.61	3.68
1907483.96	32838340.89	3.98	1794763.34	32801095.86	3.97	2058893.18	32580200.15	3.68
1907468.58	32838334.96	3.98	1794781.47	32801078.72	3.97	2058882.42	32580227.69	3.68
1907450.91	32838329.08	3.98	1794799.10	32801062.06	3.97	2058871.36	32580256.01	3.68
1907432.28	32838323.55	3.98	1794817.23	32801044.92	3.97	2058860.61	32580283.55	3.68
1907413.65	32838318.02	3.98	1794835.37	32801027.78	3.97	2058849.85	32580311.09	3.68
1907395.03	32838312.49	3.98	1794854.03	32801011.21	3.97	2058838.80	32580339.40	3.68
1907376.88	32838306.48	3.98	1794876.86	32800994.48	3.97	2058828.04	32580366.94	3.67
1907358.76	32838300.44	3.98	1794899.06	32800978.22	3.97	2058817.29	32580394.48	3.67
1907340.64	32838294.41	3.98	1794921.89	32800961.50	3.97	2058806.23	32580422.80	3.67
1907322.52	32838288.37	3.99	1794944.12	32800947.14	3.97	2058795.47	32580450.34	3.67
1907304.40	32838282.34	3.99	1794967.01	32800933.43	3.97	2058785.22	32580477.98	3.67
1907286.28	32838276.31	3.99	1794989.26	32800920.11	3.97	2058775.69	32580506.60	3.67
1907268.16	32838270.27	3.99	1795012.14	32800906.41	3.97	2058766.42	32580534.44	3.67
1907250.87	32838263.33	3.99	1795035.02	32800892.71	3.97	2058757.15	32580562.28	3.67
1907233.86	32838256.09	3.99	1795057.28	32800879.39	3.97	2058747.39	32580590.14	3.67
1907216.85	32838248.85	3.99	1795080.15	32800865.70	3.97	2058737.82	32580616.98	3.67

Line 1 PL-2			Line 2 PL-2			Line 3 PL-2		
X	Y	Time	X	Y	Time	X	Y	Time
1907982.73	32838532.43	4.01	1794747.39	32803660.88	4.05	2056511.43	32586189.88	3.77
1907966.50	32838525.89	4.01	1794731.23	32803639.64	4.05	2056502.10	32586215.20	3.77
1907950.27	32838519.36	4.01	1794715.50	32803618.98	4.05	2056494.34	32586242.43	3.77
1907934.03	32838512.82	4.01	1794699.34	32803597.74	4.05	2056486.59	32586269.67	3.77
1907917.80	32838506.28	4.01	1794683.61	32803577.08	4.05	2056478.60	32586297.67	3.77
1907901.57	32838499.75	4.01	1794667.45	32803555.84	4.05	2056469.03	32586322.94	3.77
1907885.34	32838493.21	4.01	1794652.93	32803533.10	4.05	2056459.06	32586347.78	3.77
1907869.11	32838486.67	4.01	1794638.22	32803509.33	4.05	2056449.08	32586372.61	3.77
1907852.88	32838480.14	4.02	1794623.52	32803485.56	4.05	2056438.64	32586398.12	3.77
1907836.64	32838473.60	4.02	1794609.22	32803462.44	4.05	2056427.86	32586422.86	3.77
1907819.99	32838467.30	4.02	1794594.52	32803438.67	4.04	2056417.08	32586447.60	3.77
1907801.47	32838462.07	4.02	1794580.22	32803415.55	4.04	2056406.00	32586473.03	3.77
1907782.95	32838456.84	4.02	1794565.51	32803391.78	4.04	2056396.21	32586498.91	3.77
1907764.42	32838451.61	4.02	1794551.21	32803368.66	4.04	2056386.99	32586525.45	3.77
1907746.77	32838446.15	4.02	1794536.51	32803344.89	4.04	2056377.51	32586552.74	3.77
1907729.76	32838440.52	4.02	1794522.21	32803321.77	4.04	2056368.29	32586579.27	3.77
1907712.75	32838434.89	4.02	1794507.65	32803297.70	4.04	2056359.08	32586605.81	3.77
1907695.74	32838429.26	4.02	1794494.22	32803271.22	4.04	2056349.60	32586633.10	3.77
1907678.83	32838422.36	4.02	1794481.16	32803245.48	4.04	2056340.38	32586659.63	3.77
1907661.93	32838415.42	4.02	1794467.74	32803219.01	4.04	2056331.87	32586686.04	3.78
1907645.02	32838408.48	4.02	1794457.58	32803195.78	4.04	2056323.99	32586713.02	3.78
1907627.49	32838401.61	4.02	1794449.72	32803174.12	4.04	2056316.33	32586739.25	3.78
1907608.86	32838394.88	4.02	1794442.08	32803153.06	4.04	2056308.68	32586765.49	3.78
1907590.24	32838388.14	4.02	1794434.30	32803131.03	4.04	2056298.76	32586791.59	3.78
1907571.61	32838381.40	4.02	1794511.81	32802589.12	4.04	2056288.79	32586816.82	3.78
1907556.58	32838374.28	4.02	1794590.77	32802040.26	4.04	2056278.81	32586842.06	3.78
1907542.70	32838367.04	4.02	1794671.84	32801476.96	4.04	2056268.76	32586868.12	3.78
1907528.83	32838359.80	4.02	1794727.48	32801130.49	4.04	2056259.49	32586893.75	3.78
1907514.73	32838352.76	4.02	1794745.71	32801112.52	4.04	2056250.22	32586919.39	3.78
1907499.35	32838346.82	4.02	1794763.34	32801095.86	4.04	2056240.70	32586945.75	3.78
1907483.96	32838340.89	4.02	1794781.47	32801078.72	4.04	2056231.98	32586971.18	3.78
1907468.58	32838334.96	4.02	1794799.10	32801062.06	4.04	2056223.52	32586996.52	3.78
1907450.91	32838329.08	4.02	1794817.23	32801044.92	4.04	2056214.82	32587022.57	3.78
1907432.28	32838323.55	4.02	1794835.37	32801027.78	4.04	2056206.29	32587047.88	3.78
1907413.65	32838318.02	4.02	1794854.03	32801011.21	4.04	2056197.12	32587072.91	3.78
1907395.03	32838312.49	4.02	1794876.86	32800994.48	4.04	2056187.69	32587098.65	3.78
1907376.88	32838306.48	4.02	1794899.06	32800978.22	4.04	2056178.53	32587123.69	3.78
1907358.76	32838300.44	4.02	1794921.89	32800961.50	4.04	2056170.13	32587148.01	3.78
1907340.64	32838294.41	4.02	1794944.12	32800947.14	4.04	2056162.25	32587172.32	3.78
1907322.52	32838288.37	4.02	1794967.01	32800933.43	4.03	2056154.59	32587195.95	3.78
1907304.40	32838282.34	4.02	1794989.26	32800920.11	4.03	2056146.94	32587219.58	3.78
1907286.28	32838276.31	4.03	1795012.14	32800906.41	4.03	2056136.79	32587249.06	3.78
1907268.16	32838270.27	4.03	1795035.02	32800892.71	4.03	2056126.72	32587278.20	3.78
1907250.87	32838263.33	4.03	1795057.28	32800879.39	4.03	2056116.64	32587307.34	3.78
1907233.86	32838256.09	4.03	1795080.15	32800865.70	4.03	2056106.84	32587336.48	3.78
1907216.85	32838248.85	4.03	1795100.84	32800854.03	4.03	2056098.38	32587363.21	3.78
1907199.63	32838241.69	4.03	1795120.48	32800843.76	4.03	2056089.92	32587389.95	3.78

Line 1 Acoustic Basement			Line 2 Acoustic Basement			Line 3 Acoustic Basement		
X	Y	Time	X	Y	Time	X	Y	Time
1907998.96	32838538.97	4.05	1794747.39	32803660.88	4.14	2059192.42	32579423.79	3.82
1907982.73	32838532.43	4.05	1794731.23	32803639.64	4.14	2059181.29	32579451.98	3.82
1907966.50	32838525.89	4.05	1794715.50	32803618.98	4.14	2059170.13	32579480.81	3.82
1907950.27	32838519.36	4.03	1794699.34	32803597.74	4.14	2059160.15	32579508.35	3.82
1907934.03	32838512.82	4.03	1794683.61	32803577.08	4.14	2059150.18	32579535.89	3.82
1907917.80	32838506.28	4.04	1794667.45	32803555.84	4.14	2059139.92	32579564.20	3.82
1907901.57	32838499.75	4.04	1794652.93	32803533.10	4.14	2059128.90	32579591.74	3.82
1907885.34	32838493.21	4.04	1794638.22	32803509.33	4.14	2059117.31	32579619.28	3.82
1907869.11	32838486.67	4.04	1794623.52	32803485.56	4.14	2059105.40	32579647.60	3.83
1907852.88	32838480.14	4.04	1794609.22	32803462.44	4.14	2059093.77	32579675.11	3.83
1907836.64	32838473.60	4.04	1794594.52	32803438.67	4.14	2059081.48	32579702.15	3.83
1907819.99	32838467.30	4.04	1794580.22	32803415.55	4.14	2059068.84	32579729.95	3.83
1907801.47	32838462.07	4.04	1794565.51	32803391.78	4.14	2059056.55	32579756.99	3.83
1907782.95	32838456.84	4.04	1794551.21	32803368.66	4.14	2059045.67	32579784.12	3.83
1907764.42	32838451.61	4.04	1794536.51	32803344.89	4.14	2059036.39	32579811.36	3.83
1907746.77	32838446.15	4.05	1794522.21	32803321.77	4.14	2059026.86	32579839.37	3.83
1907729.76	32838440.52	4.05	1794507.65	32803297.70	4.14	2059017.60	32579866.61	3.83
1907712.75	32838434.89	4.05	1794494.22	32803271.22	4.14	2059007.71	32579894.11	3.83
1907695.74	32838429.26	4.05	1794481.16	32803245.48	4.14	2058997.46	32579922.42	3.83
1907678.83	32838422.36	4.05	1794467.74	32803219.01	4.14	2058987.49	32579949.96	3.84
1907661.93	32838415.42	4.05	1794457.58	32803195.78	4.14	2058977.51	32579977.50	3.84
1907645.02	32838408.48	4.05	1794449.72	32803174.12	4.14	2058967.26	32580005.82	3.84
1907627.49	32838401.61	4.05	1794442.08	32803153.06	4.14	2058957.28	32580033.36	3.84
1907608.86	32838394.88	4.05	1794434.30	32803131.03	4.14	2058947.31	32580060.90	3.84
1907590.24	32838388.14	4.05	1794511.81	32802589.12	4.14	2058936.50	32580089.21	3.84
1907571.61	32838381.40	4.05	1794590.77	32802040.26	4.14	2058925.74	32580116.75	3.84
1907556.58	32838374.28	4.05	1794671.84	32801476.96	4.14	2058914.99	32580144.29	3.84
1907542.70	32838367.04	4.05	1794727.48	32801130.49	4.14	2058903.93	32580172.61	3.84
1907528.83	32838359.80	4.05	1794745.71	32801112.52	4.14	2058893.18	32580200.15	3.84
1907514.73	32838352.76	4.05	1794763.34	32801095.86	4.14	2058882.42	32580227.69	3.84
1907499.35	32838346.82	4.05	1794781.47	32801078.72	4.14	2058871.36	32580256.01	3.84
1907483.96	32838340.89	4.05	1794799.10	32801062.06	4.14	2058860.61	32580283.55	3.84
1907468.58	32838334.96	4.05	1794817.23	32801044.92	4.14	2058849.85	32580311.09	3.84
1907450.91	32838329.08	4.05	1794835.37	32801027.78	4.14	2058838.80	32580339.40	3.84
1907432.28	32838323.55	4.05	1794854.03	32801011.21	4.14	2058828.04	32580366.94	3.84
1907413.65	32838318.02	4.05	1794876.86	32800994.48	4.14	2058817.29	32580394.48	3.84
1907395.03	32838312.49	4.05	1794899.06	32800978.22	4.14	2058806.23	32580422.80	3.84
1907376.88	32838306.48	4.06	1794921.89	32800961.50	4.14	2058795.47	32580450.34	3.84
1907358.76	32838300.44	4.06	1794944.12	32800947.14	4.14	2058785.22	32580477.98	3.84
1907340.64	32838294.41	4.06	1794967.01	32800933.43	4.14	2058775.69	32580506.60	3.84
1907322.52	32838288.37	4.06	1794989.26	32800920.11	4.15	2058766.42	32580534.44	3.84
1907304.40	32838282.34	4.06	1795012.14	32800906.41	4.15	2058757.15	32580562.28	3.84
1907286.28	32838276.31	4.06	1795035.02	32800892.71	4.15	2058747.39	32580590.14	3.84
1907268.16	32838270.27	4.06	1795057.28	32800879.39	4.15	2058737.82	32580616.98	3.84
1907250.87	32838263.33	4.06	1795080.15	32800865.70	4.15	2058728.25	32580643.81	3.84
1907233.86	32838256.09	4.06	1795100.84	32800854.03	4.15	2058718.41	32580671.41	3.84
1907216.85	32838248.85	4.06	1795120.48	32800843.76	4.15	2058708.84	32580698.25	3.84

Line 7 P-1			Line 8 P-1			Line 9 P-1		
X	Y	Time	X	Y	Time	X	Y	Time
2310725.85	32611143.79	3.24	2140029.30	32464818.72	3.06	2271316.07	32509318.39	3.25
2310710.84	32611123.34	3.24	2140013.65	32464871.63	3.06	2271336.47	32509337.41	3.25
2310695.41	32611102.31	3.24	2139998.22	32464923.80	3.06	2271356.87	32509356.42	3.25
2310680.39	32611081.85	3.24	2139980.13	32464981.58	3.06	2271380.01	32509375.00	3.25
2310664.96	32611060.82	3.24	2139943.20	32465085.39	3.06	2271404.42	32509394.11	3.25
2310649.94	32611040.37	3.24	2139923.33	32465133.14	3.06	2271428.83	32509413.23	3.25
2310634.93	32611019.91	3.24	2139900.33	32465183.31	3.06	2271451.69	32509431.66	3.25
2310619.49	32610998.88	3.24	2139874.24	32465233.22	3.06	2271470.53	32509448.32	3.25
2310602.30	32610976.72	3.24	2139844.97	32465281.19	3.06	2271489.37	32509464.98	3.25
2310584.17	32610953.58	3.24	2139815.70	32465329.15	3.06	2271507.71	32509481.19	3.25
2310566.54	32610931.08	3.24	2139786.02	32465377.79	3.06	2271529.31	32509497.78	3.25
2310548.99	32610909.48	3.24	2139756.76	32465425.76	3.06	2271552.06	32509514.33	3.25
2310533.58	32610892.88	3.24	2139727.08	32465474.40	3.06	2271574.83	32509530.89	3.25
2310518.16	32610876.27	3.24	2139697.81	32465522.37	3.06	2271597.72	32509547.39	3.25
2310502.30	32610859.20	3.24	2139668.21	32465571.54	3.06	2271620.66	32509563.10	3.25
2310483.89	32610841.80	3.24	2139637.10	32465625.25	3.05	2271644.23	32509579.24	3.25
2310463.38	32610823.50	3.24	2139605.67	32465675.33	3.06	2271667.81	32509595.39	3.25
2310443.44	32610805.70	3.24	2139573.31	32465721.76	3.06	2271691.40	32509611.54	3.25
2310423.43	32610787.97	3.24	2139540.48	32465768.84	3.06	2271714.99	32509627.69	3.25
2310402.10	32610770.79	3.24	2139508.12	32465815.27	3.06	2271738.57	32509643.84	3.25
2310381.35	32610754.09	3.25	2139475.30	32465862.36	3.06	2271761.45	32509659.53	3.25
2310360.00	32610736.92	3.25	2139442.98	32465908.92	3.06	2271781.14	32509675.18	3.25
2310337.31	32610719.58	3.25	2139411.63	32465958.16	3.06	2271800.82	32509690.82	3.25
2310312.63	32610701.58	3.25	2139379.84	32466008.09	3.06	2271820.49	32509706.46	3.25
2310287.26	32610683.07	3.25	2139348.48	32466057.33	3.06	2271841.96	32509722.85	3.25
2310262.58	32610665.07	3.25	2139316.69	32466107.26	3.06	2271865.55	32509740.13	3.25
2310242.32	32610651.64	3.25	2139285.33	32466156.50	3.06	2271888.48	32509756.92	3.25
2310223.18	32610639.14	3.25	2139253.01	32466204.77	3.06	2271912.06	32509774.20	3.25
2310203.50	32610626.29	3.25	2139219.71	32466253.21	3.06	2271934.92	32509789.84	3.25
2310183.58	32610613.79	3.25	2139186.88	32466300.98	3.06	2271957.68	32509805.28	3.25
2310162.02	32610601.29	3.25	2139153.58	32466349.42	3.06	2271980.44	32509820.71	3.25
2310139.85	32610588.44	3.25	2139120.74	32466397.19	3.06	2272003.48	32509835.91	3.25
2310118.30	32610575.94	3.25	2139086.98	32466445.01	3.06	2272026.41	32509850.22	3.25
2310093.85	32610564.07	3.25	2139050.07	32466493.65	3.06	2272049.99	32509864.93	3.25
2310069.27	32610552.88	3.25	2139013.67	32466541.62	3.06	2272073.58	32509879.65	3.25
2310044.69	32610541.68	3.25	2138976.75	32466590.27	3.06	2272097.35	32509895.28	3.25
2310019.05	32610530.27	3.25	2138940.35	32466638.23	3.06	2272121.17	32509911.20	3.25
2309992.16	32610519.72	3.25	2138903.94	32466686.20	3.06	2272144.99	32509927.10	3.25
2309964.51	32610508.88	3.25	2138868.77	32466733.59	3.06	2272168.16	32509942.58	3.25
2309937.61	32610498.33	3.25	2138834.35	32466780.12	3.06	2272191.99	32509958.49	3.25
2309909.96	32610487.49	3.25	2138799.45	32466827.30	3.07	2272215.81	32509974.40	3.25
2309883.07	32610476.94	3.25	2138765.04	32466873.82	3.07	2272239.64	32509990.31	3.25
2309856.17	32610466.39	3.25	2138730.61	32466920.36	3.07	2272263.45	32510006.22	3.25
2309828.52	32610455.56	3.25	2138695.71	32466967.55	3.07	2272287.28	32510022.13	3.25
2309802.42	32610446.64	3.26	2138661.29	32467014.08	3.07	2272310.45	32510037.60	3.25
2309775.60	32610437.49	3.25	2138626.39	32467061.26	3.07	2272334.04	32510053.49	3.25
2309749.52	32610428.60	3.26	2138591.97	32467107.79	3.07	2272354.48	32510069.08	3.25

Line 7 LM-1			Line 8 LM-1			Line 9 LM-1		
X	Y	Time	X	Y	Time	X	Y	Time
2251617.29	32559207.24	3.65	2108995.84	32507779.57	3.39	2267037.83	32505924.69	3.35
2251597.61	32559189.90	3.65	2108965.39	32507822.72	3.38	2267061.06	32505943.86	3.35
2251577.36	32559172.07	3.65	2108935.36	32507865.26	3.39	2267084.28	32505963.03	3.35
2251557.68	32559154.73	3.65	2108905.33	32507907.80	3.38	2267107.50	32505982.19	3.35
2251537.44	32559136.90	3.65	2108874.88	32507950.95	3.39	2267128.82	32506000.14	3.35
2251517.17	32559117.76	3.65	2108843.91	32507993.52	3.39	2267147.69	32506016.91	3.35
2251495.94	32559096.89	3.65	2108811.73	32508036.71	3.39	2267166.54	32506033.68	3.35
2251475.29	32559076.59	3.65	2108779.99	32508079.29	3.39	2267185.39	32506050.45	3.35
2251454.65	32559056.32	3.65	2108748.26	32508121.87	3.39	2267208.27	32506068.42	3.35
2251434.45	32559037.91	3.65	2108716.07	32508165.06	3.39	2267232.57	32506086.82	3.35
2251414.80	32559020.01	3.65	2108684.34	32508207.65	3.39	2267256.20	32506104.71	3.35
2251394.61	32559001.61	3.65	2108652.15	32508250.83	3.39	2267280.13	32506123.07	3.35
2251374.96	32558983.70	3.65	2108620.42	32508293.42	3.39	2267302.18	32506141.27	3.35
2251355.32	32558965.81	3.65	2108588.68	32508336.01	3.39	2267324.22	32506159.47	3.35
2251335.12	32558947.40	3.65	2108559.04	32508379.77	3.39	2267346.27	32506177.67	3.35
2251315.48	32558929.50	3.65	2108531.79	32508423.39	3.39	2267368.75	32506197.25	3.35
2251295.45	32558910.40	3.65	2108504.54	32508467.01	3.39	2267390.88	32506217.12	3.35
2251276.01	32558891.70	3.65	2108476.90	32508511.24	3.39	2267413.64	32506237.57	3.35
2251256.57	32558873.00	3.65	2108449.65	32508554.85	3.39	2267436.36	32506257.89	3.35
2251236.58	32558853.77	3.66	2108421.60	32508599.30	3.39	2267457.85	32506275.31	3.35
2251217.14	32558835.07	3.66	2108391.98	32508644.20	3.39	2267479.34	32506292.72	3.34
2251197.15	32558815.85	3.66	2108362.36	32508689.10	3.39	2267500.82	32506310.12	3.34
2251177.70	32558797.15	3.66	2108332.31	32508734.64	3.39	2267521.73	32506327.06	3.34
2251157.71	32558777.92	3.66	2108302.69	32508779.54	3.38	2267543.22	32506344.47	3.34
2251138.27	32558759.22	3.66	2108272.65	32508825.08	3.38	2267564.71	32506361.89	3.34
2251118.83	32558740.52	3.66	2108213.39	32508914.89	3.39	2267586.19	32506379.29	3.34
2251098.86	32558721.56	3.66	2108187.47	32508959.78	3.39	2267607.69	32506396.70	3.34
2251079.62	32558705.46	3.66	2108162.04	32509004.03	3.39	2267629.18	32506414.12	3.34
2251059.84	32558688.90	3.66	2108136.24	32509048.90	3.39	2267650.08	32506431.05	3.34
2251040.59	32558672.80	3.66	2108108.58	32509093.45	3.39	2267671.74	32506448.42	3.34
2251021.47	32558655.25	3.66	2108077.29	32509138.46	3.39	2267693.75	32506465.73	3.34
2251001.92	32558635.74	3.66	2108045.55	32509184.12	3.39	2267715.75	32506483.04	3.34
2250982.90	32558616.77	3.66	2108014.27	32509229.14	3.39	2267737.76	32506500.35	3.34
2250963.35	32558597.26	3.66	2107982.53	32509274.80	3.39	2267759.17	32506517.19	3.34
2250944.34	32558578.28	3.66	2107951.24	32509319.81	3.39	2267781.16	32506534.49	3.34
2250924.78	32558558.77	3.66	2107916.14	32509363.22	3.39	2267803.17	32506551.80	3.34
2250905.77	32558539.80	3.66	2107880.48	32509407.21	3.39	2267825.18	32506569.11	3.34
2250886.76	32558520.82	3.66	2107845.32	32509450.60	3.39	2267847.18	32506586.42	3.34
2250867.21	32558501.31	3.66	2107809.66	32509494.59	3.39	2267869.19	32506603.73	3.34
2250848.19	32558482.34	3.66	2107774.49	32509537.97	3.39	2267890.58	32506620.56	3.34
2250828.64	32558462.83	3.66	2107739.33	32509581.35	3.39	2267914.62	32506638.64	3.34
2250809.63	32558443.85	3.66	2107703.67	32509625.35	3.39	2267939.74	32506657.14	3.34
2250790.61	32558424.87	3.66	2107668.51	32509668.74	3.39	2267964.87	32506675.65	3.34
2250771.06	32558405.37	3.66	2107632.85	32509712.73	3.39	2267989.45	32506693.86	3.34
2250751.75	32558386.29	3.66	2107597.69	32509756.11	3.39	2268009.02	32506709.50	3.34
2250730.42	32558366.19	3.66	2107563.07	32509799.13	3.39	2268028.04	32506724.71	3.34
2250709.67	32558346.64	3.66	2107530.20	32509841.27	3.39	2268047.61	32506740.35	3.34

Line 7 LM-1a			Line 8 LM-1a			Line 9 LM-1a		
X	Y	Time	X	Y	Time	X	Y	Time
2308359.89	32610445.74	3.57	2111476.96	32504387.82	3.40	2206341.04	32458325.07	3.29
2308329.17	32610449.35	3.57	2111445.51	32504432.45	3.40	2206360.26	32458341.07	3.29
2308297.59	32610453.06	3.57	2111413.61	32504477.72	3.40	2206379.47	32458357.06	3.29
2308267.34	32610456.40	3.57	2111382.16	32504522.35	3.40	2206398.67	32458373.06	3.29
2308209.53	32610461.09	3.57	2111350.71	32504566.98	3.40	2206417.88	32458389.05	3.29
2308181.03	32610463.40	3.57	2111318.81	32504612.24	3.40	2206437.09	32458405.05	3.29
2308148.82	32610466.93	3.57	2111287.44	32504656.97	3.40	2206455.77	32458420.61	3.29
2308115.78	32610471.04	3.57	2111257.41	32504703.38	3.39	2206475.22	32458436.77	3.29
2308081.82	32610475.27	3.57	2111166.48	32504843.91	3.39	2206498.07	32458455.27	3.29
2308049.05	32610479.37	3.57	2111136.45	32504890.32	3.39	2206520.94	32458473.77	3.29
2308022.16	32610483.28	3.57	2110936.34	32505177.02	3.39	2206543.80	32458492.26	3.29
2307994.52	32610487.30	3.57	2110907.46	32505222.21	3.38	2206565.21	32458508.54	3.29
2307967.63	32610491.21	3.57	2110878.99	32505266.76	3.38	2206586.43	32458523.57	3.29
2307938.52	32610495.16	3.57	2110850.12	32505311.94	3.38	2206607.64	32458538.60	3.29
2307908.57	32610498.92	3.57	2110818.41	32505356.08	3.38	2206628.86	32458553.62	3.29
2307878.60	32610502.68	3.57	2110785.14	32505400.03	3.38	2206648.57	32458569.61	3.29
2307847.79	32610506.55	3.57	2110751.40	32505444.60	3.38	2206668.18	32458585.66	3.29
2307817.83	32610510.31	3.57	2110718.13	32505488.55	3.38	2206687.26	32458601.26	3.29
2307787.03	32610514.18	3.57	2110684.39	32505533.13	3.38	2206706.88	32458617.31	3.29
2307757.06	32610517.94	3.57	2110651.12	32505577.07	3.38	2206726.50	32458633.36	3.29
2307727.32	32610520.95	3.57	2110617.85	32505621.03	3.38	2206746.11	32458649.40	3.29
2307697.28	32610522.10	3.57	2110584.11	32505665.60	3.38	2206765.73	32458665.45	3.29
2307668.07	32610523.21	3.57	2110453.17	32505830.13	3.38	2206786.44	32458681.86	3.29
2307638.04	32610524.35	3.57	2110420.33	32505870.75	3.39	2206806.80	32458697.90	3.29
2307607.77	32610525.11	3.57	2110387.23	32505915.90	3.38	2206827.74	32458714.39	3.29
2307576.18	32610525.74	3.57	2110353.65	32505961.69	3.38	2206848.67	32458730.88	3.29
2307545.47	32610526.35	3.57	2110320.54	32506006.85	3.38	2206869.62	32458747.37	3.29
2307515.18	32610526.89	3.57	2110286.64	32506049.97	3.39	2206890.56	32458763.86	3.29
2307487.51	32610526.90	3.57	2110251.42	32506091.60	3.39	2206911.50	32458780.35	3.29
2307460.62	32610526.91	3.57	2110216.70	32506132.64	3.39	2206931.85	32458796.38	3.29
2307432.97	32610526.91	3.57	2110181.48	32506174.28	3.39	2206952.79	32458812.87	3.29
2307406.08	32610526.44	3.57	2110146.85	32506221.29	3.39	2206973.73	32458829.36	3.29
2307379.19	32610525.55	3.57	2110112.23	32506268.96	3.39	2206994.68	32458845.90	3.29
2307351.54	32610524.63	3.57	2110077.12	32506317.28	3.39	2207015.65	32458862.72	3.29
2307324.65	32610523.74	3.57	2110042.71	32506362.67	3.39	2207036.62	32458879.55	3.29
2307296.27	32610519.67	3.57	2110008.31	32506403.38	3.39	2207057.02	32458895.92	3.29
2307184.90	32610502.98	3.56	2109974.39	32506443.52	3.39	2207077.99	32458912.75	3.29
2307156.47	32610498.72	3.56	2109940.48	32506483.66	3.39	2207098.97	32458929.59	3.29
2307128.82	32610494.58	3.56	2109907.64	32506528.58	3.39	2207119.94	32458946.41	3.29
2307099.71	32610489.40	3.56	2109875.91	32506574.62	3.39	2207140.92	32458963.25	3.29
2307071.21	32610484.10	3.57	2109843.72	32506621.31	3.39	2207161.89	32458980.08	3.29
2307042.71	32610478.81	3.56	2109811.99	32506667.34	3.39	2207182.29	32458996.44	3.29
2307013.42	32610473.21	3.56	2109780.26	32506713.38	3.39	2207203.26	32459013.27	3.29
2306985.01	32610467.11	3.56	2109748.07	32506760.07	3.39	2207224.49	32459030.62	3.29
2306955.81	32610460.85	3.56	2109716.34	32506806.10	3.39	2207246.07	32459048.66	3.29
2306927.41	32610454.75	3.56	2109684.60	32506852.14	3.39	2207267.64	32459066.71	3.29
2306901.32	32610448.66	3.56	2109652.42	32506898.82	3.39	2207288.62	32459084.25	3.29